Study of Ship Turning in Waves
(船の波浪中旋回運動の研究)

Muhammed Amirul Asyraf Bin Hasnan

Doctor Thesis
Submitted in Fullfillment of the Requirements
for the Degree of Doctor of Philosophy

September 2020

Graduate School of Engineering
Department of Transportation
and Environmental Systems
Hiroshima University,
Japan

# ABSTRACT

A 6-DOF simulation method based on two-time scale concept for ships steering in regular waves and irregular waves in time-domain are established and validated with free-running model tests in this study. Separating the basic motion equations into two groups where one is for high frequency wave-induced motion and the other is for low frequency maneuvering motion, the total 10 motion equations which are composed of 6-DOF equations for the high frequency motions and 4-DOF (surge, sway, yaw and roll) equations for the low frequency motions are treated in time-domain. The present method can simulate both the turning motion in the irregular waves and the wave-induced motions during turning with practical accuracy in short computational time, although there is some room for improvements in the low approach speed range. In final part, the newly derived theoretical formulas are useful for a better understanding of the wave-induced drift motion of ships during turning. It is concluded the drifting distance $H_D/L$ is proportional to the $H_{1/3}$ and inversely proportional to approach speed $U_A$.

# ACKNOWLEDGEMENTS

# TABLE OF CONTENTS

# LIST OF FIGURES

# LIST OF TABLES

# Chapter 1

# Introduction

## 1.1   Background

Ship maneuverability is usually studied in calm waters. Although it is convenient to study the ship maneuvering in calm water first, ship maneuvering in waves should be investigated as the next step because a large number of ships actually do sail in waves. Particularly, for the safety of ships sailing in the sea, studying the effect of waves on ship maneuvering is important. However, the understanding of the wave effect on maneuvering may be limited. Next, in order to prevent marine accidents due to human mistakes in ship navigation, prior training of crew members using a ship-handling simulator is effective. In adverse weather condition, the captain navigates the ship so as to avoid large waves visually, so it is necessary for the simulator to realistically reflect the influence of steering on the ship motions in the waves. In other words, a ship-handling simulator that rationally incorporates the three features of wave fields, maneuvering motion, and wave-induced fluctuating motions is required. However, it is not easy to construct a simple calculation method that can be mounted on a computer of the simulator, and that can handle the wave-induced motions during ship maneuvering in irregular waves with reliable accuracy.

Studies on ship turning in waves have started experimentally since approximately 40 years ago: Hirano et al.[1] conducted a free-running test in regular waves using a self-propelled Ro-Ro ship model to investigate the effects of waves on the turning trajectory. The drifting behavior during turning in regular waves was studied. Ueno et al.[2] performed free-running tests for turning, zig-zag, and stopping maneuvers in regular waves using a VLCC tanker model. It was shown that the drifting direction of a ship was different from the incoming wave direction. In addition, a large drift of the ship during turning was observed for shorter wavelengths. Nishimura and Hirayama[3] conducted turning tests in relatively longer regular waves such as $\lambda/L = 1 \sim 3$, where $\lambda/L$ is the ratio of the wave length and ship length, for a fishing boat in the variations of wave heights and wave directions. The main purpose of this study was to capture the roll characteristics during turning, and the wave effect on maneuvering was not discussed. Yasukawa[4][5][6], and Yasukawa and Nakayama[7] conducted free-running tests for turning, zig-zag, and stopping maneuvers using the S-175 container ship model. The tests were performed in

not only regular waves but also in irregular waves. The test with irregular waves was performed for just one pattern. They did not conduct tests for conditions where the wave pattern was changed with the same significant wave height and mean wave period. Lee et al.[8] conducted turning and zig-zag maneuver tests in regular waves using a VLCC model to capture the wave height effect. However, details such as $\lambda/L$ were not revealed. Sanada et al.[9] performed turning tests for the ONR Tumblehome in calm water and regular waves and presented measured time histories of 6-DOF motions during turning in waves. Moreover, Sanada et al.[10] performed repeat tests (RTs) of turning and zig-zag maneuvers for the same ONR Tumblehome in regular waves and discussed the effect of ship speed and $\lambda/L$ on maneuvering with the measured accuracy. Sprenger et al.[11] performed turning and zig-zag maneuver tests for a DTC container ship and KVLCC2 tanker models in regular waves with variations in wave directions, $\lambda/L$, etc. The obtained data was mainly used to validate the calculation method for maneuvering in waves. Thus, although tank tests have been done for regular waves, the tests for irregular waves have been rarely performed with the aim of capturing the maneuvering behaviors in waves.

In order to predict ship maneuvering in waves, a simple method is known which takes only wave-induced steady forces into account to the existing prediction method in calm water[1]. However, this method cannot treat wave-induced motion of a maneuvering ship. Such a treatment is theoretically acceptable on the assumption of a slender ship[12]. However, treatment of wave-induced motions such as heave and pitch of a maneuvering ship unable to be performed in this method. McCreight[13] presented a simulation method which is able to calculate both maneuvering and wave-induced motions. The motion equations were treated on the basis of the coordinate system fixed to the ship, and the strip method was used for estimating the hydrodynamic forces related to the wave-induced motions such as wave exciting forces, added mass and wave damping. As the calculation example, turning motions in regular waves were presented. However, wave-induced steady forces acting on the ship were not included in the calculation. Hamamoto and Saito[14], and Hamamoto and Kim[15] constructed the equation of motion under the horizontal body axes system and presented a 6-DOF motion simulation method including maneuvering in waves. The Froude-Krylov force was used as the wave-exciting force acting on the ship, and the zig-zag maneuvers in regular waves was simulated. Hamamoto's approach has been improved by Nishimura et al.[16] and Fang et al.[17]. However, these methods do not consider the wave-induced steady forces. When discussing ship maneuvering in waves, the effects of wave-induced steady forces cannot be ignored. In recent years, many papers have been published on simulation methods for ship maneuvering in waves Yasukawa[4], Yasukawa and Nakayama[7],Skejic and Faltinsen[18], Yen et al.[19], Seo and Kim[20], Cura and Uharek[21], and Zhang et al.[22]. In the methods, the hydrodynamic forces acting on the ship with steering in waves are estimated by the captive model test, the empirical formulas, the potential theory, CFD, their combinations, etc. However, most of them deal with maneuvering in regular waves. In the methods, the hydrodynamic forces acting on the ship with steering in waves are estimated by several methods such as the captive model test, the empirical formulas, the potential theory, CFD, their combinations, etc. However, there is no example of detailed validation of the calculation method for items such as 6-DOF motions (trajectory, rotational motions and wave-induced motions) together with the hydrodynamic properties such as rudder normal force and propeller thrust in waves, so far. Studying in regular waves is useful for a better understanding of

2

the wave effects on the ship maneuvering. However, to discuss the safety of ships sailing in the actual sea, investigating in regular waves is inadequate as the sea comprises irregular waves. Skejic and Faltinsen[23] have presented a simulation method of ship maneuvering in irregular waves. As the external disturbance forces act on the ships in irregular waves, not only the wave-induced steady forces but also the slowly varying second-order wave forces were considered in the turning simulations in irregular waves with six random patterns. However, it has not been validated by free-running model tests in irregular waves till date.

## 1.2   Objective and outline of the thesis

The main objective of this study is to establish a method for simulating a ship maneuvering in irregular waves. The validation for the simulation method for a ship turning in irregular waves which consists of ship trajectories, time histories motions and wave-induced motions are very limited so far, thus is conducted in this study. The second objective of this study is to understand the phenomena for a ship turning in irregular waves. An analytical study for steady turning in irregular waves by taking the drift effect due to wave-induced steady forces into account. Understanding the influence of lateral drift during maneuvering in irregular waves is important for the current and future experiment and simulation researches on ship maneuvering in actual sea.

In order to achieve the main objective, firstly turning test in regular waves was conducted in a square tank of National Research Institute of Fisheries Engineering, Japan by using KCS container ship as studied ship. The model tests with one approach speed $U_A = 14.5$ kn at full scale and rudder angle $\pm 35°$ were performed in calm water first, followed by head waves at the time of approaching with wave amplitude $h_a = 0.024$ m and $\lambda/L = 1.0$ for regular waves. Thus, in chapter 2 describes the conducted free-running model test for a KCS container ship model in calm water and regular waves. The chapter defines firstly the coordinate system used, followed by the descriptions of test outline, selected approach speed and propeller revolution for the ship, water condition for the regular waves and drifting indices for the analysis of the ship drifting for turning in waves. Drifting indices that represent the effect of drifting during turning in waves consist of drifting distance $H_D$ and drifting direction $\mu_D$ are mainly used across the analysis in this study. The results of the repeat test of turning in calm water and regular waves from this chapter is crucial as a base for the turning test in irregular waves because irregular waves is a superposition of regular waves. Besides that, the data is for the validation of the simulation method of ship turning in regular waves in chapter 4.

Continuation from the chapter 2, turning test in irregular waves was conducted. The model tests were conducted in a square tank of National Research Institute of Fisheries Engineering, Japan by using KVLCC2 tanker and KCS container ship as studied ships. The model tests with are varied approach speeds ranging from $U_A = 5$ kn to 15 kn and rudder angle $\pm 35°$ were performed in calm water first, followed by head waves at the time of approaching with significant wave height 4.5 m for KVLCC2, and 3.0 m for KCS in full-scale for irregular wave. Thus, in the chapter 3 describes the conducted free-running model

test for a KVLCC2 tanker and KCS container ship model in calm water and irregular waves. The chapter used the same coordinate system and drifting indices used in regular waves, followed by the descriptions of test outline, selected approach speed and propeller revolution for the ship, water condition for the irregular waves. As for the test outline, it can be summarized as follows. First, the RT is conducted for KCS and KVLCC2, in which the turning test of rudder angle $\pm 35°$ is repeated five times in the exact same wave pattern both in regular and irregular waves. Next, five waves are generated with different patterns on a time history basis, although the wave conditions (significant wave height, mean wave period, and main wave direction) are the same, and the turning tests are conducted for KVLCC2 and KCS in those waves. From the obtained test results, the average values and standard deviations of turning indices (advance $A_D$ and tactical diameter $D_T$) and drifting indices in waves (drifting distance $H_D$ and drifting direction $\mu_D$) are obtained. The wave patterns are varied in order to investigate the effect of slowly varying second order wave forces during turning. The results from this chapter is necessary for the decision of a suitable simulation method to be used, and the method for estimating wave-induced steady forces and moment. The results which consisted of trajectories for ship turning with rudder angle $\pm 35°$ and their time histories motions are necessary for the purpose of validation for the simulation method of ship turning in irregular waves in chapter 5. In this chapter, it is found a simulation method based on two-time scale concept is valid to be used in treating maneuvering and seakeeping problems. It is also experimentally confirmed that mean values for the wave-induced steady forces is majorly influencing the drifting effect during turning in irregular waves and the effect of slowly varying second order wave forces is negligible during turning.

In chapter 4, a simulation method for a ship turning in regular waves is established and outlined. The chapter describes a coordinate system that is used for the base for both simulation method in regular and irregular waves. In particular, the coordinate system is called as horizontal body axes system (HBA system). Next, ship motion is assumed to be expressed as the sum of the maneuvering motion regarded as low frequency motion and wave-induced motion regarded as high frequency motion, according to the concept of the two time-scale method. By assuming a hip maneuvering motion is very slow comparing with wave-induced motion, the basic motion equations are separated into two groups where one is for high frequency wave-induced motion and the other is for low frequency maneuvering motion based on the two time-scale method concept. The simulation results of ship turning in regular waves which consists of turning trajectories, time histories motions during turning and wave-induced motions during turning with $\delta = \pm 35°$ are presented and compared with the previous model tests results in chapter 2. The agreement of results comparisons in the validation between simulation and tests in this chapter confirms the estimation of the wave-induced steady forces in the present turning in regular waves are sufficient to be used in the estimation of the wave-induced steady forces for simulation method for turning in irregular waves.

In chapter 5, a simulation method for a ship turning in irregular waves is then established and outlined. The chapter used the same coordinate system, concept, assumptions, motion equations that are used in the method for simulating turning in regular waves. In other words, the 6-DOF method in regular waves is extended by changing the wave-induced steady forces and wave exciting forces based on irregular waves condition. The

simulation results of ship turning in regular waves which consists of turning trajectories, time histories motions during turning and wave-induced motions during turning with $\delta = \pm 35°$ are presented and compared with the previous model tests results in chapter 3. The agreement of results comparisons in the validation between simulation and tests in this chapter confirms the estimation of the wave-induced steady forces in the present turning in irregular waves are sufficient. It is also confirmed the two-time scale concept is valid to be used for a method simulating a 6-DOF motions of ship behaviors in irregular waves.

Next, in chapter 6, an analytical study for steady turning in irregular waves by taking the drift effect due to wave-induced steady forces into account is conducted. The calculated drifting distance $H_D$ and drifting direction $\mu_D$ from the theoretical study are compared with the results from the conducted model tests for a KVLCC2 and KCS models. The linear assumption in the theory formulation confirmed the non-linearity effect is exist. Finally, the conclusion and several recommendations for future research are given in chapter 7.

# Chapter 2

# Turning tests in regular waves

## 2.1 Studied ship

### 2.1.1 KCS containership

The studied ship is a KCS container ship (SIMMAN 2008)[24]. Table 2.1 shows the principal particulars of the ship hull and the propeller. The scale ratio is 1/75.238. In the table, $L$ is length between perpendiculars, $B$ is the ship's breadth, $D$ is the ship's depth, $d$ is the ship's draft, $\nabla$ is displacement volume, $x_G$ is the coordinate in the length direction of the center of gravitation (ahead of midship is positive), and $C_b$ is the block coefficient. Furthermore, $\overline{GM}$ is the metacentric height, $\overline{KM}$ is the metacenter height above baseline, $Z$ is the number of propeller blades, $D_P$ is the propeller diameter, and $p$ is the propeller pitch ratio. Table 2.2 shows rudder dimensions of KCS. A mariner rudder was attached to this ship. In the table, $H_R$ is the rudder span length, $B_R$ is the average chord length of the rudder, and $A_R$ is the rudder area including the horn part. A mariner rudder was attached to this ship, but bilge keels were not installed. Fig.2.1 shows the body plan of KCS. Fig.2.2 shows the photograph of the KCS model. The full load condition is considered.
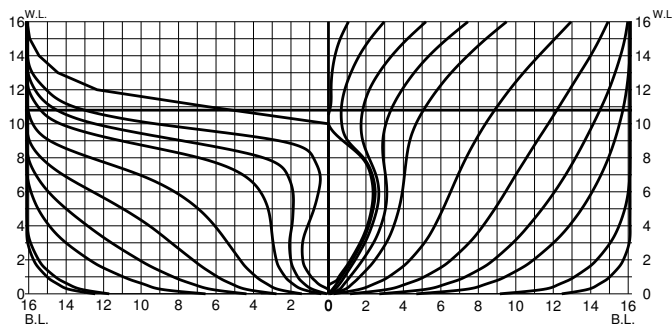


Fig. 2.1: Body plan of KCS

Table 2.1: Principal particulars of KCS

|  | full-scale | model |
|---|---|---|
| $L$ (m) | 230.0 | 3.057 |
| $B$ (m) | 32.2 | 0.428 |
| $D$ (m) | 18.0 | 0.239 |
| $d$ (m) | 10.8 | 0.144 |
| $\nabla$ (m$^3$) | 52040 | 0.122 |
| $x_G$ (m) | -3.39 | -0.045 |
| $C_b$ | 0.651 | 0.651 |
| $\overline{GM}$ (m) | 0.60 | 0.008 |
| $\overline{KM}$ (m) | 14.1 | 0.187 |
| $Z$ | 5 | 5 |
| $D_P$ (m) | 7.90 | 0.105 |
| $p$ | 0.997 | 0.997 |



Fig. 2.2: Side profile of a KCS model

Table 2.2: Rudder dimensions of KCS

|  | fullscale | model | remarks |
|---|---|---|---|
| $H_R$ (m) | 9.90 | 0.132 |  |
| $B_R$ (m) | 5.50 | 0.073 | including horn |
| $A_R$ (m$^2$) | 54.5 | 0.0096 | including horn area |

## 2.2 Test outline

The model tests were conducted in a square tank of National Research Institute of Fisheries Engineering, Japan (Tank length: 60 m, width: 25 m, depth: 3.2 m). The test coordinate system, test procedure, test measurements, test conditions and test analysis are described. In this chapter, free-running model tests in calm water and regular waves are considered.

### 2.2.1 Coordinate systems

Fig.2.3 shows the coordinate systems used in this experimental study. Specifically, the space-fixed coordinate system was denoted as $o_s - x_s y_s z_s$, where the $x_s - y_s$ plane coincided with the still water surface, and the $z_s$-axis pointed vertically downward. The horizontally

moving body-fixed coordinate system proposed by Hamamoto and Kim[26], denoted as $o - xyz$ where $o$ is located at the midship position on the still water surface of the moving ship, and $x$, $y$, and $z$ axes point toward the ship's bow, toward the starboard, and vertically downwards, respectively. Heading angle $\psi$ is defined as the angle between $x_s$ and $x$-axes, $\delta$ is the rudder angle, and $r$ is the yaw rate. $u$ and $v_m$ denote the velocity components in $x$ and $y$ directions, respectively. $\beta$ is the drift angle at midship position, and $U$ is the total velocity defined by ($U = \sqrt{u^2 + v_m^2}$).

The wave propagation direction is defined as an angle against $x_s$-axis by $\chi$. Then, the head waves of the ship in approaching are assumed to be $\chi = 0°$ in this study.
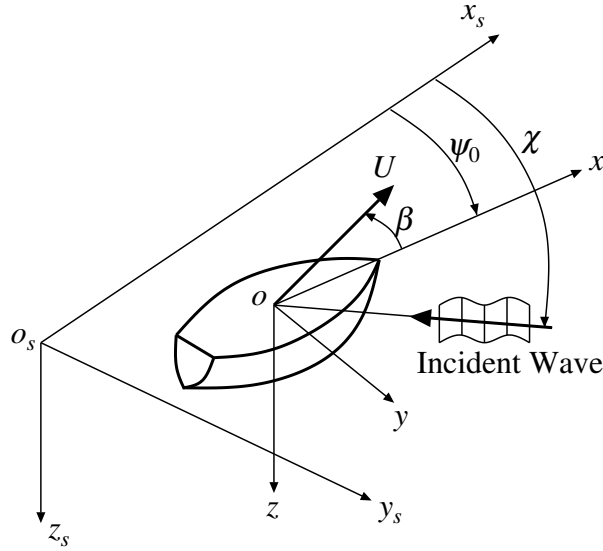


Fig. 2.3: Coordinate systems

## 2.2.2   Procedure

The regular waves are generated first. After the regular waves cover the tank completely, the ship model is launched at a certain approach speed by a catapult set at the tank shore (wave absorber) and runs straight on $x_s$-axis using an autopilot with PD controller. After reaching the target approach speed ($U_A$) and the target heading angle ($\psi_T = 0$), the model is steered by a radio controller for turning. Then, the midship position is defined as $(x_s, y_s) = (0, 0)$ when the steering is started.

The turning test of rudder angle $\pm 35°$ was repeated five times in both conditions: calm water and regular waves. The steering rate is set to be equivalent to $2.32(°/s)$ for full-scale ships: $20.1(°/s)$ in the model tests. The radius of pitch gyration was set to $k_{zz} = 0.25L$. The radius of roll gyration including the added moment of inertia was $k_{xx} = 0.49B$.

In the tests, the 3D position $(x_s, y_s, z_s)$ of the ship model was measured by a total station system by Matsuda et al.[28]. The heading angle ($\psi$), yaw rate ($r$), roll angle ($\phi$),

and pitch angle ($\theta$) were measured using a gyroscope on the model. The rudder angle ($\delta$), rudder normal force ($F_N$) and propeller thrust ($T_P$) during turning were measured using dynamo-meters equipped on the model. Ship velocity ($U$) was calculated by differentiating the position of the ship model.

### 2.2.3   Approach speeds and propeller revolutions

As for waves condition, the characteristics of the regular waves are kept similar along the repetition. Average values and standard deviations of turning indices and drifting indices in waves are obtained from the measured turning test data, and used to ascertain the variation in test results. Table 2.3 shows combinations of the approach speed $U_A$ and propeller revolution $n_P$ for the turning tests. The propeller revolution is kept constant during the test. The approach speed was kept constant for calm water and regular waves by adjusting the propeller revolution.

Table 2.3: Approach speed ($U_A$) and propeller revolution ($n_P$) in the tank tests

|  | Calm (EXP) | Waves (EXP) |
|---|---|---|
| $U_A$ in full-scale (kn) | 14.5 | 14.5 |
| $U_A$ in model (m/s) | 0.860 | 0.860 |
| $n_P$ in model (rps) | 10.4 | 13.2 |

### 2.2.4   Wave conditions

The target values of the wave amplitude $h_a$ and the wave-length $\lambda$ in the tests are shown in Table 2.4. As the wave direction, $\chi = 0°$ is assumed. This is the head wave condition when the ship is approaching at zero heading $\psi_T = 0°$.

Table 2.4: Target value of wave condition in the tank test

|  | Full-scale | Model |
|---|---|---|
| $h_a$ (m) | 3.61 | 0.024 |
| $\lambda/L$ | 1.0 | 1.0 |

### 2.2.5   Analysis: turning and drifting indices in waves

Turning indices such as advance $A_D$ and tactical diameter $D_T$ are used to characterize the turning performance in both calm water and waves. Drifting indices during turning in waves such as drifting distance $H_D$ and drifting direction $\mu_D$ are used. The definition of the indices is summarized as follows: $A_D$ is a longitudinal distance ($x_s$-coordinate)

from $y_s$-axis where the ship reaches $\psi = 90°$, and $D_T$ is a lateral distance ($y_s$-coordinate) from $x_s$-axis where the ship reaches $\psi = 180°$. $H_D$ is the distance between successive ship positions at each $\psi = 90°$. $\mu_D$ is the offset angle between the wave direction and the moving direction of the ship drifted away at each $\psi = 90°$.

Here, the successive ship positions in $\psi = 90°$, $450°$, $810°$, etc. during turning are numbered as 1, 2, 3 and so on, as shown in Fig.2.4. Then, $A_{D1}$ and $A_{D2}$ are defined as the advances at position 1 and 2, respectively. Do the same for $D_{T1}$ and $D_{T2}$. $H_{D1}$ and $H_{D2}$ are defined as the distances of ship drifting from 1 to 2 and 2 to 3, respectively. Similarly, $\mu_{D1}$ and $\mu_{D2}$ are defined as angles of the ship drifting from 1 to 2 and 2 to 3, respectively. In case of $\delta = +35°$, positive $\mu_{D1}$ means that the ship drifts away from the steering position $(x_s, y_s) = (0, 0)$, while negative $\mu_{D1}$ indicates it is drifting towards the steering position. Conversely, in case of $\delta = -35°$, positive $\mu_{D1}$ is defined when the ship drifts towards the steering position $(x_s, y_s) = (0, 0)$. Meanwhile, $H_{D1}$ are similar in both $\delta = \pm 35°$ cases and are not subjected to turning direction.
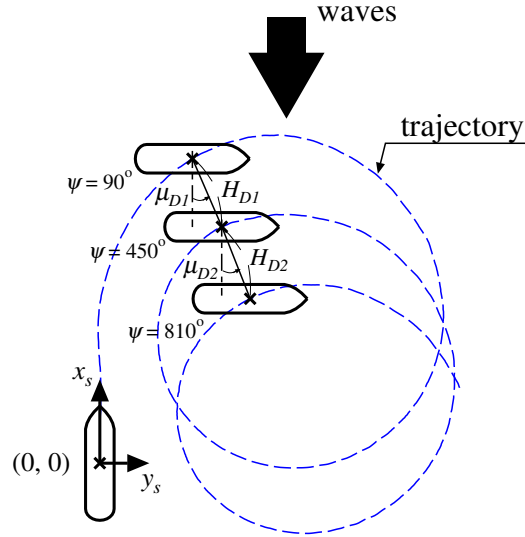


Fig. 2.4: Definition of drifting distance $H_D$ ($H_{D1}$ and $H_{D2}$) and drifting direction $\mu_D$ ($\mu_{D1}$ and $\mu_{D2}$)

## 2.3 Test results

### 2.3.1 Wave measurement

The turning test was repeated five times in each calm water and regular waves. Namely, 20 turning tests in total were performed: 10 in calm water and 10 in regular waves. It was confirmed the actual wave condition of $h_a$ based on the measured wave data. Table 2.5 show the measured incident wave amplitude of $h_a$ in the tests. In the table, AVG denotes the average value, STD denotes the standard deviation, and RSD denotes the

relative standard deviation, which is defined by $(\text{RSD} \equiv \text{STD}/\text{AVG})$. The average value of the $h_a$ is adequately close to the target wave condition (24.0 mm) shown in Table 2.4. The RSD of the $h_a$ is smaller than 5%.

Table 2.5: Measured incident wave amplitude $h_a$ in the turning tests

| $h_a$ | | |
|---|---|---|
| | AVG (mm) | 24.14 |
| | STD (mm) | 0.85 |
| | RSD (%) | 3.51 |

## 2.3.2 Turning trajectories in waves: repeat test results

Figs. 2.5 and 2.6 show the turning trajectories of repeat test (RT) with $\delta = \pm 35°$ in calm water and regular waves. The test was repeated five times, namely Test1, Test2, Test3, Test4 and Test5 for both port and starboard turnings. The turning of the ship in the calm water enters the steady turning condition when the heading angle exceeds 180° and the circular motion continues until the circle is complete. In contrast, the turning in regular waves leads to the circular trajectory which gradually shifting under the influence of the waves. For the first turn of the circular motion, the five trajectories are almost in agreement, but the difference becomes significant during the second turn. Slight variations in incoming waves and initial condition at the time of approaching create such differences. Table 2.6 and Table 2.7 show AVG, STD, and RSD of turning and drifting indices from RT. The AVG and RSD for the approach speed in $\delta = \pm 35°$ are listed in the table. The RSDs of both turning and drifting indices are smaller than 2%, where the $A_{D1}/L$ is the largest.
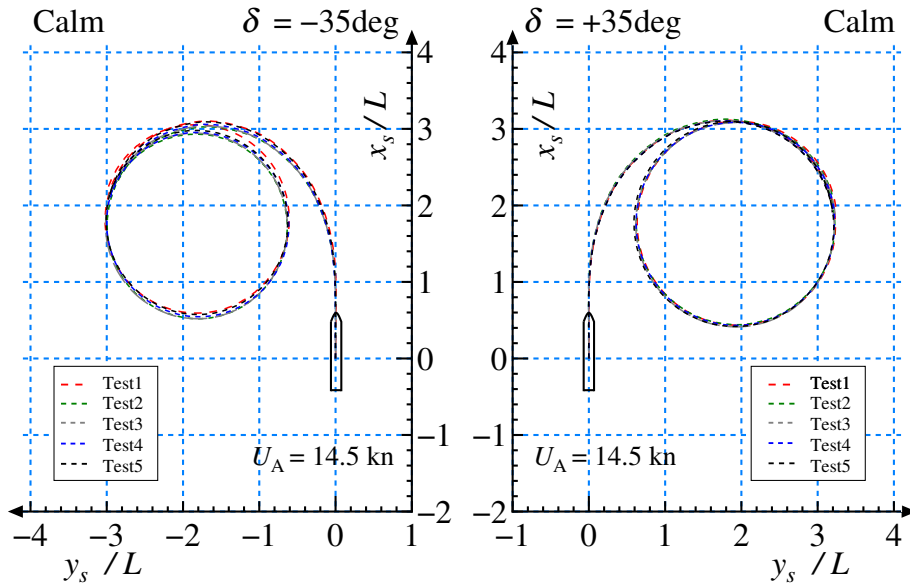


Fig. 2.5: Repeat test results: turning trajectories with $\delta = \pm 35°$ in calm water

11
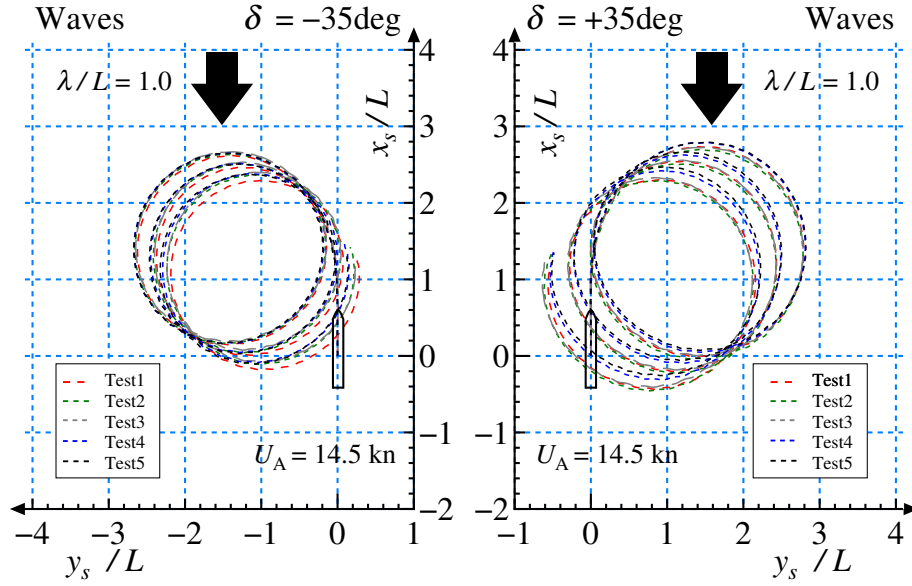
Fig. 2.6: Repeat test results: turning trajectories with $\delta = \pm 35°$ in regular waves

The obtained results of turning circle motions with rudder angle $\delta = \pm 35°$ of Test1 is used in the comparison with simulation results in chapter 4. The turning indices, drifting indices, time histories motions and wave-induced motions are also compared in the chapter.

Table 2.6: Repeat test results: turning indices in calm water and regular waves

| | | Calm | | Waves | |
|---|---|---|---|---|---|
| | | $\delta = -35°$ | $\delta = +35°$ | $\delta = -35°$ | $\delta = +35°$ |
| $A_{D1}/L$ | AVG | 3.00 | 3.05 | 2.58 | 2.70 |
| | STD | 0.03 | 0.01 | 0.01 | 0.04 |
| | RSD (%) | 1.00 | 0.33 | 0.39 | 1.48 |
| $D_{T1}/L$ | AVG | 2.95 | 3.16 | 2.59 | 2.74 |
| | STD | 0.01 | 0.01 | 0.02 | 0.01 |
| | RSD (%) | 0.34 | 0.32 | 0.77 | 0.36 |
| $A_{D2}/L$ | AVG | – | – | 2.45 | 3.53 |
| | STD | – | – | 0.02 | 0.05 |
| | RSD (%) | – | – | 0.82 | 1.42 |
| $D_{T2}/L$ | AVG | – | – | 2.37 | 2.41 |
| | STD | – | – | 0.03 | 0.03 |
| | RSD (%) | – | – | 1.27 | 1.24 |

Table 2.7: Repeat test results: drifting indices in regular waves

| | | Waves | |
|---|---|---|---|
| | | $\delta = -35°$ | $\delta = +35°$ |
| $H_{D1}/L$ | AVG | 0.19 | 0.30 |
| | STD | 0.01 | 0.02 |
| | RSD (%) | 5.26 | 6.67 |
| $H_{D2}/L$ | AVG | 0.22 | 0.35 |
| | STD | 0.03 | 0.02 |
| | RSD (%) | 13.64 | 5.71 |
| $\mu_{D1}$ (°) | AVG | 52.56 | -83.92 |
| | STD | 5.73 | 8.91 |
| | RSD (%) | 10.90 | 10.62 |
| $\mu_{D2}$ (°) | AVG | 72.76 | -72.60 |
| | STD | 7.24 | 5.86 |
| | RSD (%) | 9.95 | 8.07 |

### 2.3.3 Time histories during turning

Figs.2.7 and 2.8 show comparison of time histories of speeds ($u$ and $v$) , yaw rate ($r$) and rudder normal force ($F_N$) during $\pm35°$ turning for KCS in calm water and regular waves. Approach speed is equivalent to 14.5 kn in full-scale for all. Since the approach speed is the same in calm water and waves, the propeller revolution in the waves becomes larger than that in calm water as shown in Table 2.3. Therefore, the propeller load in the waves is higher, and $F_N$ in the waves becomes larger than that in calm water generally. The results ($u$, $v$, $r$ and $F_N$) in regular waves are characterized by the addition of high-frequency fluctuation component due to wave-induced motions to the low-frequency component. Removing the high-frequency fluctuation component from the time history results, these become similar to the results in calm water. Namely, the ship motion in waves is expressed approximately as sum of low-frequency maneuvering motion and high-frequency wave-induced motion. This means that the base assumption employed in the two-time scale method[5][7][18] is valid.

## 2.4  Summary for turning tests in regular waves

From this chapter, the summary are the followings:

1.  Model tests were conducted in a square tank of National Research Institute of Fisheries Engineering, Japan by using KCS container ship as studied ship. The model tests with one approach speed $U_A = 14.5$ kn at full scale and rudder angle $\pm35°$ were performed in calm water first, followed by head waves at the time of approaching with wave amplitude $h_a = 0.024$ m and $\lambda/L = 1.0$ for regular waves.
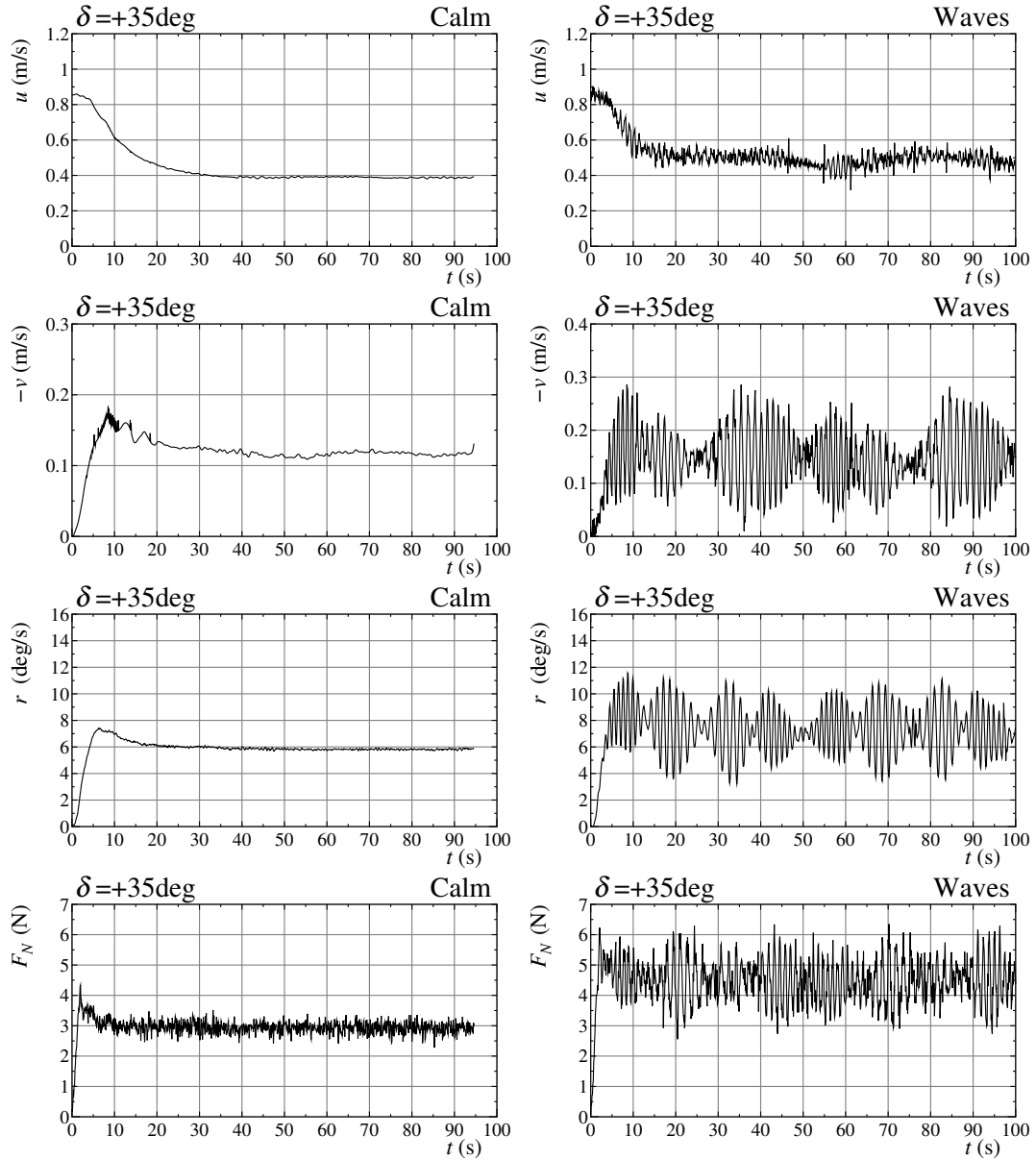
Fig. 2.7: Comparison of time histories during $+35°$ turning for KCS with $U_A = 14.5$ kn (left: calm water, right: regular waves)

2. Drifting indices that represent the effect of drifting during turning in waves consist of drifting distance $H_D$ and drifting direction $\mu_D$ are mainly used across the analysis in this study. The results of the repeat test of turning in calm water and regular waves from this chapter is crucial as a base for the turning test in irregular waves because irregular waves is a superposition of regular waves. The obtained results such as ship trajectories, turning indices, drifting indices and time histories motions from this chapter is important for the validation works for simulation method in chapter 4.
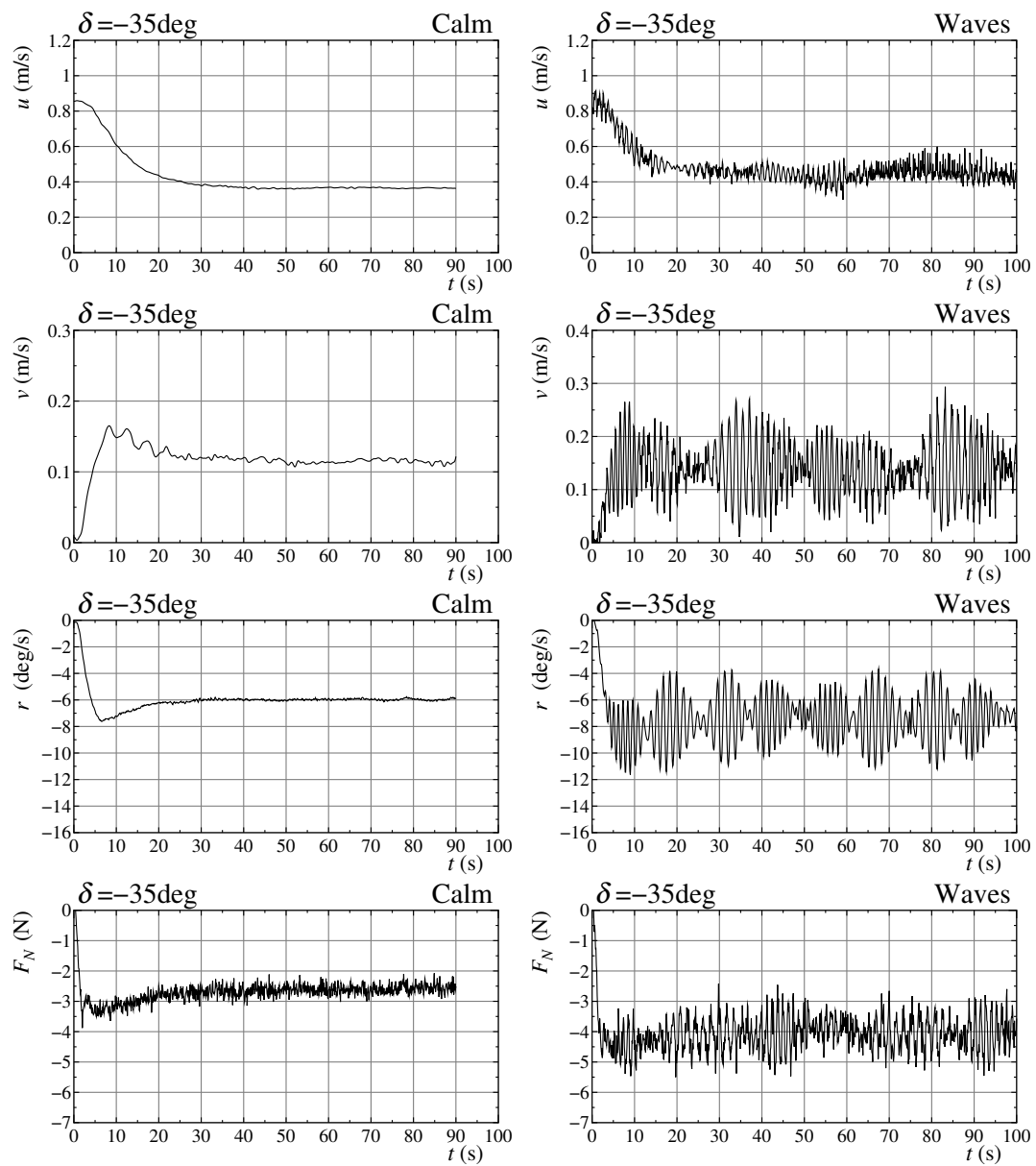
Fig. 2.8: Comparison of time histories during $-35°$ turning for KCS with $U_A = 14.5$ kn (left: calm water, right: regular waves)

# Chapter 3

# Turning tests in irregular waves

## 3.1 Studied ships

### 3.1.1 KVLCC2

Table 3.1 shows the principal particulars of the ship hull and propeller of KVLCC2 ship[24] on full- and model scale. The scale ratio of the ship model to the full-scale is 1:110. In the table, $L$ is length between perpendiculars, $B$ is the ship's breadth, $D$ is the ship's depth, $d$ is the ship's draft, $\nabla$ is displacement volume, $x_G$ is the coordinate in the length direction of the center of gravitation (ahead of midship is positive), and $C_b$ is the block coefficient. Furthermore, $\overline{GM}$ is the metacentric height, $\overline{KM}$ is the metacenter height above baseline, $Z$ is the number of propeller blades, $D_P$ is the propeller diameter, and $p$ is the propeller pitch ratio. Fig.3.1 shows the body plan of KVLCC2. Fig.3.2 shows the photograph of a ship model used in the tank tests. The full load condition is considered. Table 3.2 shows the rudder model for KVLCC2. In the table, $H_R$ is the rudder span length, $B_R$ is the average chord length of the rudder, and $A_R$ is the rudder area including the horn part. A mariner rudder was attached to this ship, but bilge keels were not installed.
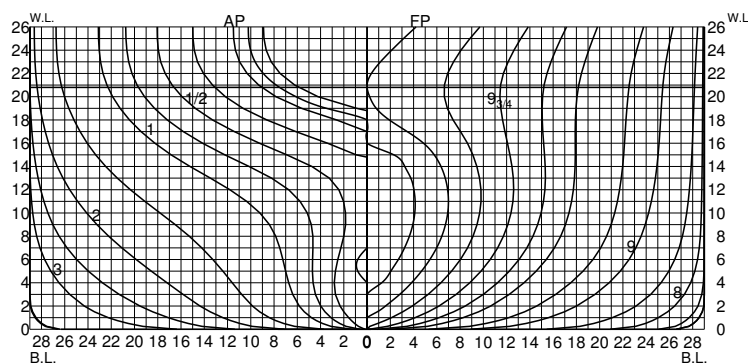


Fig. 3.1: Body plan of KVLCC2

Table 3.1: Principal particulars of KVLCC2

|  | full-scale | model |
|---|---|---|
| $L$ (m) | 320.0 | 2.909 |
| $B$ (m) | 58.0 | 0.527 |
| $D$ (m) | 26.0 | 0.236 |
| $d$ (m) | 20.8 | 0.189 |
| $\nabla$ (m$^3$) | 312600 | 0.235 |
| $x_G$ (m) | 11.1 | 0.101 |
| $C_b$ | 0.81 | 0.81 |
| $\overline{GM}$ (m) | 13.2 | 0.120 |
| $\overline{KM}$ (m) | 24.3 | 0.221 |
| $Z$ | 4 | 4 |
| $D_P$ (m) | 9.86 | 0.090 |
| $p$ | 0.721 | 0.721 |



Fig. 3.2: Side profile of a KVLCC2 model

Table 3.2: Rudder dimensions of KVLCC2

|  | full-scale | model | remarks |
|---|---|---|---|
| $H_R$ (m) | 15.80 | 0.144 | |
| $B_R$ (m) | 8.65 | 0.079 | including horn |
| $A_R$ (m$^2$) | 112.5 | 0.0093 | including horn area |

### 3.1.2  KCS

A KCS container ship model is used in this model test. The specification details was described in the chapter 2.

## 3.2 Test outline

Test outline almost similar with the test in regular waves. The coordinate system is identical with the coordinate system used in the regular waves model tests, thus is skipped in this sub-chapter.

### 3.2.1 Procedure

The ship model is launched at a certain approach speed by a catapult set at the tank shore of NRIFE and runs straight on $x_s$-axis using an autopilot. After reaching the target approach speed ($U_A$) and the target heading angle ($\psi_T = 0$), the model is steered by a radio controller for turning. Then, the midship position when the steering is started is defined as $(x_s, y_s) = (0,0)$. The steering rate is set to be equivalent to 2.32(°/s) for full-scale ships: 24.3(°/s) for KVLCC2, and 20.1(°/s) for KCS in the model tests. The propeller revolution is kept constant during the test, and the effect of torque-rich was not considered.

First, the RT was conducted for KVLCC2, in which the turning test of rudder angle ±35° was repeated five times in the exact same wave pattern. From the obtained test results, average values and standard deviations of turning indices (advance $A_D$ and tactical diameter $D_T$) and drifting indices in waves were obtained to ascertain the variation in test results.

Next, five waves were generated with different patterns on a time history basis, although the wave conditions (significant wave height, mean wave period, and main wave direction) were the same. Specifically, the wave pattern was changed by varying the phase between the elementary waves in the wave generation. Such a test is called the wave pattern variation test (WVT). From the obtained test results, the average values and standard deviations of the turning indices and the drifting indices in waves were obtained.

In the tests, the 3D position $(x_0, y_0, z_0)$ of a prism equipped to the midship of the model was measured by a total station system at NRIFE[28]. The heading angle ($\psi$), yaw rate ($r$), roll angle ($\phi$), rudder angle ($\delta$), rudder normal force ($F_N$) and propeller thrust ($T_P$) were measured in the tests using a three-axis gyro and dynamo-meters equipped on the model. However, it is skipped to present the measured results in detail. The radius of pitch gyration was set to $0.25L$ for both the KVLCC2 and KCS models.

### 3.2.2 Approach speeds and propeller revolutions

Table 3.3 shows combinations of the approach speed $U_A$ and propeller revolution $n_P$ for the turning tests. Three approach speeds were changed to capture the speed effect on the turning in waves. In the fastest speed case (15.5 kn in calm water) for KVLCC2, the propeller revolution (17.2 rps for model) was kept constant for calm water and irregular waves. Then, the approach speed became 13.0 kn in irregular waves owing to the added

resistance. For the medium and low speeds (10.0 kn and 5.0 kn), the approach speed was same in calm water and irregular waves. In three speeds (15.0 kn, 10.0 kn and 5.0 kn) for KCS, the approach speed was kept constant for calm water and irregular waves by adjusting the propeller revolution. The reason 15 kn was selected as the maximum speed for KCS in the test is because there was a possibility of water inflow into the ship model over the free-board due to excessive roll angle during turning in the service speed case 24 kn in the full-scale.

Table 3.3: Approach speed ($U_A$) and propeller revolution ($n_P$) in the tank tests

| KVLCC2 | Calm water | | | Irregular waves | | |
|---|---|---|---|---|---|---|
| $U_A$ in full-scale (kn) | 15.5 | 10.0 | 5.0 | 13.0 | 10.0 | 5.0 |
| $U_A$ in model (m/s) | 0.760 | 0.491 | 0.245 | 0.636 | 0.491 | 0.245 |
| $n_P$ in model (rps) | 17.2 | 11.6 | 6.0 | 17.2 | 14.0 | 8.3 |

| KCS | Calm water | | | Irregular waves | | |
|---|---|---|---|---|---|---|
| $U_A$ in full-scale (kn) | 15.0 | 10.0 | 5.0 | 15.0 | 10.0 | 5.0 |
| $U_A$ in model (m/s) | 0.890 | 0.593 | 0.290 | 0.890 | 0.593 | 0.297 |
| $n_P$ in model (rps) | 10.9 | 7.5 | 3.8 | 11.7 | 8.0 | 4.6 |

### 3.2.3 Wave conditions

The turning tests were conducted for short-crested irregular waves with the International Towing Tank Conference (ITTC) wave spectrum. The $\cos^4$-function distribution was employed as wave directional distribution. The average wave direction was set to be head waves in ship approaching ($\chi = 0°$). Table 3.4 shows target values of the significant wave height ($H_{1/3}$) and the average wave period ($T_0$) in the tests. About 40 mm of $H_{1/3}$ was selected for the tests.

Table 3.4: Target value of wave conditions in the tank test

| | KVLCC2 | | KCS | |
|---|---|---|---|---|
| | Full-scale | Model | Full-scale | Model |
| $H_{1/3}$ (m) | 4.5 | 0.041 | 3.0 | 0.040 |
| $T_0$ (s) | 10.5 | 1.00 | 7.8 | 0.90 |

### 3.2.4 Analysis: turning and drifting indices in waves

Turning indices such as advance $A_D$ and tactical diameter $D_T$ are used to characterize the turning. The definition of the indices was summarized as described in chapter 2.

## 3.3 Test results

### 3.3.1 Turning trajectories in calm water

In advance of the turning tests in irregular waves, turning tests in calm water were conducted. The turning trajectories are shown in Figs. 3.5 and 3.6 together with the test results in waves. Tables 3.5 and 3.6 show the non-dimensionalized turning indices $(A_D/L, D_T/L)$ for both KVLCC2 and KCS, respectively. For comparison, the non-dimensionalized drifting distance $H_{D1}/L$ during the turning-in calm water is shown in the tables. As expected, $H_{D1}/L$ is smaller for ship speeds for KVLCC2 and KCS. The shift during the turning is not significant in calm water.

Table 3.5: Test results: turning indices in calm water (KVLCC2)

|            | $\delta = -35°$ | | | $\delta = +35°$ | | |
| --- | --- | --- | --- | --- | --- | --- |
| $U_A$ (kn)  | 15.5 | 10.0 | 5.0  | 15.5 | 10.0 | 5.0  |
| $A_D/L$     | 2.99 | 2.90 | 2.73 | 3.11 | 2.96 | 2.77 |
| $D_T/L$     | 3.01 | 3.01 | 2.99 | 3.18 | 3.09 | 3.06 |
| $H_{D1}/L$  | 0.23 | 0.62 | –    | 0.31 | 0.22 | –    |

Table 3.6: Test results: turning indices in calm water (KCS)

|            | $\delta = -35°$ | | | $\delta = +35°$ | | |
| --- | --- | --- | --- | --- | --- | --- |
| $U_A$ (kn)  | 15.0 | 10.0 | 5.0  | 15.0 | 10.0 | 5.0  |
| $A_D/L$     | 2.87 | 2.91 | 2.72 | 3.06 | 2.89 | 2.90 |
| $D_T/L$     | 2.74 | 2.86 | 2.95 | 2.82 | 2.97 | 3.06 |
| $H_{D1}/L$  | 0.19 | 0.16 | 0.11 | 0.17 | 0.20 | 0.19 |

### 3.3.2 Wave measurement

The turning tests in WVT are conducted for five different wave patterns with same $H_{1/3}$ and $T_0$ for one steering and one approach speed condition. Therefore, 10 tests were conducted in case of $\delta = \pm35°$ turning for each of the three different approach speeds, and a total of 30 tests were carried out. Tables 3.7 and 3.8 show the measured wave conditions such as $H_{1/3}$ and $T_0$ in the turning tests for KVLCC2 and KCS models, respectively. In the tables, AVG denotes the average value, STD denotes the standard deviation, and RSD denotes the relative standard deviation, which is defined by (RSD $\equiv$ STD/AVG). The average values of the $H_{1/3}$ and $T_0$ are adequately close to the target wave conditions shown in Table 3.4. For all cases, the RSDs of the $H_{1/3}$ and $T_0$ are smaller than 8% for KVLCC2 and 5% for KCS.

As an example of the directional wave spectrum for short-crested irregular waves, analysis results of the frequency distribution $S(\omega)$ and the angular distribution function $D(\gamma)$

Table 3.7: Measured wave conditions in the turning tests (KVLCC2)

| $U_A$ (kn) | | 13.0 | 10.0 | 5.0 | all |
|---|---|---|---|---|---|
| $H_{1/3}$ (m) | AVG | 0.040 | 0.039 | 0.040 | 0.040 |
| | STD | 0.003 | 0.003 | 0.003 | 0.003 |
| | RSD (%) | 7.5 | 7.7 | 7.5 | 7.5 |
| $T_0$ (s) | AVG | 1.01 | 1.02 | 1.02 | 1.01 |
| | STD | 0.07 | 0.10 | 0.06 | 0.08 |
| | RSD (%) | 6.9 | 9.8 | 5.9 | 7.9 |

Table 3.8: Measured wave conditions in the turning tests (KCS)

| $U_A$ (kn) | | 15.0 | 10.0 | 5.0 | all |
|---|---|---|---|---|---|
| $H_{1/3}$ (m) | AVG | 0.041 | 0.042 | 0.041 | 0.041 |
| | STD | 0.001 | 0.002 | 0.002 | 0.002 |
| | RSD (%) | 2.4 | 4.8 | 4.9 | 4.9 |
| $T_0$ (s) | AVG | 0.89 | 0.90 | 0.91 | 0.90 |
| | STD | 0.03 | 0.03 | 0.03 | 0.03 |
| | RSD (%) | 3.4 | 3.3 | 3.3 | 3.3 |

are shown in Figs.3.3 and 3.4, respectively, under the conditions of $H_{1/3} = 40$ mm, $T_0 = 0.90$ s. The generated irregular waves were measured at a fixed point (12 m in front of the wave generators, 7m on the right side of the tank center line) in the tank using the wave height sensor array composed of three wave height probes. Using the time history data of the wave elevations, the directional wave spectrum was estimated by the Bayesian method proposed by Iseki and Ohtsu (1994)[27]. The frequency spectrum in the tank test is a little different from the target spectrum since the peak position is shifted to the lower frequency direction. The angular distribution function in the tank test is a narrow-band distribution that 0° waves are more remarkable than the target distribution expressing as $\cos^4$-function. Although the directional spectrum is a little different from the target, the significant wave height and the average wave period practically match the target values. There seems to be no problem in practical use.

### 3.3.3   Turning trajectories in waves: repeat test results

Fig.3.5 shows the comparison of the turning trajectories with $\delta = 35°$ in RT for the KVLCC2 model. For comparison, the trajectory in calm water is also plotted in the figure. The turning of the ship in the calm water enters the steady turning condition when the heading angle exceeds 180° and the circular motion continues as it is. In contrast, turning of a ship in irregular waves leads to the circular trajectory gradually shifting under the influence of the waves. For the first turn of the circular motion, the five trajectories are almost in agreement, but the difference becomes significant during the second turn. Slight variations in incoming waves and initial condition at the time of approaching create such differences.
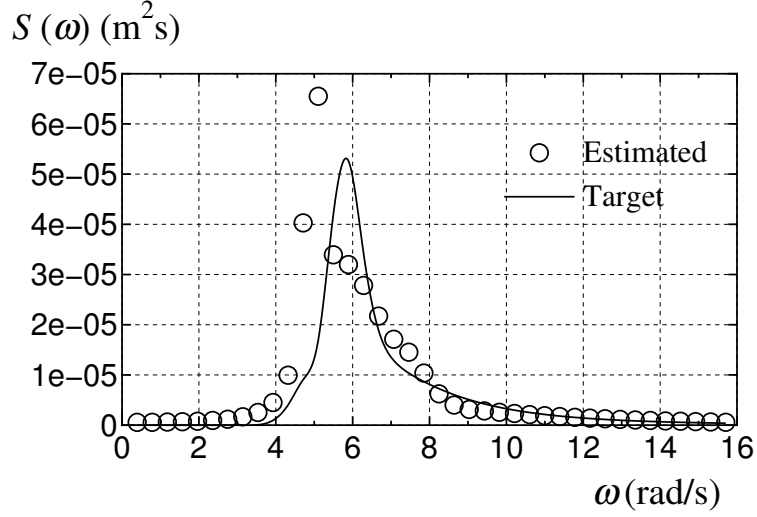
Fig. 3.3: Comparison of frequency spectrum $S(\omega)$ ($H_{1/3} = 0.040$ m, $T_0 = 0.90$ s)
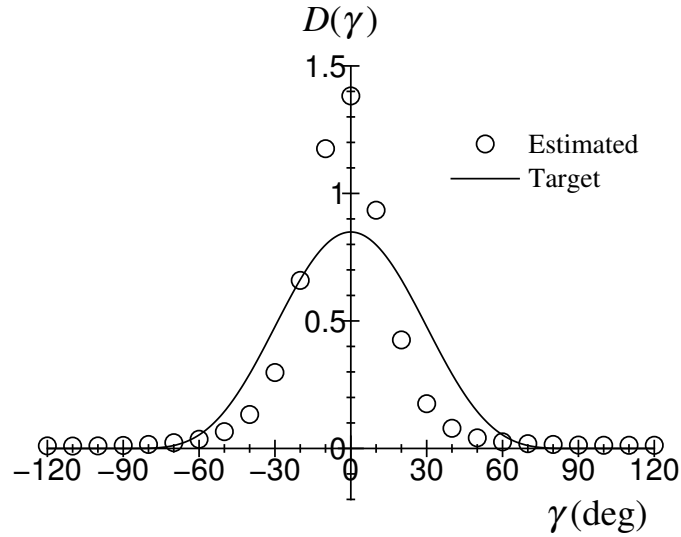


Fig. 3.4: Comparison of angular distribution function $D(\gamma)$ ($H_{1/3} = 0.040$ m, $T_0 = 0.90$ s)

Table 3.9 shows AVG, STD, and RSD of turning and drifting indices in RT. The average RSD of each RSD for the different approach speeds in $\delta = \pm 35°$ is also listed in the table. The average RSDs of $A_D/L$ and $D_T/L$ are smaller than RSD of the significant wave height of the irregular waves in the tests. The average RSD of $H_{D1}/L$ is larger than those of $A_D/L$ and $D_T/L$. This corresponds to the fact that the five trajectories are almost in agreement in the first turn of the circular motion, but the difference becomes larger in the second turn. The average RSD of $\mu_{D1}$ is remarkably large. This is because the AVG of $\mu_{D1}$ is often close to zero.
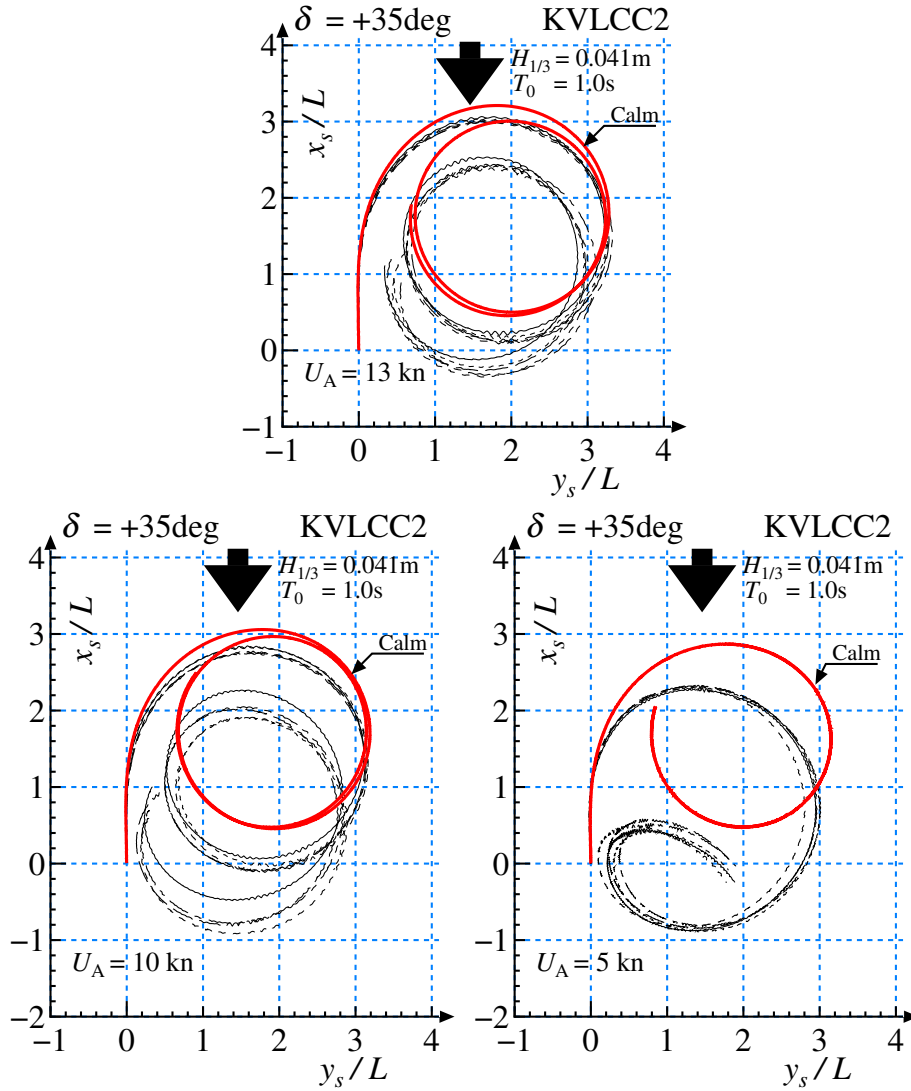
Fig. 3.5: RT results: turning trajectories with $\delta = 35°$ in irregular waves (KVLCC2)

### 3.3.4 Turning trajectories in waves: wave pattern variation test results

Fig.3.6 shows the comparison of turning trajectories with $\delta = 35°$ in WVT for KVLCC2 and KCS. The results of the five turning trajectories in the waves seem to have more variation than the results at RT. The turning circle in the waves distorts because the ship drifts in one direction due to the influence of the waves. Consequently, it does not become a circular trajectory like in the case of the calm water. The drifting direction is different from the incoming wave direction, and it becomes slightly oblique. This tendency is the same as the test results for regular waves by Ueno et al.[2] and Yasukawa[4]. $A_D/L$ in waves is smaller than that in calm water at all speeds. Particularly, when the approach speed is reduced, the ship drifts more remarkably as the influence of the waves is relatively large. For the same approach speed, KVLCC2 drifts more significantly than KCS. This may be because the damping force acting on the KCS with respect to the lateral motion

Table 3.9: RT results: turning and drifting indices for irregular waves (KVLCC2)

| $U_A$ (kn) | | $\delta = -35°$ | | | $\delta = +35°$ | | | Ave. |
|---|---|---|---|---|---|---|---|---|
| | | 13.0 | 10.0 | 5.0 | 13.0 | 10.0 | 5.0 | |
| $A_D/L$ | AVG | 2.86 | 2.69 | 2.29 | 2.95 | 2.72 | 2.27 | |
| | STD | 0.05 | 0.02 | 0.05 | 0.02 | 0.02 | 0.03 | |
| | RSD (%) | 1.7 | 0.7 | 2.2 | 0.7 | 0.7 | 1.3 | 1.2 |
| $D_T/L$ | AVG | 2.99 | 2.98 | 2.68 | 3.18 | 3.04 | 2.86 | |
| | STD | 0.06 | 0.06 | 0.08 | 0.03 | 0.05 | 0.09 | |
| | RSD (%) | 2.0 | 2.0 | 3.0 | 0.9 | 1.6 | 3.1 | 2.1 |
| $H_{D1}/L$ | AVG | 0.56 | 0.72 | 1.63 | 0.58 | 0.73 | 1.84 | |
| | STD | 0.05 | 0.05 | 0.15 | 0.04 | 0.12 | 0.05 | |
| | RSD (%) | 8.9 | 6.9 | 9.2 | 6.9 | 16.4 | 2.7 | 8.5 |
| $\mu_{D1}$ (°) | AVG | -3.28 | 1.06 | 11.4 | 5.97 | -1.11 | -12.9 | |
| | STD | 10.6 | 7.04 | 4.58 | 5.93 | 6.27 | 1.68 | |
| | RSD (%) | 323 | 664 | 40 | 99 | 564 | 13 | 284 |

is larger than that on the KVLCC2.

Tables 3.10 and 3.11 show AVG, STD, and RSD of turning and drifting indices for KVLCC2 and KCS, respectively. For KVLCC2, the AVGs of $A_D/L$, $D_T/L$ and $H_{D1}/L$ are slightly different from the values at RT shown in Table 3.9. Moreover, the average RSD of $A_D/L$ is 2.5 % in WVT (1.2 % in RT), that of $D_T/L$ is 2.3 % in WVT (2.1 % in RT), and that of $H_{D1}/L$ is 9.3 % in WVT (8.5 % in RT). The average RSDs in WVT become larger than those in RT. This may come from the influence of the slowly varying second-order wave forces. However, the influence is insignificant. The average RSDs of $A_D/L$, $D_T/L$ and $H_{D1}/L$ for KCS are of the same order as those for KVLCC2. The order of magnitude of AVGs of $H_{D1}/L$ and $H_{D2}/L$ is almost the same, although the average RSD of $H_{D2}/L$ is slightly larger than that of $H_{D1}/L$. This tendency is roughly the same for $\mu_{D1}$ and $\mu_{D2}$.

Fig.3.7 shows the comparison of the turning and drifting indices in irregular waves for KVLCC2 and KCS to capture the effect of the approach speed $U_A$. With a decrease in $U_A$, $A_D/L$ decreases, and $D_T/L$ decreases slightly for KVLCC2 and does not change very much for KCS. This tendency is the same as the test result for regular waves by Sanada et al.[10]. Generally, as the approach speed decreases, the influence of the waves becomes relatively larger in the same irregular wave condition. The tank tests were conducted for the head wave condition at the time of approaching. Then, the waves are significantly influenced on $A_D/L$, which is the longitudinal distance during turning. In contrast, as $D_T/L$ denotes the lateral distance during turning, the wave effect on it is relatively small. This implies that the effect of the approach speed on the turning indices depends on the wave direction.

$H_{D2}$ is almost the same with $H_{D1}$, and they increase significantly with decrease in $U_A$ for KCS. As $U_A$ is reduced in the same irregular wave condition, the influence of the waves becomes relatively larger and the drifting distances $H_{D1}$ and $H_{D2}$ increase. $\mu_{D1}$ and $\mu_{D2}$

also increase significantly with a decrease in $U_A$, and the tendency of the ship drifting to the location $(x_s, y_s) = (0, 0)$ of rudder executing point becomes more remarkable.

### 3.3.5 Time histories during turning

Fig.3.8 shows comparison of time histories of speed drop ($U/U_A$), non-dimensional yaw rate ($r' = rL/U_A$), rudder normal force coefficient ($F_N' = F_N/(0.5\rho L d U_A^2)$) and roll angle ($\phi$) during $+35°$ turning for KVLCC2 in calm water and irregular waves. Fig.3.9 also shows comparison of time histories of $U/U_A$, $r'$, $F_N'$ and $\phi$ during $+35°$ turning for KCS. The shown time histories in the irregular waves results are called as "Species 1" for each ship.

Approach speed is equivalent to 10 kn in full-scale for all. Since the approach speed is the same in calm water and waves, the propeller revolution in the waves becomes larger than that in calm water as shown in Table 3.3. Therefore, the propeller load in the waves is higher, and $F_N'$ in the waves becomes larger than that in calm water generally.

The results ($U/U_A$, $r'$, and $F_N'$) in irregular waves are characterized by the addition of high-frequency fluctuation component due to wave-induced motions to the low-frequency component. Removing the high-frequency fluctuation component from the time history results, these become similar to the results in calm water. Namely, the ship motion in waves is expressed approximately as sum of low-frequency maneuvering motion and high-frequency wave-induced motion. This means that the base assumption employed in the two-time scale method[5][7][18] is valid.

In calm water, $\phi$ of KVLCC2 is almost zero since the ship sheed is low and $\overline{GM}$ is large. In the waves, the absolute value of $\phi$ increases at time $t$ when the heading angle is $90°$, $180°$, and $270°$. On the other hand, for KCS, a typical heel change during turning appears in calm water: appearance of inward heel just after steering and change to outward heel[25]. (In the figures of $\phi$, plus value is the inward heel, and minus value is the outward heel.) In waves, the roll period is relatively long, which is different from the tendency of KVLCC2. This comes from significantly different rolling characteristics in beam waves between KCS and KVLCC2.

## 3.4 Summary for turning tests in irregular waves

Our study investigated the turning behavior of ships in short-crested irregular waves using free-running model tests. Two types of ship were selected for the investigation: a KVLCC2 large tanker and a KCS container ship. The tests were performed in head waves at the time of approaching with the significant wave height 4.5 m and 3.0 m for KVLCC2 and KCS respectively. First, a repeat test was conducted for KVLCC2, in which the turning test of rudder angle $\pm 35°$ was repeated five times for the same wave pattern. Next, five waves with different patterns were generated with the same wave conditions (significant wave height, mean wave period, and main wave direction). Turning tests were conducted

for KVLCC2 and KCS in these waves. From the obtained test results, the average values and standard deviations of turning indices (advance $A_D$ and tactical diameter $D_T$), and drifting indices in waves (drifting distance $H_D$ and drifting direction $\mu_D$) were obtained. As a result, the following conclusions are obtained:

1. With a decrease in the approach speed $U_A$ of the ships running in the same wave condition, $A_D$ decreases and $D_T$ does not change significantly. For the head wave condition in approaching, the wave effect on $A_D$, which is the longitudinal distance during turning, is significant. In contrast, the wave effect on $D_T$ is relatively small as it signifies the lateral distance during turning.

2. When reducing $U_A$ in the same wave condition, the drifting distance $H_D$ increases as the influence of the waves on the ships becomes relatively larger. The drifting direction $\mu_D$ also increases with decrease in $U_A$, and the tendency of the ship to drift towards the location $(x_s, y_s) = (0, 0)$ of rudder executing point becomes more remarkable. Thus, $\mu_D$ depends on $U_A$, even though the reason for this change is unclear. The analytical study is performed in chapter 6 to further understand this phenomena.

3. Based on the results of $U/U_A$, $r'$, and $F'_N$ in irregular waves, the ship motion in waves is expressed approximately as sum of low-frequency maneuvering motion and high-frequency wave-induced motion. Removing the high-frequency fluctuation component from the time history results, these become similar to the results in calm water. This means that the base assumption employed in the two-time scale method[5][7][18] is valid.

4. A variation in turning trajectories was observed. This may have resulted from the influence of the slowly varying second-order wave forces acting on the ship models. However, the influence on the trajectories is negligible in view of practical purposes. This confirms the only mean value for estimation of wave-induced steady forces is sufficient for a two-time scale simulation[5][7].

5. The experimental data shown in this chapter is useful for the validation of the simulation method of ship maneuvering in irregular waves in the next chapter 5.
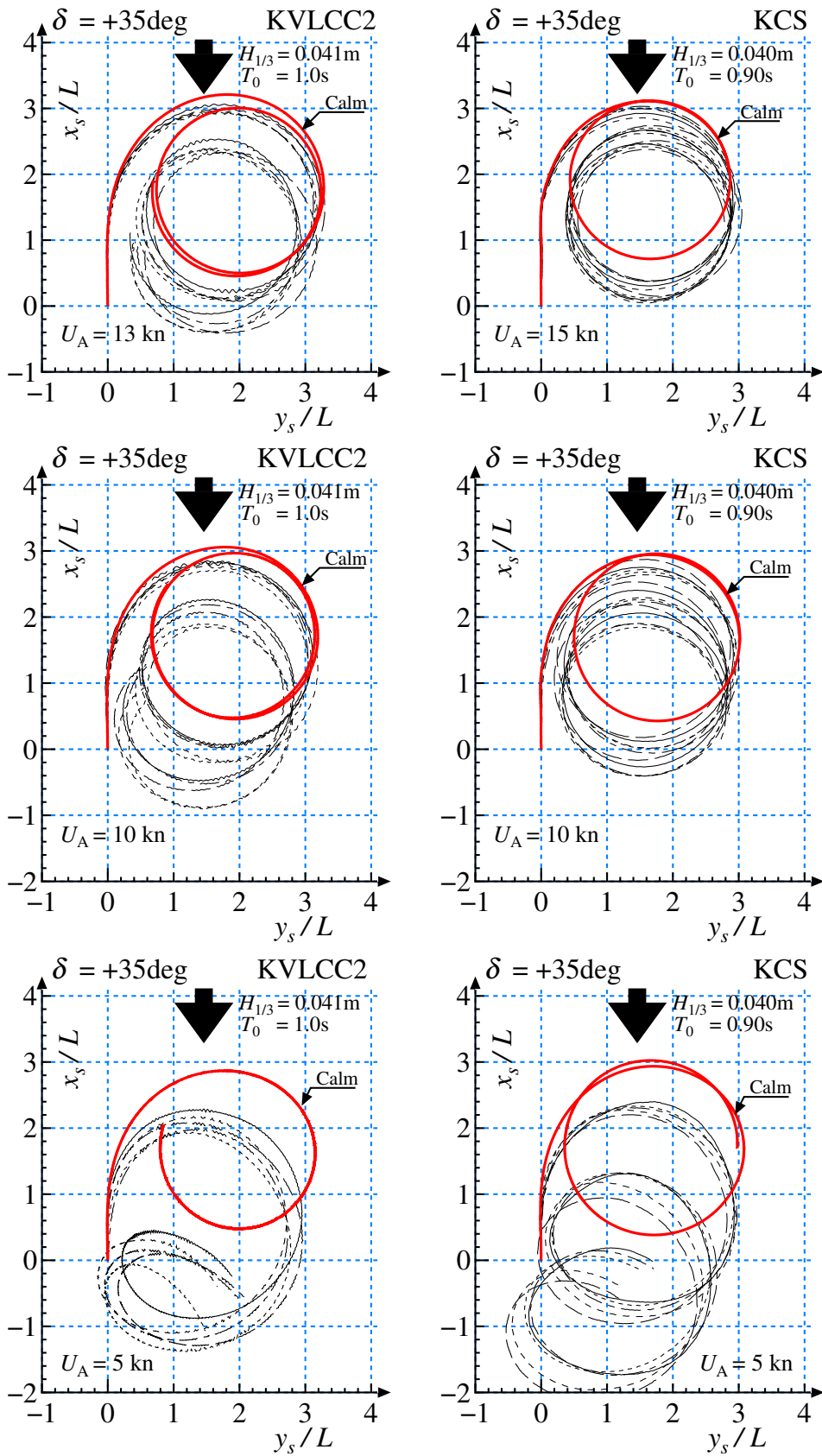
Fig. 3.6: WVT results: turning trajectories with $\delta = 35°$ in irregular waves for KVLCC2 and KCS

Table 3.10: WVT results: turning and drifting indices in irregular waves (KVLCC2)

| | | $\delta = -35°$ | | | $\delta = +35°$ | | | |
|---|---|---|---|---|---|---|---|---|
| $U_A$ (kn) | | 13.0 | 10.0 | 5.0 | 13.0 | 10.0 | 5.0 | Ave. |
| $A_D/L$ | AVG | 2.74 | 2.66 | 2.18 | 2.90 | 2.72 | 2.07 | |
| | STD | 0.05 | 0.06 | 0.05 | 0.05 | 0.03 | 0.11 | |
| | RSD (%) | 1.8 | 2.3 | 2.3 | 1.7 | 1.1 | 5.3 | 2.5 |
| $D_T/L$ | AVG | 3.01 | 2.94 | 2.56 | 3.09 | 3.01 | 2.76 | |
| | STD | 0.05 | 0.04 | 0.08 | 0.06 | 0.06 | 0.10 | |
| | RSD (%) | 1.7 | 1.4 | 3.1 | 1.9 | 2.0 | 3.6 | 2.3 |
| $H_{D1}/L$ | AVG | 0.57 | 0.70 | 1.71 | 0.60 | 0.73 | 1.98 | |
| | STD | 0.05 | 0.03 | 0.16 | 0.07 | 0.12 | 0.10 | |
| | RSD (%) | 8.8 | 4.3 | 9.4 | 11.7 | 16.4 | 5.1 | 9.3 |
| $\mu_{D1}$ (°) | AVG | -7.16 | -0.92 | 13.5 | 0.37 | -3.97 | -15.7 | |
| | STD | 3.72 | 8.95 | 4.68 | 9.37 | 5.33 | 3.55 | |
| | RSD (%) | 52 | 973 | 35 | 2532 | 134 | 23 | 625 |

Table 3.11: Wave pattern variation test results: Turning and drifting indices in irregular waves (KCS)

| | | $\delta = -35°$ | | | $\delta = +35°$ | | | |
|---|---|---|---|---|---|---|---|---|
| $U_A$ (kn) | | 15.0 | 10.0 | 5.0 | 15.0 | 10.0 | 5.0 | Ave. |
| $A_D/L$ | AVG | 2.85 | 2.61 | 2.22 | 2.92 | 2.69 | 2.28 | |
| | STD | 0.16 | 0.03 | 0.05 | 0.07 | 0.08 | 0.06 | |
| | RSD (%) | 5.6 | 1.1 | 2.3 | 2.4 | 3.0 | 2.6 | 2.8 |
| $D_T/L$ | AVG | 2.77 | 2.78 | 2.70 | 2.85 | 2.89 | 2.88 | |
| | STD | 0.03 | 0.05 | 0.07 | 0.02 | 0.04 | 0.05 | |
| | RSD (%) | 1.1 | 1.8 | 2.6 | 0.7 | 1.4 | 1.7 | 1.5 |
| $H_{D1}/L$ | AVG | 0.36 | 0.39 | 1.08 | 0.31 | 0.38 | 1.11 | |
| | STD | 0.04 | 0.07 | 0.06 | 0.04 | 0.04 | 0.11 | |
| | RSD (%) | 11.1 | 17.9 | 5.6 | 12.9 | 10.5 | 9.9 | 11.3 |
| $H_{D2}/L$ | AVG | 0.25 | 0.37 | 1.18 | 0.23 | 0.37 | 1.28 | |
| | STD | 0.07 | 0.07 | 0.12 | 0.03 | 0.03 | 0.09 | |
| | RSD (%) | 28.0 | 18.9 | 10.2 | 13.0 | 8.1 | 7.0 | 14.2 |
| $\mu_{D1}$ (°) | AVG | -29.7 | -3.47 | 8.69 | 28.0 | -1.40 | -12.7 | |
| | STD | 2.19 | 8.45 | 3.04 | 4.65 | 3.41 | 2.28 | |
| | RSD (%) | 7.4 | 244 | 35 | 17 | 244 | 18 | 94 |
| $\mu_{D2}$ (°) | AVG | -6.36 | 12.8 | 13.3 | 4.99 | -7.33 | -16.8 | |
| | STD | 10.7 | 6.29 | 5.46 | 11.5 | 6.62 | 2.85 | |
| | RSD (%) | 168 | 49 | 41 | 230 | 90 | 17 | 99 |
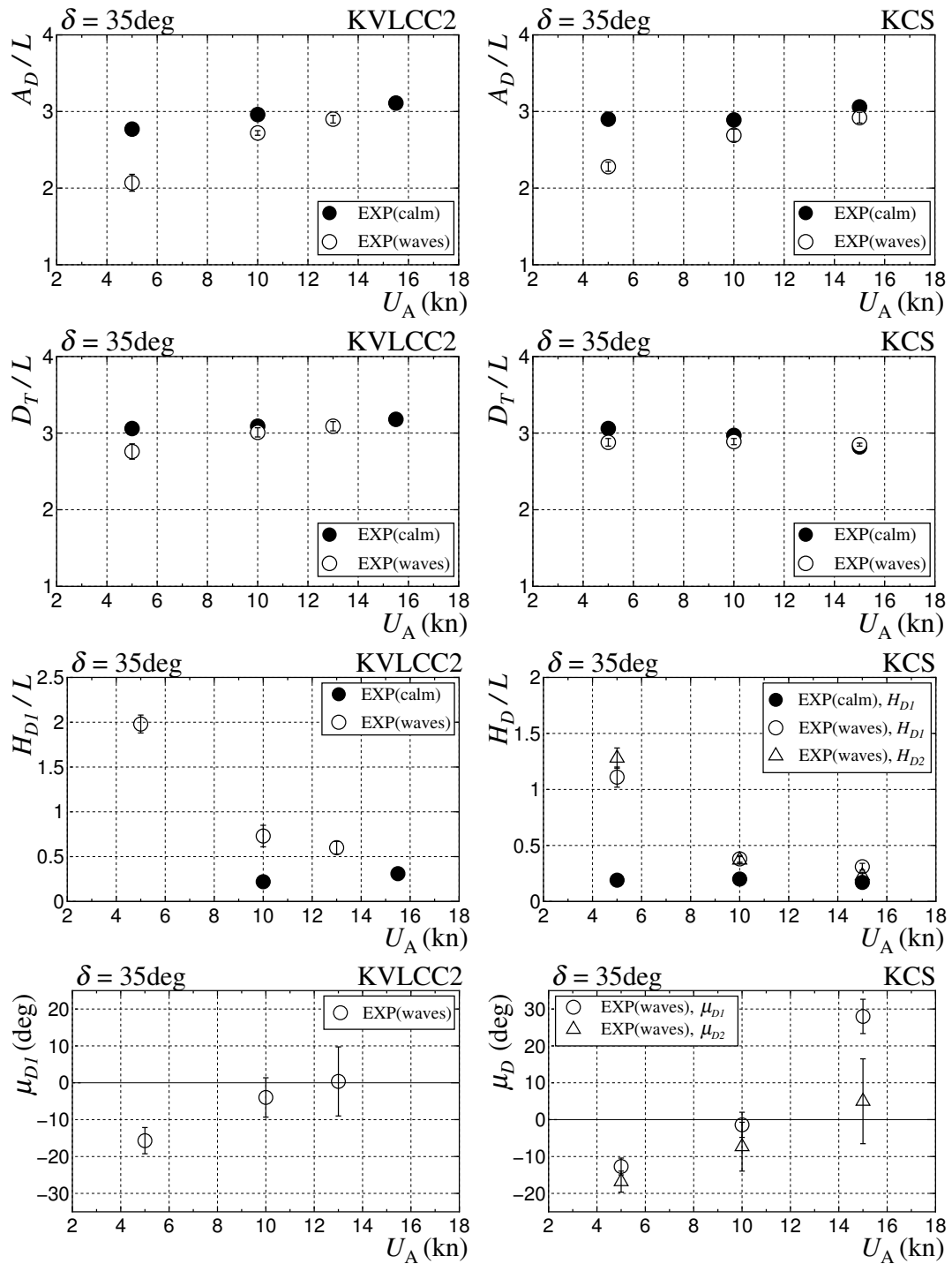
Fig. 3.7: Approach speed effect on turning and drifting indices in irregular waves for KVLCC2 and KCS
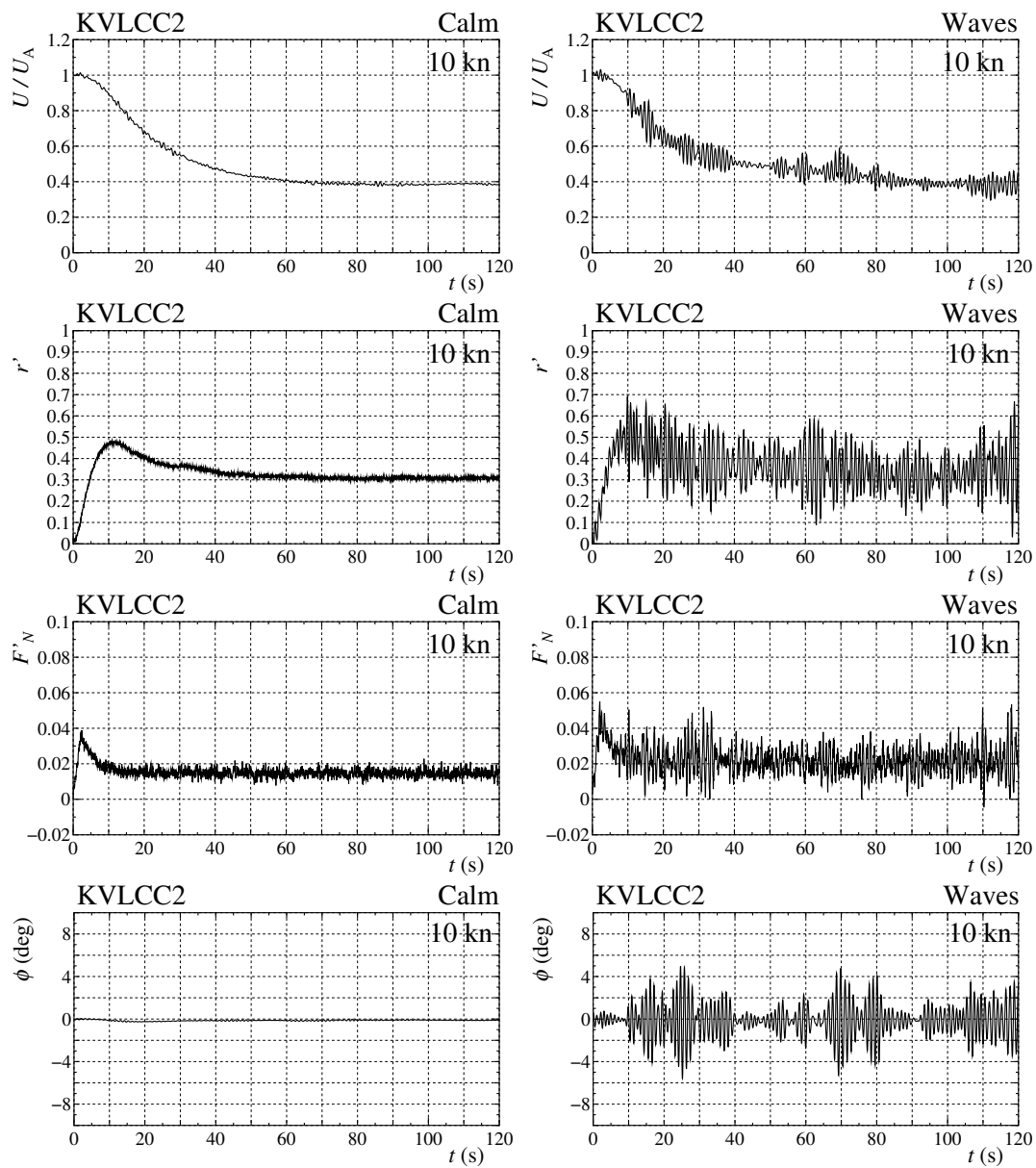
Fig. 3.8: Comparison of time histories during $+35°$ turning for KVLCC2 with $U_A = 10$ kn (left: calm water, right: irregular waves)
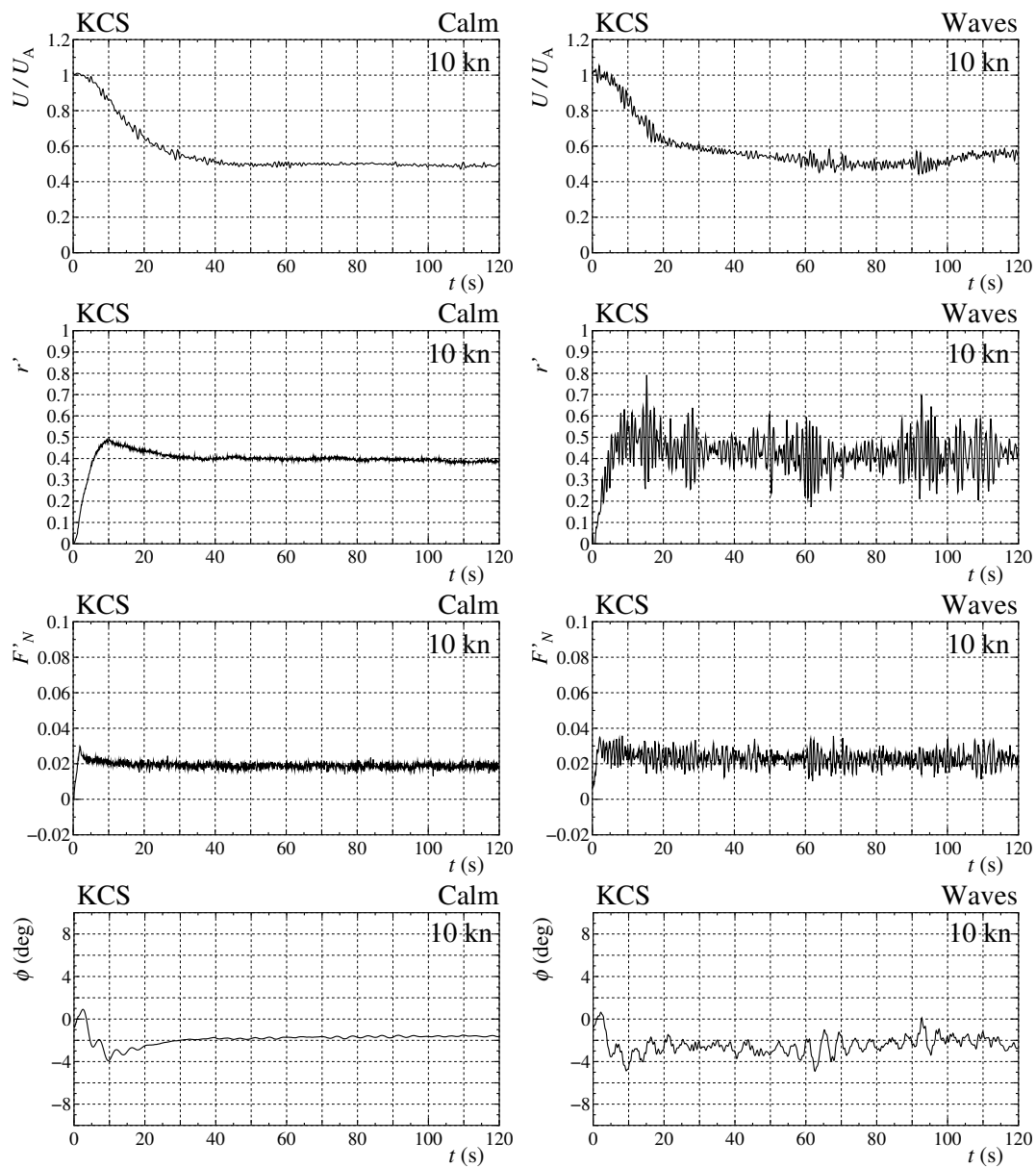
Fig. 3.9: Comparison of time histories during $+35°$ turning for KCS with $U_A = 10$ kn (left: calm water, right: irregular waves)

# Chapter 4

# Turning simulation of a ship in regular waves

## 4.1  Studied Ship

A KCS container ship model is used in this simulation. The specification details was described in the chapter 2.

## 4.2  6-DOF motion simulation method of a ship maneuvering in regular waves

## 4.3  Coordinate systems and notations

Fig. 4.1 shows two coordinate systems used in the simulation: firstly is a space-fixed coordinate system $o_s - x_s y_s z_s$, and secondly the moving ship-fixed coordinate system which located in average position of wave-induced motions and moving with the maneuvering motion of the ship $o - xyz$. The $x_s - y_s$ and $x - y$ planes coincide with the still water surface. The $z$-axis passes through the ship's center of gravity $G$ and points vertically downward. Then, these two coordinate systems have following relations:

$$\left. \begin{array}{rcl} x_s &=& x\cos\psi_0(t) - y\sin\psi_0(t) + x_0(t) \\ y_s &=& x\sin\psi_0(t) + y\cos\psi_0(t) + y_0(t) \\ z_s &=& z \end{array} \right\} \tag{4.1}$$

where $(x_0(t),\, y_0(t))$ and $\psi_0(t)$ mean the average horizontal position and heading angle of the maneuvering ship, respectively, whereby $t$ is time. In the figure, $U$ is the ship speed and $\beta$ the hull drift angle. The wave propagation direction is defined as an angle against $x_s$-axis by $\chi$. The similar coordinate is used in the free-running tests.
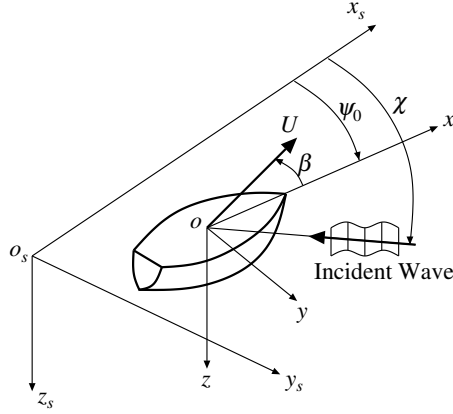
Fig. 4.1: Coordinate systems and notations

Additionally, a coordinate system fixed to the ship namely the Horizontal Body Axes System (HBA system) $o' - x'y'z'$ is defined according to Hamamoto and Kim[14][15]. The moving coordinate system $o - xyz$ is fixed to the ship at average position of wave-induced motions, however, the HBA system $o' - x'y'z'$, only $x'$-axis is fixed to the ship and $z'$-axis takes vertically.

## 4.4 Base motion equations

Next, this study consider base motion equations. Ship motion is assumed to be expressed as the sum of the maneuvering motion regarded as low frequency motion and wave-induced motion regarded as high frequency motion, according to the concept of the two-time scale method by Yasukawa[5].

### 4.4.1 Low-frequency maneuvering motions

Ship maneuvering motion is very slow relatively compared with wave-induced motion. The motion equations for low frequency motion are expressed at midship based on HBA system as described in Yasukawa et al.[35]:

$$
\left.
\begin{aligned}
(m + m_x)\dot{u}_0 - (m + m_y)v_0 r_0 - m x_G r_0^2 + m z_G r_0 \dot{\phi}_0 &= X \\
(m + m_y)\dot{v}_0 + (m + m_x)u_0 r_0 + x_G m \dot{r}_0 - (m_y \alpha_z + m z_G)\ddot{\phi}_0 &= Y \\
(I_{zz} + J_{zz} + m x_G^2)\dot{r}_0 + m x_G(\dot{v}_0 - z_G \ddot{\phi}_0 + u_0 r_0) &= N \\
(I_{xx} + J_{xx} + m z_G^2)\ddot{\phi}_0 - (m_y \alpha_z + m z_G)\dot{v}_0 - m z_G(x_G \dot{r}_0 + u_0 r_0) &= K
\end{aligned}
\right\}
\tag{4.2}
$$

where $m$ is ship's mass, and $I_{xx}$ are $I_{zz}$ the moment of inertias for roll and yaw, respectively. $m_x$, $m_y$, $J_{xx}$, and $J_{zz}$ are terms of added mass. $\alpha_z$ is the acting vertical height of $m_y$. $x_G$ is the coordinate in the length direction of the center of gravitation (ahead of midship is positive), and $z_G$ is the vertical coordinate of the center of gravitation. The dot notation

33

is an ordinary differentiation with respect to time. $u_0$ and $v_0$ are longitudinal and lateral velocities for the low frequency motion, respectively. $r_0$ is yaw rate and $\phi_0$ is heel angle. $u_0$, $v_0$, $r_0$, and $\phi_0$ are unknown variables in eq.(4.2).

$X$ is the longitudinal force, $Y$ is the lateral force, $N$ is the yaw moment about the midship, and $K$ is the roll moment about the $x'$-axis. They are represented by the following form:

$$\left.\begin{array}{rcl} X & = & X_H + X_R + X_P + X_W \\ Y & = & Y_H + Y_R + Y_W \\ N & = & N_H + N_R + N_W \\ K & = & -Y_H z_H - Y_R z_R - Y_W z_W - mg\overline{GM}\phi_0 + K_{\dot{\phi}}\dot{\phi}_0 + K_{\dot{\phi}\dot{\phi}}\dot{\phi}_0|\dot{\phi}_0| \end{array}\right\} \quad (4.3)$$

The subscripts $H, R, P$ and $W$ mean hull, rudder, propeller and wave-induced steady forces, respectively. The forces with subscript $H$, $R$ and $P$ are predicted by the MMG method by Yasukawa et al.[35] and Yasukawa and Yoshimura[29]. $z_H$ is the vertical acting point of the hull lateral force $Y_H$, $z_R$ is the vertical acting point of the rudder lateral force $Y_R$, and $z_W$ is the vertical acting point of the wave-induced lateral force $Y_W$. $\overline{GM}$ is the metacentric height, and $K_{\dot{\phi}}$ and $K_{\dot{\phi}\dot{\phi}}$ are the roll damping coefficients.

Here, only the terms with $H$ and $W$ are specifically shown. Hydrodynamic forces acting on the ship hull ($X_H$, $Y_H$, $N_H$) are expressed as follows:

$$\left.\begin{array}{rcl} X_H & = & (1/2)\rho L d U_0^2 \; X_H'(v_0', r_0', \phi_0) \\ Y_H & = & (1/2)\rho L d U_0^2 \; Y_H'(v_0', r_0', \phi_0) \\ N_H & = & (1/2)\rho L^2 d U_0^2 \; N_H'(v_0', r_0', \phi_0) \end{array}\right\} \quad (4.4)$$

where $\rho$ is the water density, $L$ is ship length between perpendiculars, $d$ is ship draft and $U_0$ is the ship speed defined by $\sqrt{u_0^2 + v_0^2})$. $v_0'$ is the non-dimensionalized lateral velocity defined by $v_0' / U_0$, and $r_0'$ is the non-dimensinoalized yaw rate defined by $r_0'L / U_0$. Here, $X_H'$, $Y_H'$ and $N_H'$ are expressed as follows:

$$\left.\begin{array}{l} X_H'(v_0', r_0', \phi_0) = -R_0' + X_{vv}'v_0'^2 + X_{vr}'v_0'r_0' + X_{rr}'r_0'^2 + X_{vvvv}'v_0'^4 + X_{v\phi}'v_0'\phi_0 \\ \qquad\qquad\qquad +X_{r\phi}'r_0'\phi_0 + X_{\phi\phi}'\phi_0^2 \end{array}\right\} \quad (4.5)$$

$$\left.\begin{array}{l} Y_H'(v_0', r_0', \phi_0) = Y_v'v_0' + Y_r'r_0' + Y_{vvv}'v_0'^3 + Y_{vvr}'v_0'^2r_0' + Y_{vrr}'v_0'r_0'^2 + Y_{rrr}'r_0'^3 \\ \qquad\qquad\qquad +Y_\phi'\phi_0 + Y_{vv\phi}'v_0'^2\phi_0 + Y_{v\phi\phi}'v_0'\phi_0^2 + Y_{rr\phi}'r_0'^2\phi_0 + Y_{r\phi\phi}'r_0'\phi_0^2 \end{array}\right\} \quad (4.6)$$

$$\left.\begin{array}{l} N_H'(v_0', r_0', \phi_0) = N_v'v_0' + N_r'r_0' + N_{vvv}'v_0'^3 + N_{vvr}'v_0'^2r_0' + N_{vrr}'v_0'r_0'^2 + N_{rrr}'r_0'^3 \\ \qquad\qquad\qquad +N_\phi'\phi_0 + N_{vv\phi}'v_0'^2\phi_0 + N_{v\phi\phi}'v_0'\phi_0^2 + N_{rr\phi}'r_0'^2\phi_0 + N_{r\phi\phi}'r_0'\phi_0^2 \end{array}\right\} \quad (4.7)$$

In eq.(4.5), $R_0'$ is the resistance coefficient in straight moving, and $X_{vv}'$, $Y_v'$ and $N_v'$, and so on are the hydrodynamic derivatives on maneuvering. Additionally, $X_H'$ is expressed

as the sum of $R'_0$ and $2^{nd}$ order polynomial function of $v'_0, r'_0$ and $\phi_0$ except for the $X_{vvvv}$-term, and $Y'_H$ and $N'_H$ are expressed as $1^{st}$ and $3^{rd}$ order polynomial functions of $v'_0, r'_0$ and $\phi_0$.

In regular waves, the wave-induced steady forces, $X_W$, $Y_W$ and $N_W$, are expressed as:

$$\left.\begin{array}{rcl} X_W & = & \rho g h_a^2 L\ C_{XW}(U_0, \lambda/L, \chi_0) \\ Y_W & = & \rho g h_a^2 L\ C_{YW}(\lambda/L, \chi_0) \\ N_W & = & \rho g h_a^2 L^2\ C_{NW}(\lambda/L, \chi_0) \end{array}\right\} \tag{4.8}$$

where $h_a$ is the incident wave amplitude. $X_W$ is expressed as the function of the ship speed $U_0$, the wave-length $\lambda$ of the incident waves and the relative main wave direction $\chi_0 (= \chi - \psi_0)$. $Y_W$ and $N_W$ are assumed to be no-relation with $U_0$. $C_{XW}$, $C_{YW}$ and $C_{NW}$ are the wave-induced steady force coefficients in regular waves, and are estimated by the theoretical methods such as strip method and/or zero speed 3D panel method as described in Yasukawa et al.[34].

## 4.4.2   High-frequency wave-induced motions

Using $\xi_1$, $\eta_1$ and $\zeta_1$ (surge, sway, heave) as the wave-induced motion components, $\phi_1$, $\theta_1$ and $\psi_1$ (roll, pitch, yaw) as the wave-induced angular motion components defined on the $o - xyz$ coordinate system, the motion equations for the high frequency motions are expressed as:

$$\left.\begin{array}{rcl} m\ddot{\xi}_1 + C_{11}\xi_1 & = & E_1 \\ (m + A_{22})\ddot{\eta}_1 + B_{22}\dot{\eta}_1 + C_{22}\eta_1 + A_{24}\ddot{\phi}_1 + B_{24}\dot{\phi}_1 + C_{24}\phi_1 + A_{26}\ddot{\psi}_1 + B_{26}\dot{\psi}_1 & = & E_2 \\ (m + A_{33})\ddot{\zeta}_1 + B_{33}\dot{\zeta}_1 + C_{33}\zeta_1 + A_{35}\ddot{\theta}_1 + B_{35}\dot{\theta}_1 + C_{35}\theta_1 & = & E_3 \\ (I_{xx} + A_{44})\ddot{\phi}_1 + B_{44}\dot{\phi}_1 + C_{44}\phi_1 + A_{42}\ddot{\eta}_1 + B_{42}\dot{\eta}_1 + C_{42}\eta_1 + A_{46}\ddot{\psi}_1 + B_{46}\dot{\psi}_1 & = & E_4 \\ (I_{yy} + A_{55})\ddot{\theta}_1 + B_{55}\dot{\theta}_1 + C_{55}\theta_1 + A_{53}\ddot{\zeta}_1 + B_{53}\dot{\zeta}_1 + C_{53}\zeta_1 & = & E_5 \\ (I_{zz} + A_{66})\ddot{\psi}_1 + B_{66}\dot{\psi}_1 + C_{66}\psi_1 + A_{64}\ddot{\phi}_1 + B_{64}\dot{\phi}_1 + A_{62}\ddot{\eta}_1 + B_{62}\dot{\eta}_1 & = & E_6 \end{array}\right\} \tag{4.9}$$

where $A_{ij}$, $B_{ij}$ and $C_{ij}$ denote added mass, wave damping coefficient, and restoring force coefficient with respect to the $i$-th force induced by motion of the $j$-th mode, respectively. $E_j$ is wave exciting force of $j$-th mode as follows:

$$E_j(t) = F_{jc}(\omega_e)\cos(\omega t + \varepsilon) - F_{js}(\omega_e)\sin(\omega t + \varepsilon) \tag{4.10}$$

The encounter frequency of the wave $\omega_e$ and phase $\varepsilon$ are expressed as:

$$\omega_e = \omega + \nu\left(\dot{x}_0\cos\chi + \dot{y}_0\sin\chi\right) \tag{4.11}$$

$$\varepsilon = \nu(x_0\cos\chi + y_0\sin\chi) \tag{4.12}$$

where $\omega$ and $\nu$ are the frequency and wave number of the incident wave, respectively. $(x_0, y_0)$ is the ship average horizontal position. $A_{ij}$, $B_{ij}$, $C_{ij}$ and $E_j$ are calculated by new strip method (NSM) by Watanabe, at al.[31]. Generally, as $u_0$, $v_0$, $\psi_0$, $x_0$, and $y_0$

change during maneuvering, the encounter frequency of the wave $\omega_e$ and ship speed $U_0$ also change. Then, those above-described hydrodynamic force coefficients change in time domain, too. Normally, $A_{ij}$ and $B_{ij}$ should take into account the memory effects with respect to changing $\omega_e$. However, $A_{ij}$ and $B_{ij}$ are treated quasi-steadily here for simplicity.

## 4.5 Ship position

The ship average horizontal position $(x_0, y_0)$ of the center of gravity defined in the space fixed coordinate system is expressed as:

$$\left.\begin{aligned} \dot{x}_0 &= u_0 \cos\psi_0 - v_0 \sin\psi_0 \\ \dot{y}_0 &= u_0 \sin\psi_0 + v_0 \cos\psi_0 \end{aligned}\right\} \tag{4.13}$$

In the same manner, displacements with respect to wave-induced motions $(x_1, y_1, z_1)$ are expressed as:

$$\left.\begin{aligned} \dot{x}_1 &= (\dot{\xi}_1 + v_0\psi_1)\cos\psi_0 - (\dot{\eta}_1 - u_0\psi_1)\sin\psi_0 \\ \dot{y}_1 &= (\dot{\xi}_1 + v_0\psi_1)\sin\psi_0 + (\dot{\eta}_1 - u_0\psi_1)\cos\psi_0 \\ \dot{z}_1 &= \dot{\zeta}_1 \end{aligned}\right\}$$

$$\tag{4.14}$$

Therefore, actual ship position included wave-induced motions is derived by adding the displacement obtained from eq.(4.14) to the position obtained from eq.(4.13). Eventually, the 6-DOF motion in waves can be obtained from numerically solving total 10 motion equations expressed as eqs.(4.2) and (4.9), and 5 supporting differential equations expressed as eqs.(4.13) and (4.14). Then, actual velocity and angular velocity components $(u, v, r)$ in waves are expressed as:

$$\left.\begin{aligned} u &= u_0 + v_0\psi_1 + \dot{\xi}_1 \\ v &= v_0 - u_0\psi_1 + \dot{\eta}_1 \\ r &= (\dot{\psi}_0 + \dot{\psi}_1)\cos\phi_0 - \dot{\theta}_1 \sin\phi_0 \end{aligned}\right\} \tag{4.15}$$

## 4.6 Turning simulation of a ship in regular

Turning simulations of KCS model with rudder angle $\delta = \pm 35°$ in calm water and regular waves were performed by the method proposed. The results obtained were compared with free-running test results in chapter 2. Here, we consider the following ship turning situation: The ship runs straight with the approach speed $(U_A)$ on $x_s$-axis (see Figure 4.1) in calm water or head waves $(\chi = 0°)$. This ship heading is defined as $\psi = 0°$. The ship is steered for turning, and the midship position when the steering is started is defined as $(x_s, y_s) = (0, 0)$. This position is called "steering position". Note that a positive $\delta$ means

a starboard turn and a negative $\delta$ means a port turn.

### 4.6.1 Data used in the simulations

To calculate the low frequency maneuvering motion, hydrodynamic derivatives and other hydrodynamic parameters are to be determined. The hydrodynamic derivatives and parameters for the simulations were mainly estimated by the captive model tests. The details are as follows:

- Hull resistance was calculated by a 3-dimensional extrapolation method based on Schoenherr's frictional resistance coefficient formula. Wave resistance coefficient and form factor were obtained by the tank tests.

- The derivatives with no-related to roll were estimated based on the captive model tests conducted in National Maritime Research Institute (NMRI) for SIMMAN 2008[30]. Roll-related derivatives were estimated based on the captive model tests conducted in Hiroshima University (HU)[35]. Table 4.1 shows the hydrodynamic derivatives on maneuvering, including roll-related derivatives used in the simulations.

- Hydrodynamic parameters related to rudder force and hull-rudder interaction terms were estimated by captive test data by NMRI[30].

- Added mass coefficients ($m'_x$, $m'_y$, $J'_{zz}$) for ship maneuvering were estimated by Motora's empirical charts. The values are $m'_x = 0.0061$, $m'_y = 0.1521$, and $J'_{zz} = 0.0089$.

- When the propeller open water thrust coefficient $K_T$ is expressed as $k_0 + k_1 J + k_2 J^2$ where $J$ is propeller advance ratio, the constants $k_0$, $k_1$ and $k_2$ were 0.4892, $-0.4053$ and $-0.0994$, respectively. Those were obtained by the propeller open water test.

### 4.6.2 Wave conditions: regular waves

The simulations were conducted in regular waves. Table 4.2 shows the wave conditions $(h_a, \lambda/L)$ in the simulation. The head waves of the ship in approaching are assumed to be $\chi = 0°$ in this study.

### 4.6.3 Wave-induced steady forces in regular waves

The wave-induced steady force coefficients in regular waves, $C_{XW}$, $C_{YW}$ and $C_{NW}$, were predicted by theoretical methods based on the potential theory. In zero speed case, $C_{XW}$, $C_{YW}$ and $C_{NW}$ were predicted by a 3D panel method by Kashiwagi et al.[33]. In non-zero

Table 4.1: The hydrodynamic derivatives on maneuvering used in the simulations

| Symbol | Value | Remarks | Symbol | Value | Remarks |
|---|---|---|---|---|---|
| $X'_{vv}$ | $-0.0726$ | NMRI | $X'_{v\phi}$ | $0.0200$ | HU |
| $X'_{vr}$ | $-0.0424$ | NMRI | $X'_{r\phi}$ | $0.0205$ | HU |
| $X'_{rr}$ | $-0.0139$ | NMRI | $X'_{\phi\phi}$ | $0.0013$ | HU |
| $Y'_v$ | $-0.2310$ | NMRI | $Y'_\phi$ | $-0.0157$ | HU |
| $Y'_r$ | $0.0424$ | NMRI | $Y'_{vv\phi}$ | $0.5748$ | HU |
| $Y'_{vvv}$ | $-1.635$ | NMRI | $Y'_{v\phi\phi}$ | $0.2288$ | HU |
| $Y'_{vvr}$ | $-0.3090$ | NMRI | $Y'_{r\phi\phi}$ | $-0.1759$ | HU |
| $Y'_{vrr}$ | $-0.805$ | NMRI | $N'_\phi$ | $-0.0137$ | HU |
| $Y'_{rrr}$ | $0.005$ | NMRI | $N'_{vv\phi}$ | $-0.2948$ | HU |
| $N'_v$ | $-0.1130$ | NMRI | $N'_{v\phi\phi}$ | $-0.0271$ | HU |
| $N'_r$ | $-0.0446$ | NMRI | $N'_{r\phi\phi}$ | $0.1383$ | HU |
| $N'_{vvv}$ | $-0.1653$ | NMRI | $z_H/d$ | $0.368$ | HU |
| $N'_{vvr}$ | $-0.6094$ | NMRI | $z_R/d$ | $0.57$ | estimation |
| $N'_{vrr}$ | $-0.0349$ | NMRI | $z_W/d$ | $0.2$ | estimation |
| $N'_{rrr}$ | $-0.0344$ | NMRI | | | |

Table 4.2: Wave conditions in the simulation

| Symbol | Value |
|---|---|
| $h_a$ (m) | $0.024$ |
| $\lambda/L$ | $1.0$ |

speed case, the speed effect on $C_{YW}$ and $C_{NW}$ were assumed to be negligible by Yasukawa et al.[34]. On the contrary, the speed effect on the added resistance coefficients $C_{XW}$ cannot be neglected. In the framework of the strip theory, the far field theory presented by Maruo[36] was applied for the added resistance prediction with the empirical correction of the added resistance in short wave-length referring to Takahashi[37].

Fig.4.2 shows $C_{XW}$, $C_{YW}$ and $C_{NW}$ in regular waves of $\lambda/L = 1.0$. In the figures, $\chi_0$ means relative wave direction, and $\chi_0 = 0°$ the heading waves, $\chi_0 = 90°$ the beam waves and $\chi_0 = 180°$ the following waves. $F_n$ is the Froude number based on $L$. In advance of the simulations, a data base was made based on the results of $C_{XW}$, $C_{YW}$ and $C_{NW}$ as functions of $U_0$, $\lambda/L$ and $\chi_0$. On the assumption of quasi-steady treatment, the wave-induced steady forces at the moment of the low frequency motion are estimated by an interpolation technique based on the data base.
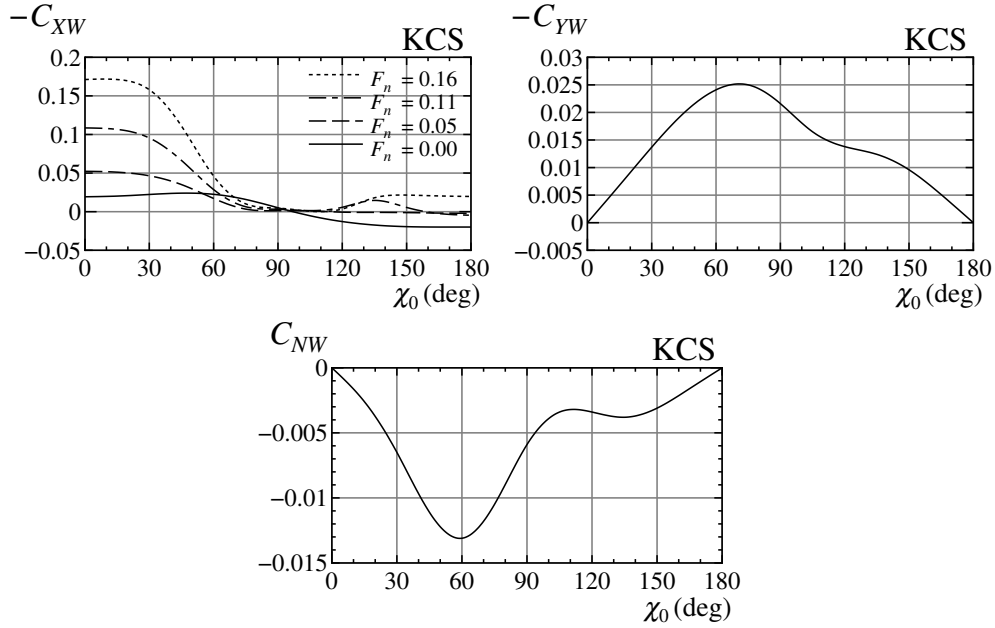
Fig. 4.2: Wave-induced steady force coefficients $(C_{XW}, C_{YW}, C_{NW})$ in regular waves of $\lambda/L = 1.0$

## 4.7 Comparison with Test Results

### 4.7.1 Straight moving

First, the relationship between the ship speed $U$ and the propeller revolution $n_P$ when sailing straight at zero rudder angle $(\delta = 0°)$ was examined. In calm water, $n_P$ at a given $U$ was calculated by the present method, then was followed by the $n_P$ calculation at a given $U$ in regular head waves. $U$ was set to be 14.5 kn in full-scale (0.860 m/s in the model) for calm water and regular waves, respectively. Table 4.3 shows a comparison of $n_P$ in calm water and regular waves. The calculated $n_P$ agrees with the experimental value for both calm water and regular waves. The $n_P$ in waves is about 30% higher than that in calm water. Since the calculated $n_P$ in waves matches with the experiment, the calculation accuracy of the added resistance in head waves is considered sufficient.

Table 4.3: Propeller revolution $(n_P)$ of ship model when sailing straight with $U = 0.860$ m/s in calm water and regular waves

|  | Calm | | Waves | |
|---|---|---|---|---|
|  | EXP | CAL | EXP | CAL |
| $n_P$ (rps) | 10.4 | 10.4 | 13.2 | 13.2 |

## 4.7.2 Turning trajectories

Next, the turning simulations in calm water and regular waves were conducted at the same approach speed condition in straight moving ($U = 0.860$ m/s for model). The rudder angle was set to be $\delta = \pm 35°$. Figs. 4.3 and 4.4 show comparisons of turning trajectories of KCS container ship model between experiment (EXP) and calculation (CAL) in calm water and regular waves, respectively. Result of Test1 from the experiment is used in the comparison. In the graphs, positions of the midship when the ship heading reaches $\pm 90°$ or $\pm 180°$ are represented by triangles mark. The positions when the ship heading reaches $\pm 450°$ or $\pm 540°$ are represented by circles and the positions when the ship heading reaches $\pm 810°$ or $\pm 900°$ are represented by squares. In calm water, the calculated trajectories with $\delta = -35°$ agrees well with the experiment, although the circle with $\delta = +35°$ turning is slightly larger than the experiment. In regular waves, obvious difference is observed compared to the result in calm water as follows. The turning circle distorts in the waves, where it does not become a circular trajectory like in the case of the calm water. During the turning in waves, the drifts towards the location $(x_s, y_s) = (0, 0)$ of rudder executing point, whereas no such significant drifting motion appears in calm water. This tendency is the same as the experimental result for other ship models in head waves in Yasukawa and Nakayama[7], Sanada et al.[9], Kim et al.[32] and Hasnan et al.[38]. The present method captures the tendencies observed in the experiments. However, the calculated drifting direction is different. This is probably because the calculation accuracy of the wave-induced steady force is insufficient.
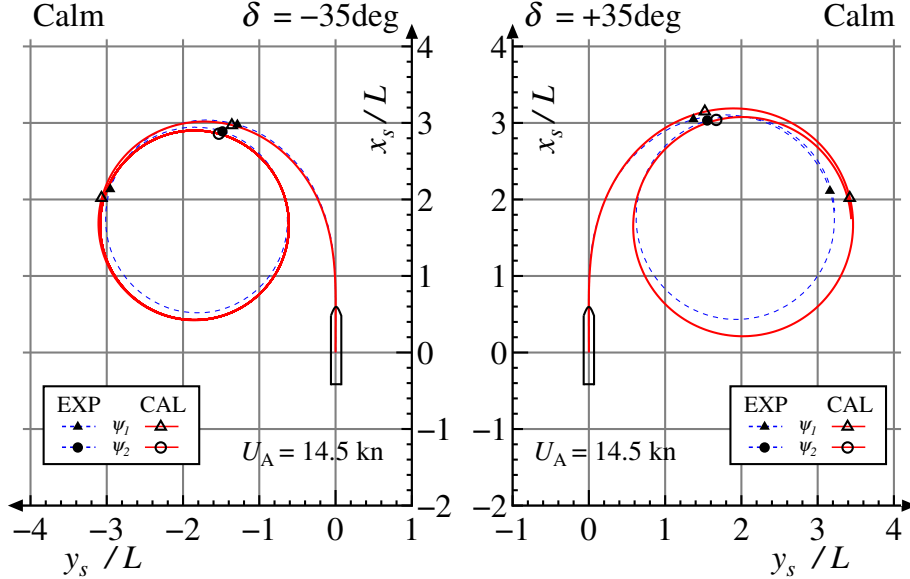


Fig. 4.3: Comparison of turning trajectories in calm water with $\delta = \pm 35°$

Next, the turning indices and the drifting indices during turning in calm water and in waves are compared. As for the experiment results for comparisons, the analysis results as described in chapter 2 were used. Table 4.4 shows comparison of turning indices $(A_{D1}/L, D_{T1}/L)$ in calm water. In the table, the error of the calculation result with respect to the average value of the test results is shown. A negative value means that the
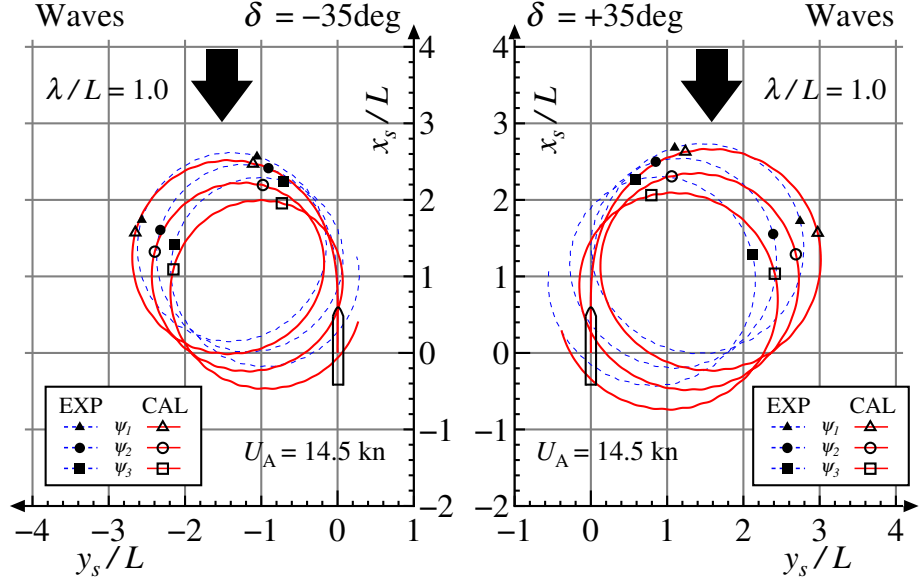
Fig. 4.4: Comparison of turning trajectories in regular waves with $\delta = \pm 35°$

absolute value of the calculation result is smaller than the test result, and a positive value means that the absolute value is larger than the test result. In the case of $\delta = -35°$, the present calculation result (CAL) agrees with the experiment result (EXP) within the error (err) of 4%. On the other hand, $\delta = +35°$ the present calculation result is slightly larger than the experiment result, and the accuracy is inferior to that in the case of $\delta = -35°$. This corresponds to the fact that the calculation result of the turning trajectory is larger than the experimental result, as shown in Fig. 4.3. Table 4.5 shows comparison of turning indices $(A_{D1}/L, D_{T1}/L), (A_{D2}/L, D_{T2}/L)$ in regular waves.

Table 4.6 show drifting indices in waves such as the drifting distance ($H_{D1}/L$ and $H_{D2}/L$) and drifting direction ($\mu_{D1}$ and $\mu_{D2}$), which are defined in chapter 2. The calculated results of $H_{D1}/L$ and $H_{D2}/L$ are about 60% larger than the test results. Also, the calculated results of $\mu_{D1}$ and $\mu_{D2}$ are about 60% less than the test results. This is because the drifting tendency of the ship turning in the waves is different between the calculation and the experiment, as shown in Fig. 4.4. The over-estimation of calculated wave-induced steady lateral force and wave-induced steady yaw moment might be the reason for such difference. Further investigation is performed by using analytical approach in chapter 6 to understand the phenomena.

Table 4.4: Comparison of turning indices during turning in calm water

|  | Calm | | | | | |
|  | $\delta = -35°$ | | | $\delta = +35°$ | | |
|  | EXP | CAL | Diff (%) | EXP | CAL | Diff (%) |
|---|---|---|---|---|---|---|
| $A_{D1}/L$ | 3.00±0.03 | 2.97 | -1.00 | 3.05±0.01 | 3.15 | 3.28 |
| $D_{T1}/L$ | 2.95±0.01 | 3.07 | 4.07 | 3.16±0.01 | 3.42 | 8.23 |

Table 4.5: Comparison of turning indices during turning in regular waves

| | Waves | | | | | |
| | $\delta = -35°$ | | | $\delta = +35°$ | | |
| | EXP | CAL | Diff (%) | EXP | CAL | Diff (%) |
|---|---|---|---|---|---|---|
| $A_{D1}/L$ | 2.58±0.01 | 2.47 | -4.26 | 2.70±0.04 | 2.63 | -2.59 |
| $D_{T1}/L$ | 2.59±0.01 | 2.65 | 2.32 | 2.74±0.01 | 2.97 | 8.39 |
| $A_{D2}/L$ | 2.45±0.02 | 2.19 | -10.6 | 2.53±0.05 | 2.31 | -8.70 |
| $D_{T2}/L$ | 2.37±0.03 | 2.40 | 1.27 | 2.41±0.03 | 2.69 | 11.6 |

Table 4.6: Comparison of drifting indices during turning in regular waves

| | Waves | | | | | |
| | $\delta = -35°$ | | | $\delta = +35°$ | | |
| | EXP | CAL | Diff (%) | EXP | CAL | Diff (%) |
|---|---|---|---|---|---|---|
| $H_{D1}/L$ | 0.19±0.01 | 0.31 | 63.2 | 0.30±0.02 | 0.37 | 23.3 |
| $H_{D2}/L$ | 0.22±0.01 | 0.34 | 54.6 | 0.35±0.02 | 0.36 | 2.9 |
| $\mu_{D1}$ (°) | -52.6±5.7 | 24.9 | 52.6 | -83.9±8.9 | -29.1 | -65.4 |
| $\mu_{D2}$ (°) | 72.8±7.2 | 46.2 | -36.5 | -72.6±5.9 | -47.5 | -34.6 |

## 4.7.3 Time histories during turning

Fig. 4.5 shows the time histories of longitudinal speed component $u$, lateral speed component $v$, yaw rate $r$, rudder normal force $F_N$ and propeller thrust $T_P$ during the turning with $\delta = +35°$ in the calm water and regular waves. In calm water, $u$ gradually decreases due to influence of the resistance increase during turning, and reaches the steady speed which is approximately 50% of the approach speed ($U_A = 0.860$ m/s). The calculation agrees well with the experiment. $v$ and $r$ reach their maximum values after steering, and gradually decrease and converge to steady values. Although the calculated $v$ and $r$ are slightly under-predicted, the calculation accuracy is acceptable. $F_N$ rapidly increases after steering, reaches a peak value and gradually converges to a steady value. The calculated $F_N$ is under-estimated. This is one of the reasons why the calculation result of the turning circle is larger than the test result. $T_P$ gradually increases due to the effect speed drop and converges to a steady value. The calculated $T_P$ is slightly under-estimated. The calculated $F_N$ and $T_P$ are not oscillated, although small oscillation with high frequency is observed in the measurements.

In regular waves, $u$ also decrease during turning, that is basically similar to the calm water case, however, never reaches the steady value as in calm water. Further, the high frequency oscillation is observed in the experiment. The calculated $u$ agrees well with the experiment. In time histories, of $v$ and $r$, a periodic oscillation appears. The present method captures well the oscillations and the periodic patterns, although a phase lead of $v$ and $r$ are observed in the calculation. It is noted that the high frequency oscillations components in $u$, $v$ and $r$ are coming from the effect of high-frequency wave-induced motion components such as $\dot{\xi}_1$, $\dot{\eta}_1$, $\dot{\psi}_1$ and $\dot{\phi}_1$ in eq.(4.15). Next, averaged values of $F_N$ and $T_P$ in waves are larger than those in calm water. The reason is that the propeller revolution increased in order to keep the same ship speed in calm water even in waves.

The calculated $F_N$ and $T_P$ are slightly under-estimated, however, the present method capture the overall tendency. The high frequency oscillations in $F_N$ and $T_P$ come from the wave-induced motions during turning. However, in the present method, high frequency oscillations in $F_N$ and $T_P$ are not calculated.

Fig. 4.6 shows comparisons of time histories of $u$, $v$, $r$, $F_N$ and $T_P$ during turning with $\delta = -35°$ in the calm water and regular waves. The overall tendency is the same as the results for $\delta = +35°$ shown in Fig. 4.5. However, the agreement between the calculation and the experiment is improved in the case of $\delta = -35°$. The present method can capture the behavior of $u$, $v$, $r$, $F_N$ and $T_P$ during turning with $\delta = -35°$ in the calm water and regular waves.

## 4.7.4 Wave-induced motions during turning

Fig. 4.7 shows a comparisons of time histories of heave $z$, pitch $\theta$ and roll/heel $\phi$ during turning 40s after steering, at the beginning of turning. The rudder angle is $\delta = +35°$ The present calculation well captures the feature that the pitch is small and the heave is large near $t = 14$s ( relative wave direction 90° : beam waves), and the motion period becomes longer and the heave becomes smaller near $t = 25$s ( relative wave direction 180° : beam waves). The oscillations and their periodic patterns in $z$ and $\theta$ are captured well. For $\phi$, the inward heel occurred just after steering, and changed to the outward hell after that, including the high frequency roll. The present calculations captures the roll/heel behavior during turning.

Fig. 4.8 shows comparisons of $z$ and $\theta$ histories versus heading angle $\psi$ in the range of 0° to 800° during turning. In the graphs, $z$ and $\theta$ are plotted versus not time $t$ but heading angle $\psi$ to capture the relationship of the wave-induced motions and the $\psi$. The histories of $z$ and $\theta$ in the calculation agree well with those in the experiment. This agreement shows that the heave and pitch motions are captured well with respect to the heading angle or the relative wave direction of the ship.
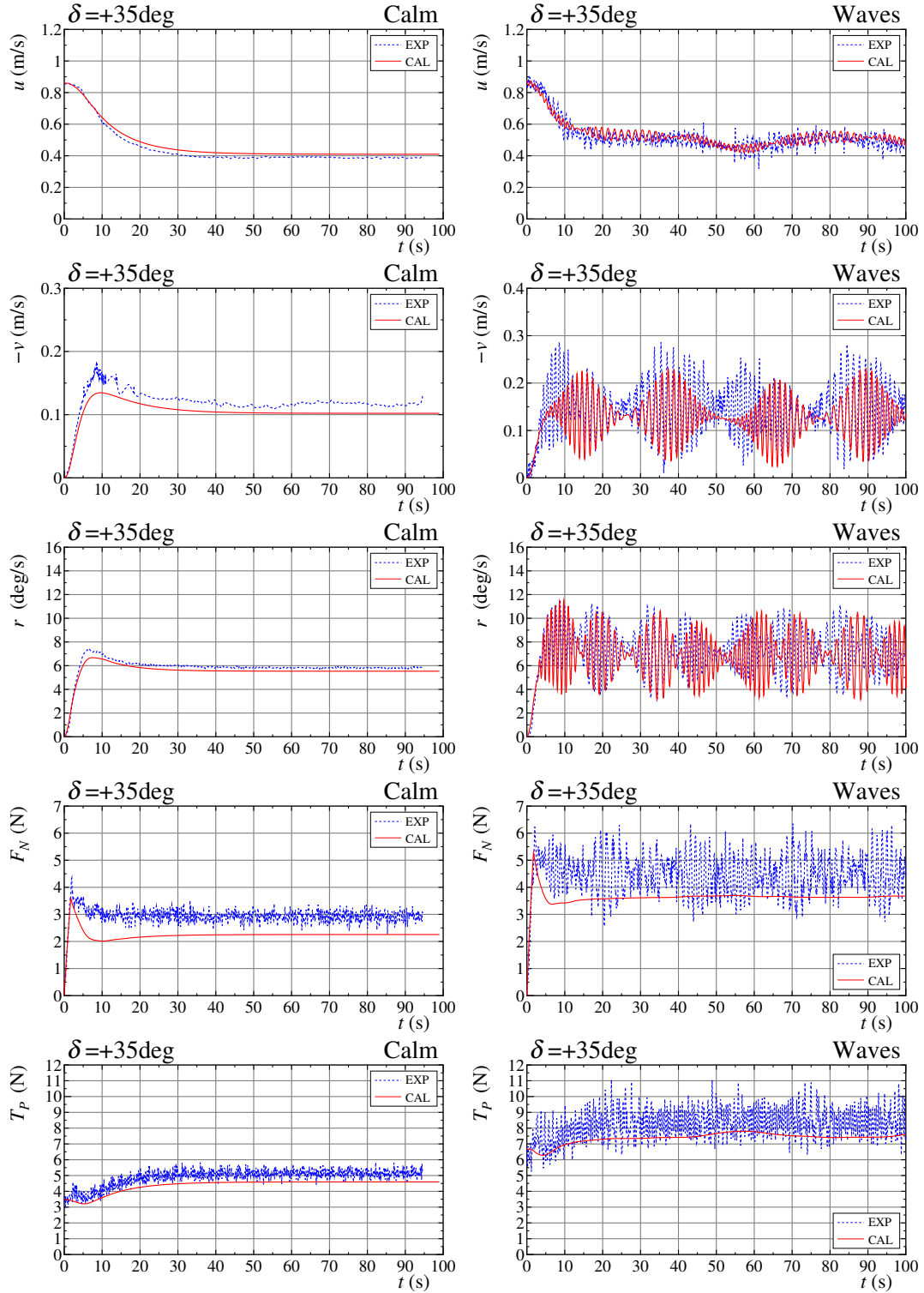
Fig. 4.5: Time histories of $u$, $v$, $r$, $F_N$ and $T_P$ during $\delta = +35°$ turning in calm water (left) and regular waves for KCS
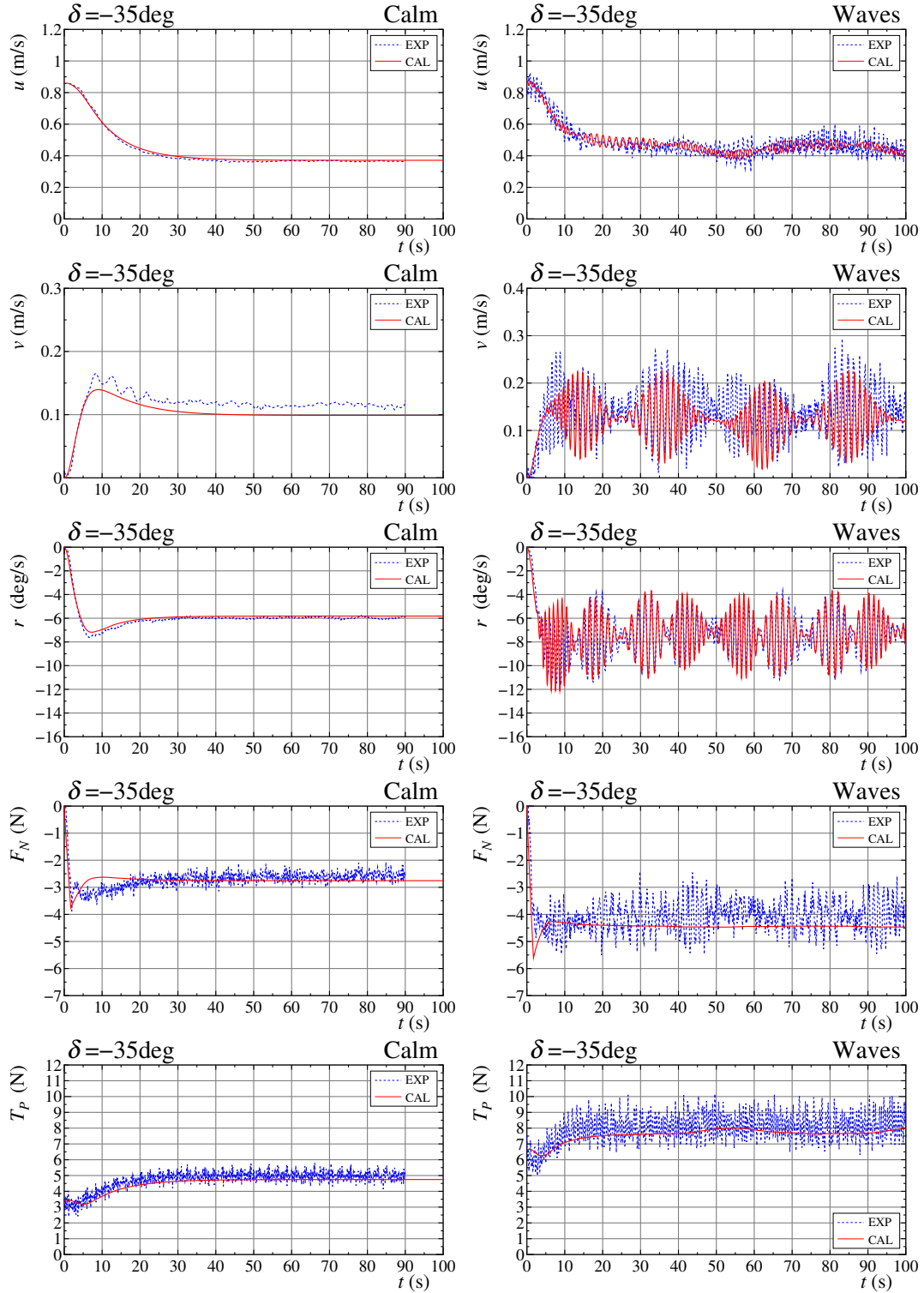
Fig. 4.6: Time histories of $u$, $v$, $r$, $F_N$ and $T_P$ during $\delta = -35°$ turning in calm water (left) and regular waves for KCS
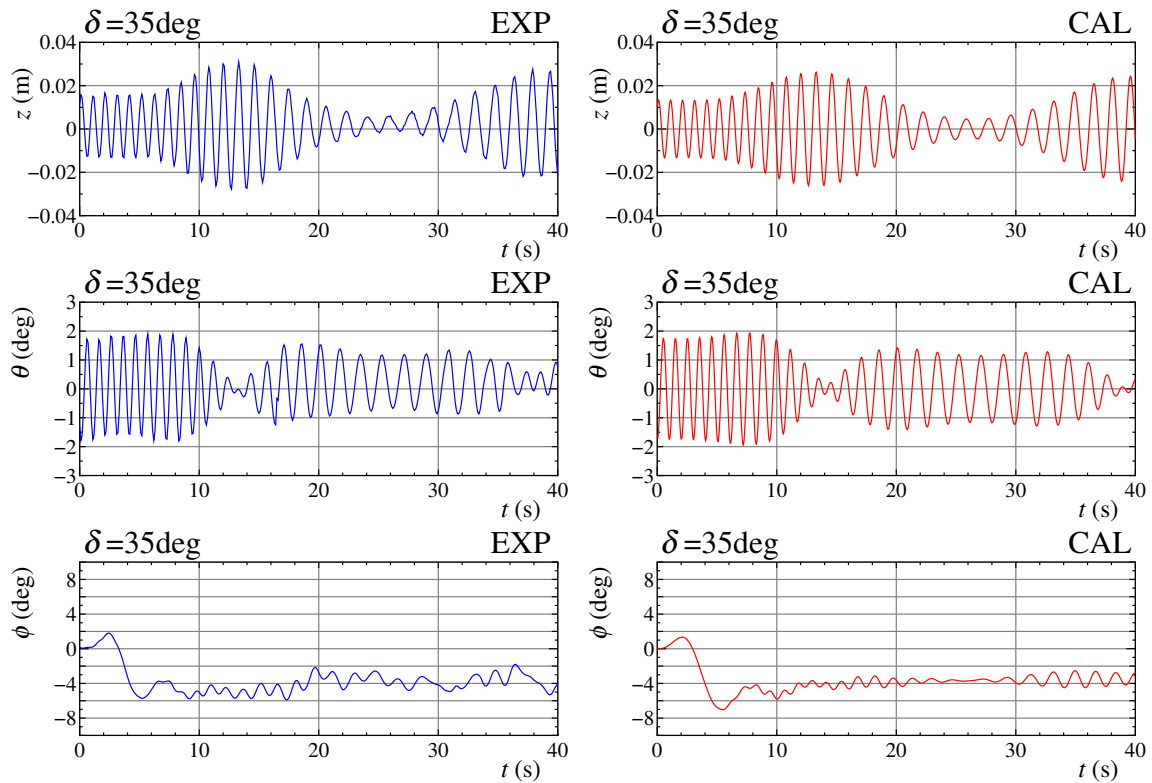
Fig. 4.7: Comparison of time histories of $z$, $\theta$ and $\phi$ during $\delta = +35°$ turning in regular waves between experiment(left) and calculation
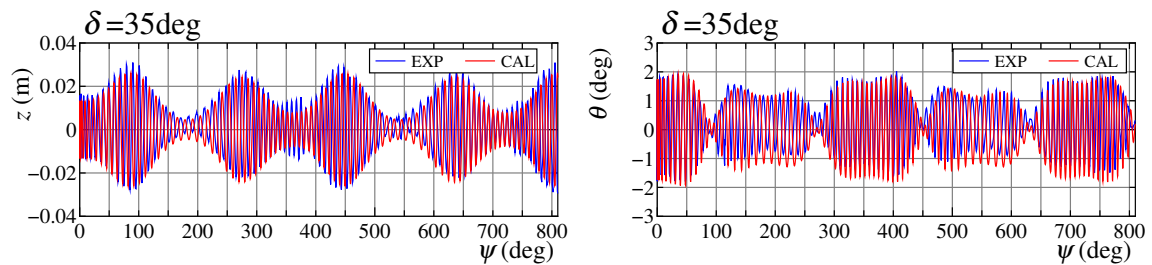


Fig. 4.8: Comparison of heading histories for $z$ and $\theta$ during $\delta = +35°$ turning in regular waves between experiment(left) and calculation

## 4.8 Summary for simulation in regular waves

From this chapter, the summary are the followings:

1. The obtained results such as ship trajectories, turning indices, drifting indices, time histories motions and wave-induced motions were compared and validated with the conducted free-running model test for both port and starboard turning. The validation shows that the present method can simulate both the maneuvering turning motion and the wave-induced motions in regular waves during turning with practical accuracy in short computational time, although there is some room for improvement in the prediction of wave-induced steady forces.

2. The validation of turning in regular waves is important before is extended to the method for turning in irregular waves. The estimation of mean wave-induced steady forces of ship turning in irregular waves is based on the combination of mean values of wave-induced steady forces of ship turning in regular waves. Based on the validation works in this chapter, it confirms the wave-induced steady forces are estimated sufficiently in regular waves, and is useful for the estimation of mean wave-induced steady forces in irregular waves in next chapter.

# Chapter 5

# Turning simulation of a ship in irregular waves

## 5.1 Studied Ship

A KVLCC2 large tanker model is used in this simulation. The specification details was described in the previous chapter 3.

## 5.2 6-DOF motion simulation method of a ship maneuvering in irregular waves

## 5.3 Coordinate systems and notations

The coordinate systems is similar with the coordinate systems for simulation method in regular waves, thus the explanation is skipped here.

## 5.4 Base motion equations

Similarly with maneuvering in regular waves, ship motion is assumed to be expressed as the sum of the maneuvering motion regarded as low frequency motion and wave-induced motion regarded as high frequency motion in irregular waves. The base motion equations for maneuvering in irregular waves are basically similar with the simulation method for regular waves, thus some explanations are skipped here. Wave-induced steady forces for low frequency maneuvering motions and wave exciting forces for high-frequency wave-induced motions are specifically described.

## 5.4.1 Low-frequency maneuvering motions

In irregular waves, the motion equations for low-frequency maneuvering motions is similar with motion equations in regular waves as shown in eq. (4.2). As for $X_W, Y_W$ and $N_W$, the mean values of the wave-induced steady forces in irregular waves are employed in this study. The mean values are calculated by applying the short-term prediction technique based on the wave-induced steady force coefficients in regular waves. However, the second order wave forces in irregular waves has several force components such as the slowly-varying second order wave forces. Therefore, it is necessary to check whether the mean value is enough without considering the other force component in the maneuvering simulation in irregular waves. Skejic and Faltinsen[23] conducted the maneuvering simulations considering the slowly-varying second order wave force components. However, in the previous chapter 3, it is experimentally confirmed that the effect of the slowly-varying second order wave forces on the turning motion in irregular waves was not significant. It is considered that the effect is negligible since the turning motion with $\delta = \pm 35°$ in waves is not a long-term motion. In this study, from a practical point of view, it is decided to consider only the mean values of the wave-induced steady forces. Then, $X_W, Y_W$ and $N_W$ are expressed as:

$$
\left.
\begin{aligned}
X_W &= \rho g H_{1/3}^2 L \ \overline{C_{XW}}(U_0, T_0, \chi_0) \\
Y_W &= \rho g H_{1/3}^2 L \ \overline{C_{YW}}(T_0, \chi_0) \\
N_W &= \rho g H_{1/3}^2 L^2 \ \overline{C_{NW}}(T_0, \chi_0)
\end{aligned}
\right\}
\tag{5.1}
$$

where $g$ is the gravity acceleration, $H_{1/3}$ is the significant wave height and $L$ is the ship length. $X_W$ is expressed as the function of the ship speed $U_0 (= \sqrt{u_0^2 + v_0^2})$, the averaged wave period $T_0$ and the relative main wave direction $\chi_0 (= \chi - \psi_0)$. $Y_W$ and $N_W$ are assumed to be no-relation with $U_0$. The mean wave-induced steady force coefficients in irregular waves $(\overline{C_{XW}}, \overline{C_{YW}}, \overline{C_{NW}})$ are expressed as:

$$
\left.
\begin{aligned}
\overline{C_{XW}}(U_0, T_0, \chi_0) &= 2 \int_{-\pi}^{\pi} G(\gamma) d\gamma \int_0^{\infty} C_{XW}(U_0, \omega, \chi_0) \frac{S_{\zeta\zeta}(\omega)}{H_{1/3}^2} d\omega \\[2mm]
\overline{C_{YW}}(T_0, \chi_0) &= 2 \int_{-\pi}^{\pi} G(\gamma) d\gamma \int_0^{\infty} C_{YW}(\omega, \chi_0) \frac{S_{\zeta\zeta}(\omega)}{H_{1/3}^2} d\omega \\[2mm]
\overline{C_{NW}}(T_0, \chi_0) &= 2 \int_{-\pi}^{\pi} G(\gamma) d\gamma \int_0^{\infty} C_{NW}(\omega, \chi_0) \frac{S_{\zeta\zeta}(\omega)}{H_{1/3}^2} d\omega
\end{aligned}
\right\}
\tag{5.2}
$$

Here, $H_{1/3}$ is the significant wave height and $L$ is the ship length. $X_W$ is expressed as the function of the ship speed $U_0 (= \sqrt{u_0^2 + v_0^2})$, the averaged wave period $T_0$ and the relative main wave direction $\chi_0 (= \chi - \psi_0)$. $Y_W$ and $N_W$ are assumed to be no-relation with $U_0$. In eq.(5.2), $S_{\zeta\zeta}(\omega)$ is the wave spectrum, and $G(\gamma)$ the wave direction distribution function. $C_{XW}$, $C_{YW}$ and $C_{NW}$, which are the mean wave-induced steady force coefficients in regular waves, are estimated by the theoretical methods such as strip method and/or zero speed 3D panel method as previously described in chapter 4. In advance of the simulations, a database of $C_{XW}$, $C_{YW}$ and $C_{NW}$ is made as functions of $U_0$, $T_0$ and

$\chi_0$. On the assumption of quasi-steady treatment, the wave-induced steady forces at the moment of the low frequency motion are estimated by an interpolation technique based on the database.

### 5.4.2 High-frequency wave-induced motions

Using the eq.(4.9), the wave exciting force of $j$-th mode $E_j$ for irregular waves is expressed as the sum of the exciting force component induced by the elementary wave as follows:

$$E_j(t) = \sum_{n=1}^{N_e} h_n \left[ F_{jc}(\omega_{en}) \cos \omega_n^* - F_{js}(\omega_{en}) \sin \omega_n^* \right] \quad (5.3)$$

where $F_{jc}$ and $F_{js}$ are the wave exciting force components calculated by taking the sum of Froude-Krylov force and diffraction force components. $h_n$ is the amplitude of the $n$-th component of the elementary wave. $\omega_{en}$ and $\omega_n^*$ are expressed as

$$\omega_{en} = \omega_n + \nu_n \left( \dot{x}_0 \cos \chi + \dot{y}_0 \sin \chi \right) \quad (5.4)$$

$$\omega_n^* = \omega_n t + \nu_n (x_0 \cos \chi + y_0 \sin \chi) + \epsilon_n \quad (5.5)$$

where $\omega_n$, $\nu_n$ and $\epsilon_n$ are the frequency, wave number and phase of the $n$-th component of the elementary wave, respectively. $\epsilon_n$ gives a uniform random number in $0 \sim 2\pi$. $N_e$ represents the number of the elementary wave components.

Generally, as $u_0$, $v_0$, $\psi_0$, $x_0$, and $y_0$ change during maneuvering, the encounter frequency of the elementary wave $\omega_{en}$ and ship speed $U_0$ also change. Then, those above-described hydrodynamic force coefficients change in time domain, too.

## 5.5 Ship position

The explanation of ship position is similar with the ship position for simulation method in regular waves, thus the explanation is skipped here.

## 5.6 Turning simulation of a ship in irregular

Turning simulations of KVLCC2 model with rudder angle $\delta = \pm 35°$ in calm water and irregular waves were performed by the method proposed. The results obtained were compared with free-running test results in chapter 3. Here, we consider the following ship turning situation: The ship runs straight with the approach speed ($U_A$) on $x_s$-axis (see Figure 4.1) in calm water or head waves ($\chi = 0°$). This ship heading is defined as $\psi = 0°$. The ship is steered for turning, and the midship position when the steering is

started is defined as $(x_s, y_s) = (0, 0)$. This position is called "steering position". Note that a positive $\delta$ means a starboard turn and a negative $\delta$ means a port turn.

## 5.6.1 Data used in the simulations

To calculate the low frequency maneuvering motion, hydrodynamic force coefficients and other parameters for KVLCC2 are to be determined. The most coefficients and parameters have been already published in the paper by Yasukawa and Yoshimura[29], and were used for the present turning simulations. More details are as follows:

- Hull resistance was calculated by a 3-dimensional extrapolation method based on Schoenherr's frictional resistance coefficient formula. Wave resistance coefficient and form factor were obtained by the tank tests.

- When the propeller open water thrust coefficient $K_T$ is expressed as $k_0 + k_1 J + k_2 J^2$ where $J$ is propeller advance ratio, the constants $k_0$, $k_1$ and $k_2$ were 0.2811, $-0.2603$ and $-0.1831$, respectively. Those were obtained by the tank tests.

- Added mass for surge, added mass for sway and added moment of inertia for yaw ($m_x$, $m_y$, $J_z$) were estimated by Motora's empirical charts.

The radius of pitch gyration was set to be $0.25L$, and steering rate was $24.3°/\text{s}$ for model ($2.32°/\text{s}$ for full-scale). These are the same as the tank test conditions.

## 5.6.2 Wave conditions: irregular waves

The simulations were conducted in short-crested irregular waves. As the wave spectrum $S_{\zeta\zeta}(\omega)$ and the wave direction distribution function $G(\gamma)$ in eq.(5.2), the Pierson-Moskowitz type frequency spectrum and the $\cos^4$-function, respectively were employed in the simulations.

The target values of the significant wave height $H_{1/3}$ and the average wave period $T_0$ are shown in Table 5.1. This condition is the same as the wave condition in the tank test. The main wave direction was set to be head waves in ship approaching ($\chi = 0°$).

Table 5.1: Wave conditions in the simulation

|              | Full-scale | Model |
|--------------|------------|-------|
| $H_{1/3}$ (m) | 4.5        | 0.041 |
| $T_0$ (s)     | 10.5       | 1.00  |

### 5.6.3 Wave-Induced Steady Force Coefficients in Irregular Waves

The wave-induced steady force coefficients in regular waves, $C_{XW}$, $C_{YW}$ and $C_{NW}$, were predicted by theoretical methods based on the potential theory as previously explained in chapter 4 for simulation method in regular waves. Then, the short-term prediction technique based on the wave-induced steady force coefficients in regular wave is applied to predict the mean values of the wave-induced steady forces in irregular waves.

Fig. 5.1 shows $\overline{C_{XW}}$ with different Froude numbers, $F_n = 0.14$, 0.09 and 0.0. Fig. 5.2 shows $\overline{C_{YW}}$ and $\overline{C_{NW}}$. In the figures, $\chi_0$ means relative wave direction, and $\chi_0 = 0°$ heading waves, $\chi_0 = 90°$ the beam waves and $\chi_0 = 180°$ the following waves. The data base was made based on the results of $\overline{C_{XW}}$, $\overline{C_{YW}}$ and $\overline{C_{NW}}$ as the functions of $U_0$, $T_0$ and $\chi_0$. On the assumption of quasi-steady treatment, the wave-induced steady forces at the moment of the low frequency motion are estimated by an interpolation technique based on the data base.
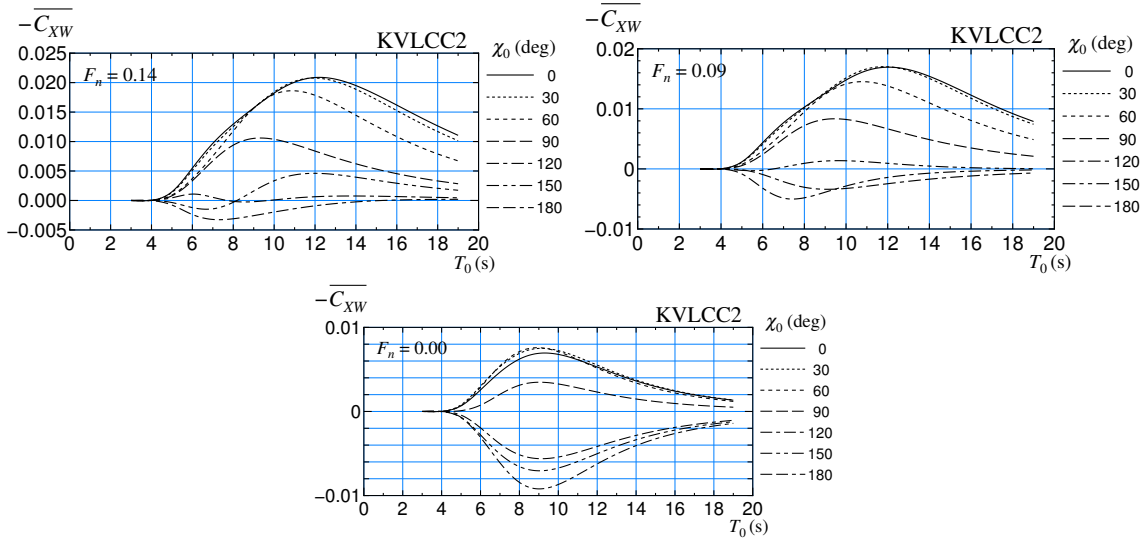


Fig. 5.1: Mean value of added resistance coefficients ($\overline{C_{XW}}$) in short-crested irregular waves
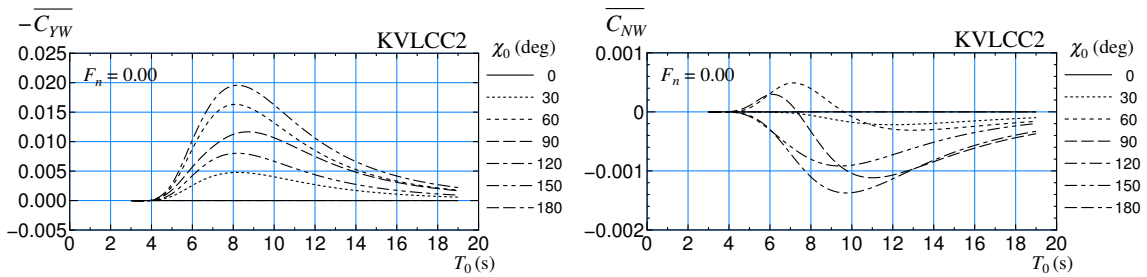


Fig. 5.2: Mean values of wave-induced lateral force and yaw moment coefficients ($\overline{C_{YW}}$, $\overline{C_{NW}}$) in short-crested irregular waves

## 5.7 Comparison with Free-Running Model Test Results

### 5.7.1 Straight moving

First, the relationship between the ship speed $U$ and the propeller revolution $n_P$ when sailing straight at zero rudder angle was checked. In calm water, $n_P$ at a given $U$ was calculated by the present method. Then, $U$ was set to 15.5 kn, 10 kn and 5 kn at full-scale. Table 5.2 shows a comparison of $n_P$ at three different $U$ in calm water between experiment (EXP) and calculation (CAL). The calculated $n_P$ almost agrees with the tank test result. In irregular head waves ($\chi_0 = 0°$), $n_P$ at a given $U$ was also calculated. Then, $U$ was set to 13 kn, 10 kn and 5 kn at full-scale. Table 5.3 shows a comparison of $n_P$ in irregular waves between EXP and CAL. The calculated $n_P$ slightly differs from the tank test result. This is probably because the calculation accuracy of the added resistance in head waves is insufficient. However, since the propeller revolution error is less than 3.5% in maximum, the special correction was not made in the motion simulations.

Table 5.2: Ship speed ($U$) and propeller revolution ($n_P$) in calm water

| $U$ in full-scale (kn) | 15.5 | 10.0 | 5.0 |
|---|---|---|---|
| $U$ in model (m/s) | 0.760 | 0.491 | 0.245 |
| $n_P$ in model (rps), EXP | 17.2 | 11.6 | 6.0 |
| $n_P$ in model (rps), CAL | 17.2 | 11.5 | 6.0 |

Table 5.3: Ship speed ($U$) and propeller revolution ($n_P$) in irregular waves

| $U$ in full-scale (kn) | 13.0 | 10.0 | 5.0 |
|---|---|---|---|
| $U$ in model (m/s) | 0.636 | 0.491 | 0.245 |
| $n_P$ in model (rps), EXP | 17.2 | 14.0 | 8.3 |
| $n_P$ in model (rps), CAL | 16.6 | 13.7 | 8.4 |

### 5.7.2 Turning trajectories

Next, the turning simulations in calm water and irregular waves were conducted at the same approach speed conditions in straight moving as shown in Tables 5.2 and 5.3. The rudder angle was set to be $\delta = \pm 35°$. Fig. 5.3 shows comparison of turning trajectories between experiment and calculation in calm water. The turning trajectory does not change much due to the difference in the approach ship speeds (15.5 kn, 10 kn and 5 kn at full-scale). For all the approach speeds, the calculation results show good agreement with the tank test results.

Fig. 5.4 shows comparison of turning trajectories in irregular waves. In Fig. 5.4, five different turning trajectories are plotted as the tank test results. These were obtained in

five different wave patterns changed by varying the phase between the elementary waves in the wave generation with keeping given significant wave height ($H_{1/3}$), mean wave period ($T_0$), and main wave direction ($\chi$)[38]. On the other hand, the influence of the difference of the wave pattern on the turning trajectory in the calculations is negligible because the effect of the difference appears only in the high-frequency motion, not in the low-frequency motion. The present method captures the following tendencies observed in the experiments:

- The turning circle distorts in the waves. It does not become a circular trajectory like in the case of the calm water.

- During turning, the ship drifts to the location $(x_s, y_s) = (0, 0)$ of rudder executing point.

- The ship drifts more remarkably while the approach speed is reduced.

However, the calculated turning trajectories in irregular waves do not agree with the experiments quantitatively. The calculated drifting amount during turning is small. This is probably because the wave-induced steady forces are under-estimated.

Table 5.4 shows the turning indices for $\delta = +35°$ in calm water. Non-dimensional advance $A_D/L$ and the tactical diameter $D_T/L$ decrease slightly with reducing the approach speed ($U_A$). Table 5.5 shows the turning and drifting indices for $\delta = +35°$ in irregular waves. In the table, 'AVG' means the average value of the results in five different irregular waves, and 'STD' means the standard deviation.

Table 5.4: Turning indices for $\delta = +35°$ turning in calm water

|  | EXP | | | CAL | | |
|---|---|---|---|---|---|---|
| $U_A$ (kn) | 15.5 | 10.0 | 5.0 | 15.5 | 10.0 | 5.0 |
| $A_D/L$ | 3.11 | 2.96 | 2.77 | 3.20 | 3.09 | 2.95 |
| $D_T/L$ | 3.18 | 3.09 | 3.06 | 3.35 | 3.30 | 3.20 |

Table 5.5: Turning and drifting indices for $\delta = +35°$ turning in irregular waves

|  |  | EXP | | | CAL | | |
|---|---|---|---|---|---|---|---|
| $U_A$ (kn) | | 13.0 | 10.0 | 5.0 | 13.0 | 10.0 | 5.0 |
| $A_D/L$ | AVG | 2.90 | 2.72 | 2.07 | 2.92 | 2.78 | 2.33 |
| | STD | 0.05 | 0.03 | 0.11 | – | – | – |
| $D_T/L$ | AVG | 3.09 | 3.01 | 2.76 | 3.08 | 2.96 | 2.53 |
| | STD | 0.06 | 0.06 | 0.10 | – | – | – |
| $H_{D1}/L$ | AVG | 0.60 | 0.73 | 1.98 | 0.47 | 0.57 | 1.28 |
| | STD | 0.07 | 0.12 | 0.10 | – | – | – |
| $\mu_{D1}$ (°) | AVG | 0.37 | -3.97 | -15.7 | 5.45 | -8.03 | -28.3 |
| | STD | 9.37 | 5.33 | 3.55 | – | – | – |

Based on the values showing in the tables, Fig. 5.5 was made for a comparison of the turning and drifting indices in experiment and calculation. $A_D/L$ and $D_T/L$ in irregular

waves decrease significantly with reducing the approach speed ($U_A$), although the effect of $U_A$ on $A_D/L$ and $D_T/L$ in calm water is not so significant. The calculated $A_D/L$ and $D_T/L$ in calm water are slightly over-estimated, but the agreement with the experiments is in acceptable level. In irregular waves, the agreement with the experiments is also in acceptable level. The present method can capture properly the change of $A_D/L$ and $D_T/L$ with varying $U_A$ both in calm water and irregular waves. The drifting distance $H_{D1}/L$ and the drifting direction $\mu_{D1}$ during turning increase with a decrease in $U_A$. The present method can capture the change of $H_{D1}/L$ and $\mu_{D1}$ with varying $U_A$ in irregular waves, although $H_{D1}$ is under-estimated.

### 5.7.3 Comparison of time histories during turning

Fig.5.6 shows a comparison of time histories of speed drop ratio $U/U_A$ during turning between experiment and calculation in both calm water and irregular waves at three different approach speeds ($U_A$). $U$ is calculated by the following formula:

$$
\begin{aligned}
U &= \sqrt{u^2 + v^2} \\
&= \sqrt{(u_0 + \dot{\xi}_1 + v_0\psi_1)^2 + (v_0 + \dot{\eta}_1 - u_0\psi_1)^2}
\end{aligned}
$$

$$(5.6)$$

Note that only one wave pattern (pat-1) was selected and presented in this comparison. In calm water, the steady values of the speed drop ratio are about 0.4 for any approach speeds. The calculations agree well with the experiments.

In irregular waves, long-period (low-frequency) fluctuation of $U/U_A$, not seen in calm water results, appear in the results. And it becomes more noticeable as $U_A$ decreases. This is closely related to the turning motion of the ship in waves. In the case of $U_A = 5$ kn, $U/U_A$ becomes minimum at about $t = 156$ s when the heading reaches 360° and the second turn starts. At this time, the relative wave direction becomes zero (head wave direction), and the added resistance in waves becomes the largest. The present method captures well the tendency of $U/U_A$ in irregular waves. At the same time, short-period (high-frequency) fluctuations of $U/U_A$, which comes from the high-frequency motion components such as $\dot{\xi}_1$, $\dot{\eta}_1$, and $\psi_1$ in eq.(5.6), appear in irregular wave results. It becomes more significant in the low approach speed case (5 kn). The calculated amplitudes of the high-frequency fluctuations are remarkably smaller to the experiments. The reason is considered due to the influence of noise in the measured data on the analysis of ship speed $U$. This is more likely than the inadequacy of the simulation method.

Fig.5.7 shows a comparison of time histories of non-dimensional yaw rate $r'$ between experiment and calculation in both calm water and irregular waves. $r'$ is defined as:

$$
\begin{aligned}
r' &= rL/U_A \\
&= \left[ (\dot{\psi}_0 + \dot{\psi}_1)\cos\phi_0 - \dot{\theta}_1 \sin\phi_0 \right] L/U_A
\end{aligned}
$$

$$(5.7)$$

In calm water, a peak appears after steering initiates, and then the $r'$ value gradually de-

creases and converges to a steady value which is about 0.3 for the three different approach speeds. The present method can capture it quantitatively at all speeds.

In irregular waves, high-frequency components appear in the time histories of $r'$. The time histories in the calculation look similar to those in the experiment for three different approach speeds. When looking at the low-frequency motion behavior, $r'$ in irregular waves is slightly larger than that in calm water as a whole. Larger $r'$ means that the turning radius is smaller. From this, we see that the ship model turns with a smaller radius on average due to the influence of waves. The present method can capture well the high- and low- frequency behaviors of $r'$ during turning in irregular waves.

Fig.5.8 shows a comparison of time histories of rudder normal force coefficient $F'_N$ between experiment and calculation in both calm water and irregular waves. $F'_N$ is defined as:

$$F'_N = \frac{F_N}{(1/2)\rho L d U_A^2} \tag{5.8}$$

Observing at the experimental data, the short-period (high-frequency) fluctuations appear in $F'_N$ regardless of whether it is in calm water or in waves. Although this may be noise mixed in the measured data, the noise is not removed by a filter in the graph. Here, only the long-period (low-frequency) fluctuation of $F'_N$ is mainly considered since the calculation of $F_N$ does not include the effect of the high-frequency components. In calm water, a peak appears soon after steering is initiated, and then the value gradually decreases and converges to a steady value. The present method can capture the behavior quantitatively. $F'_N$ on average in irregular waves becomes larger than that in calm water for $U_A = 5$ kn and 10 kn since the propeller loads are higher than the calm water cases. The present method captures well the overall behavior of $F'_N$ in irregular waves.

## 5.7.4   Comparison of wave-induced motions during turning

Next, this investigation consider the wave-induced motions such as heave and pitch during $\delta = +35°$ turning in irregular waves. Figs. 5.9 and 5.10 show comparisons of time histories of heave ($z$) and pitch ($\theta$) during turning at $U_A = 13$ kn. To capture the effect of the difference of the incident wave patterns on the wave-induced motions, the wave patterns were changed at five different patterns and are represented as pat-1, pat-2, pat-3, pat-4, and pat-5 in the experiments. In the calculations, the wave patterns were also changed and are represented by the same names. Although the name is the same between the experiment and the calculation, the wave pattern is not the same. In the figures, five different time histories in the experiment and the calculation are shown for each wave patterns. The time histories in the calculation for heave and pitch look similar to those in the experiment. In particular, the heave motion tends to decrease around $t = 40$ s in both experiments and calculations. This is because the relative wave direction is the following wave direction for the ship.

In order to quantitatively grasp the heave and pitch motions during turning, the sig-

Table 5.6: Heave significant values ($z_{1/3}$) during $\delta = +35°$ turning in three different approach speeds ($U_A$)

|  | EXP | | | CAL | | |
|---|---|---|---|---|---|---|
| $U_A$ (kn) | 13.0 | 10.0 | 5.0 | 13.0 | 10.0 | 5.0 |
| pat-1 (mm) | 28.9 | 24.1 | 22.1 | 36.7 | 37.2 | 30.1 |
| pat-2 (mm) | 24.2 | 22.9 | 23.2 | 27.3 | 32.9 | 29.4 |
| par-3 (mm) | 28.5 | 24.7 | 26.5 | 27.0 | 27.7 | 27.5 |
| pat-4 (mm) | 27.4 | 23.0 | 25.2 | 36.7 | 34.1 | 28.4 |
| par-5 (mm) | 21.6 | 24.4 | 22.7 | 28.4 | 30.7 | 34.4 |
| AVG (mm) | 26.1 | 23.8 | 23.9 | 31.2 | 32.5 | 29.9 |
| STD (mm) | 3.1 | 0.8 | 1.9 | 5.0 | 3.6 | 2.7 |

Table 5.7: Pitch significant values ($\theta_{1/3}$) during $\delta = +35°$ turning in three different approach speeds ($U_A$)

|  | EXP | | | CAL | | |
|---|---|---|---|---|---|---|
| $U_A$ (kn) | 13.0 | 10.0 | 5.0 | 13.0 | 10.0 | 5.0 |
| pat-1 (°) | 1.72 | 1.61 | 1.37 | 1.75 | 1.92 | 1.72 |
| pat-2 (°) | 1.54 | 1.61 | 1.68 | 1.58 | 1.65 | 1.65 |
| par-3 (°) | 1.68 | 1.67 | 1.61 | 1.51 | 1.43 | 1.54 |
| pat-4 (°) | 1.76 | 1.55 | 1.62 | 1.86 | 1.72 | 1.87 |
| par-5 (°) | 1.54 | 1.61 | 1.46 | 1.63 | 1.58 | 1.94 |
| AVG (°) | 1.65 | 1.61 | 1.55 | 1.67 | 1.66 | 1.74 |
| STD (°) | 0.10 | 0.04 | 0.13 | 0.14 | 0.18 | 0.16 |

nificant values were obtained by using the time history data in the range of the heading angle $0° \sim 720°$ in each for calculations and the experiments. Tables 5.6 and 5.7 show the significant values ($z_{1/3}$ and $\theta_{1/3}$) during turning in three different approach speeds ($U_A$). In the tables, average value (AVG) and standard deviation (STD) of five different significant values are shown in the model scale. The mean value of the heave ($z_{1/3}$) calculated by the present method is about 35% larger in maximum than the experimental value. The standard deviation also increases. The mean value of the pitch ($\theta_{1/3}$) calculated is about 10% larger than the experimental value. This indicates that there is some room for improvement in the calculation method in irregular waves.

Here, for reference, Fig.5.11 shows a comparison between the calculation results of the heave and pitch amplitudes ($z_a$, $\theta_a$) during straight runs in regular head waves by the present method, and the tank test results. The tank tests were conducted in Hiroshima University towing tank. In the graph, $\lambda$ is wave-length. The $z_a$ and $\theta_a$ are non-dimensionalized by using the incident wave amplitude $h_a$ and the wave slope $h_a K$, respectively. The calculated result of the heave amplitude by the present method is slightly larger than that in the tank test, which is consistent with the above-described tendency with respect to the calculation accuracy of $z_{1/3}$. However, the calculation accuracy is practically sufficient. The calculation accuracy of the pitch amplitude is also sufficient. Compared with this, the calculation accuracy of the heave and pitch during ship turning in irregular waves is inferior. Therefore, it is considered that theoretical/numerical treat-

ment related to the effects of turning motion and the effects of irregular waves should be improved in the high-frequency motion calculation part. This will be a future work.
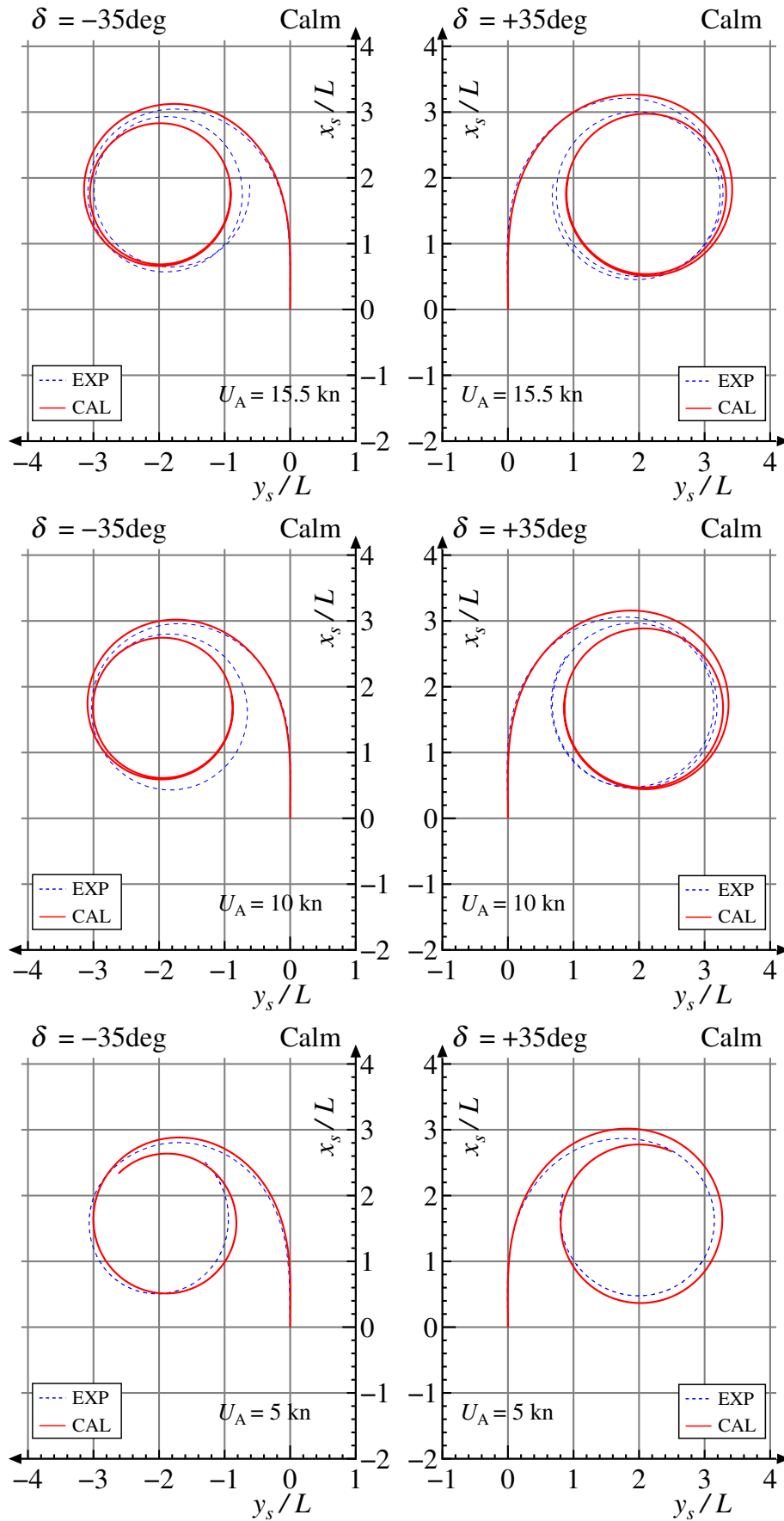
Fig. 5.3: Comparison of turning trajectories in calm water at three different approach speeds
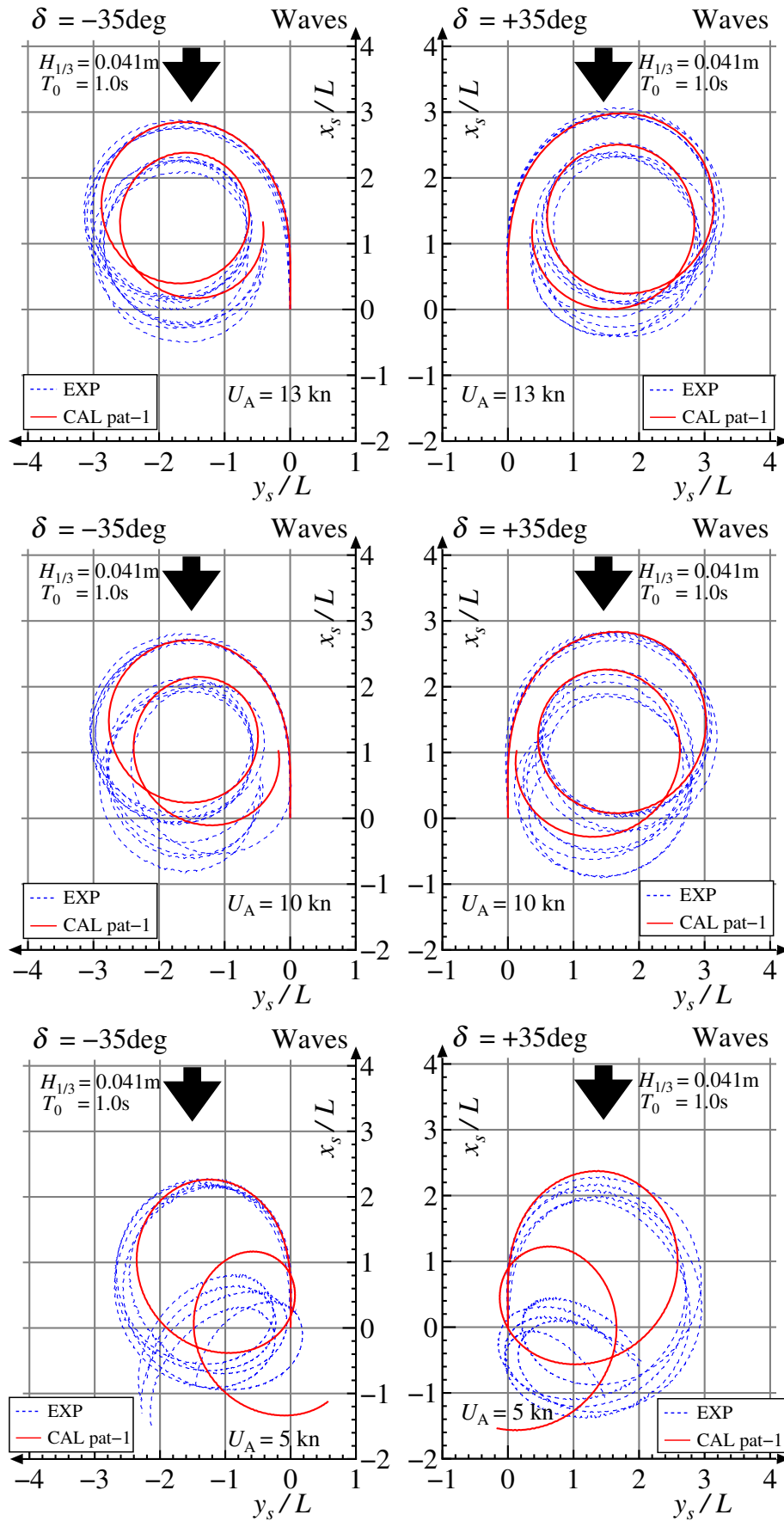
Fig. 5.4: Comparison of turning trajectories in irregular waves at three different approach speeds
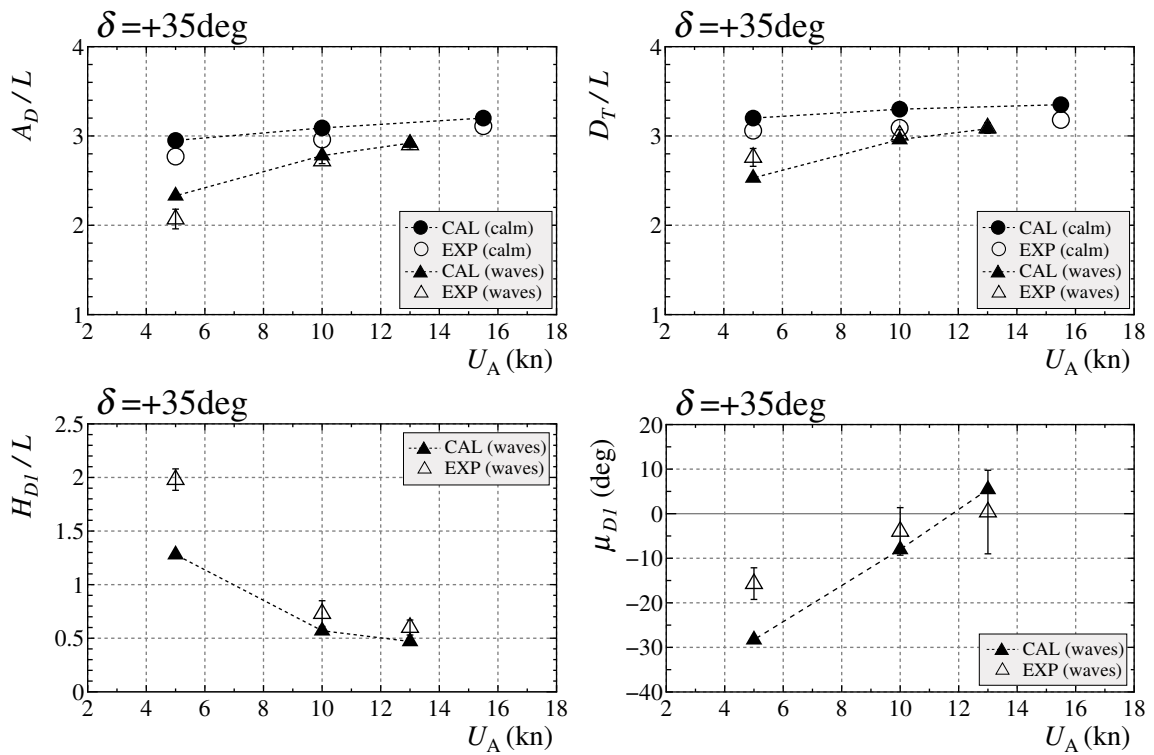
Fig. 5.5: Comparison of turning and drifting indices turning versus approach speed $U_A$ ($\delta = +35°$)
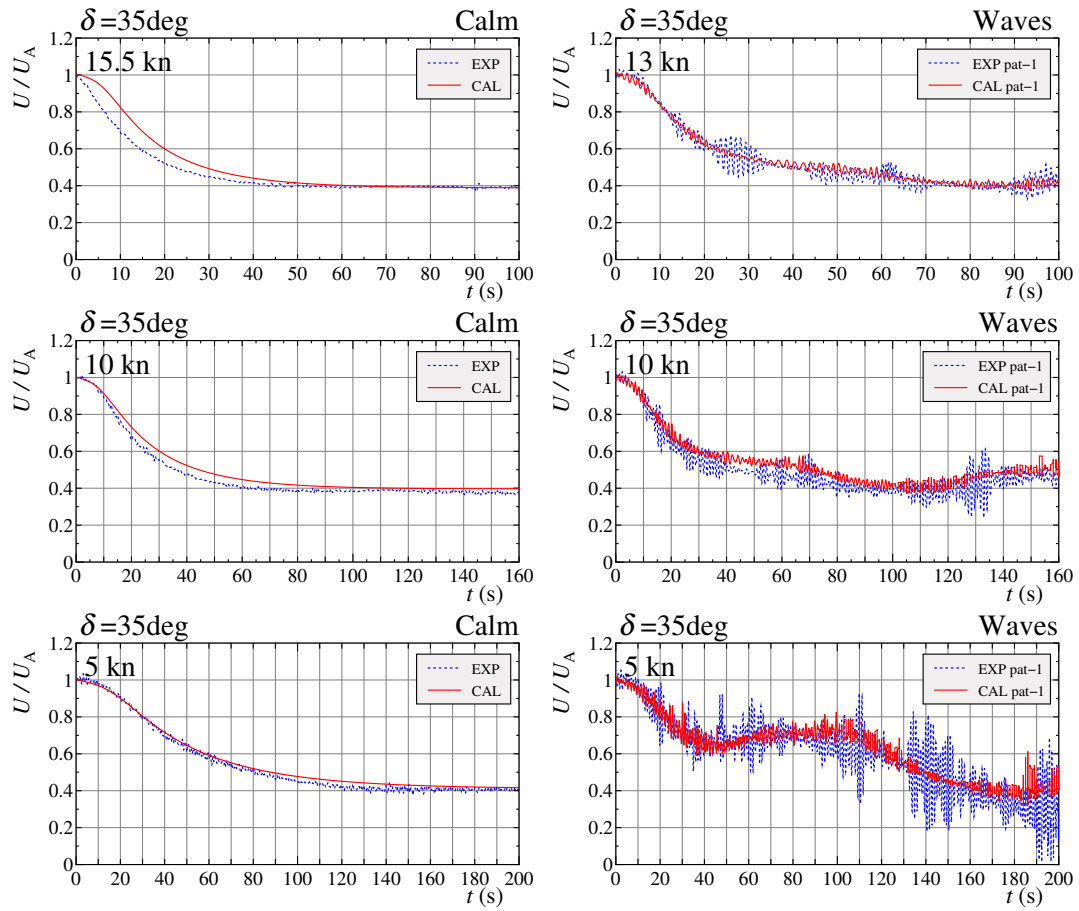
Fig. 5.6: Comparison of time histories of speed drop ratio ($U/U_A$) during $\delta = +35°$ turning in calm water and irregular waves

62
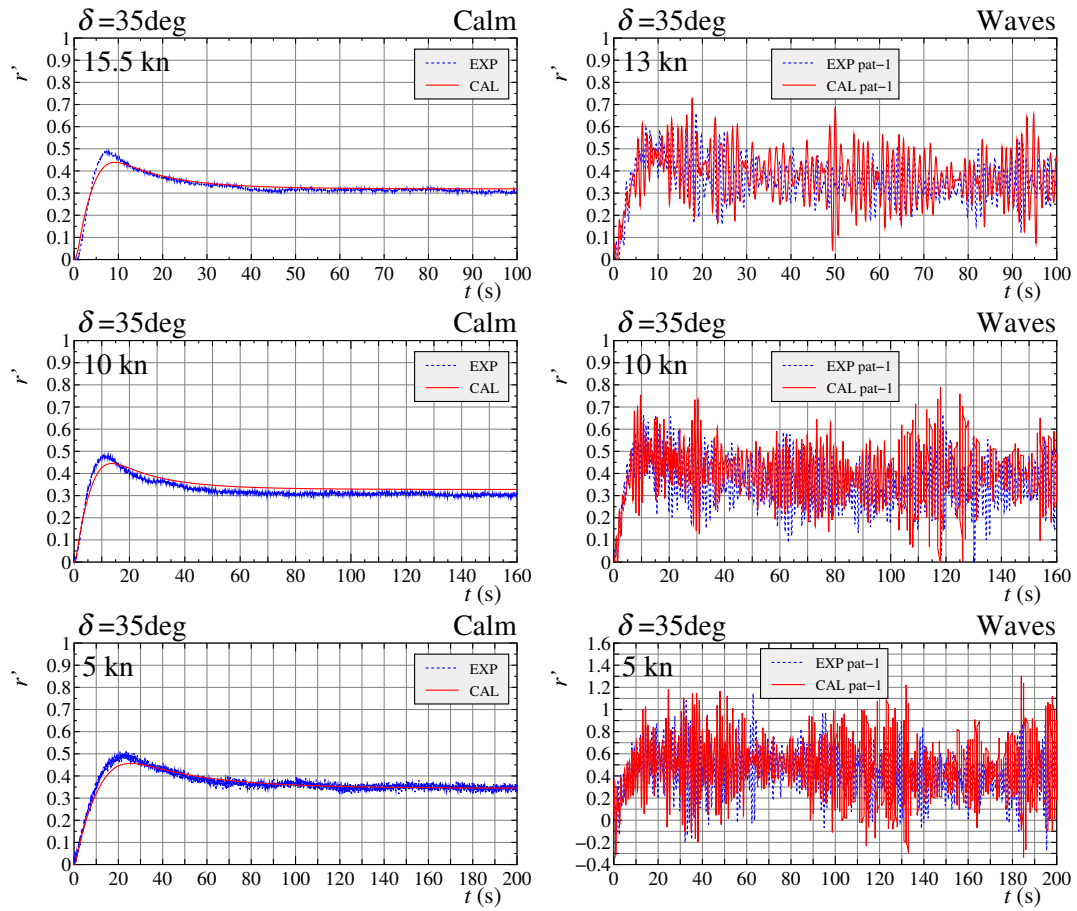
Fig. 5.7: Comparison of time histories of non-dimensional yaw rate ($r'$) during $\delta = +35°$ turning in calm water and irregular waves
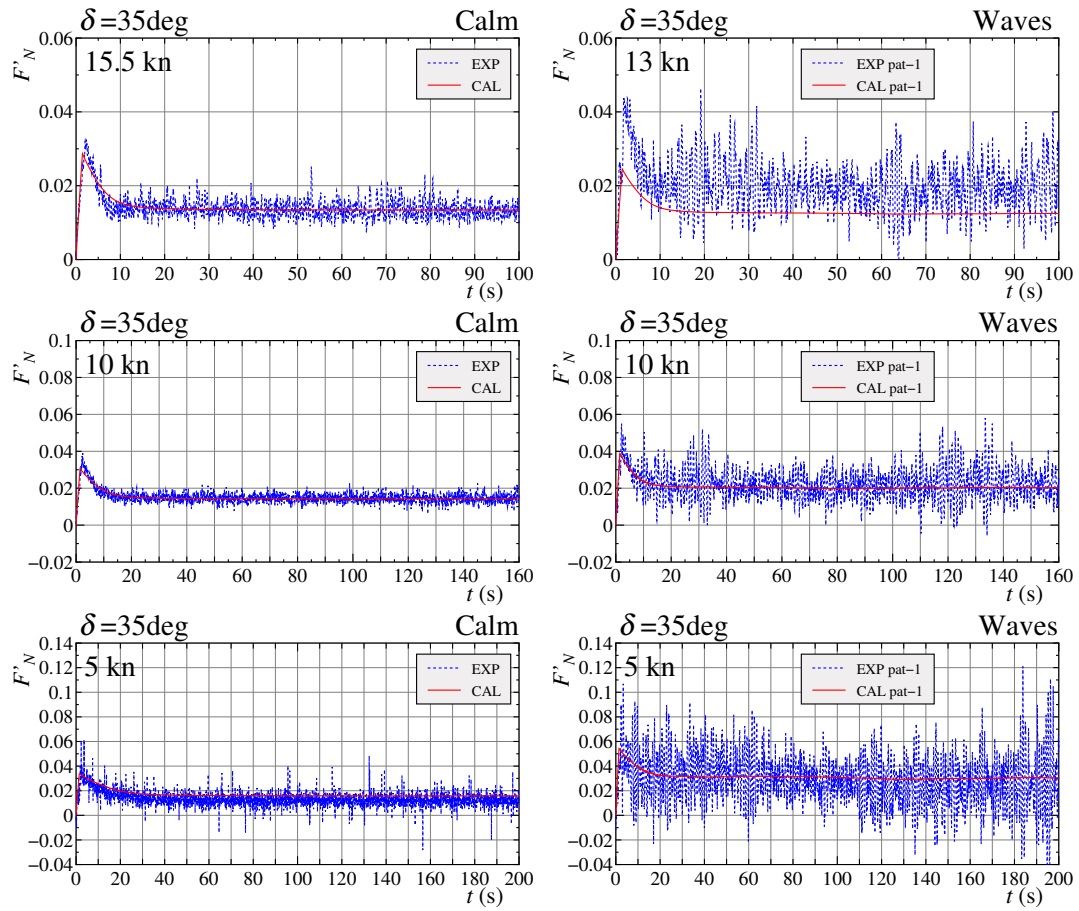
Fig. 5.8: Comparison of time histories of rudder normal force coefficient $(F'_N)$ during $\delta = +35°$ turning in calm water and irregular waves
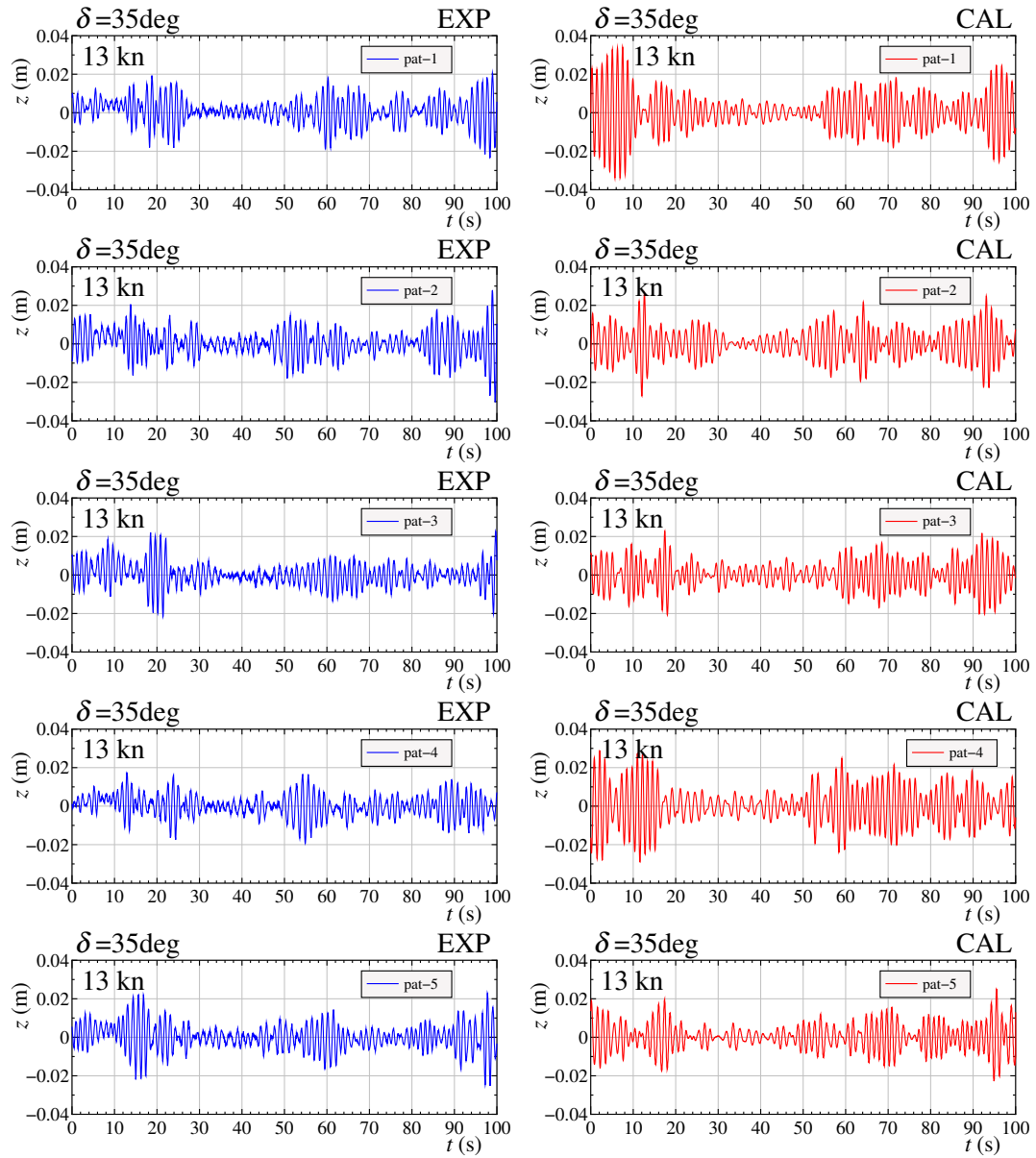
Fig. 5.9: Comparison of time histories of heave ($z$) during $\delta = +35°$ turning in irregular waves at $U_A = 13$ kn

65
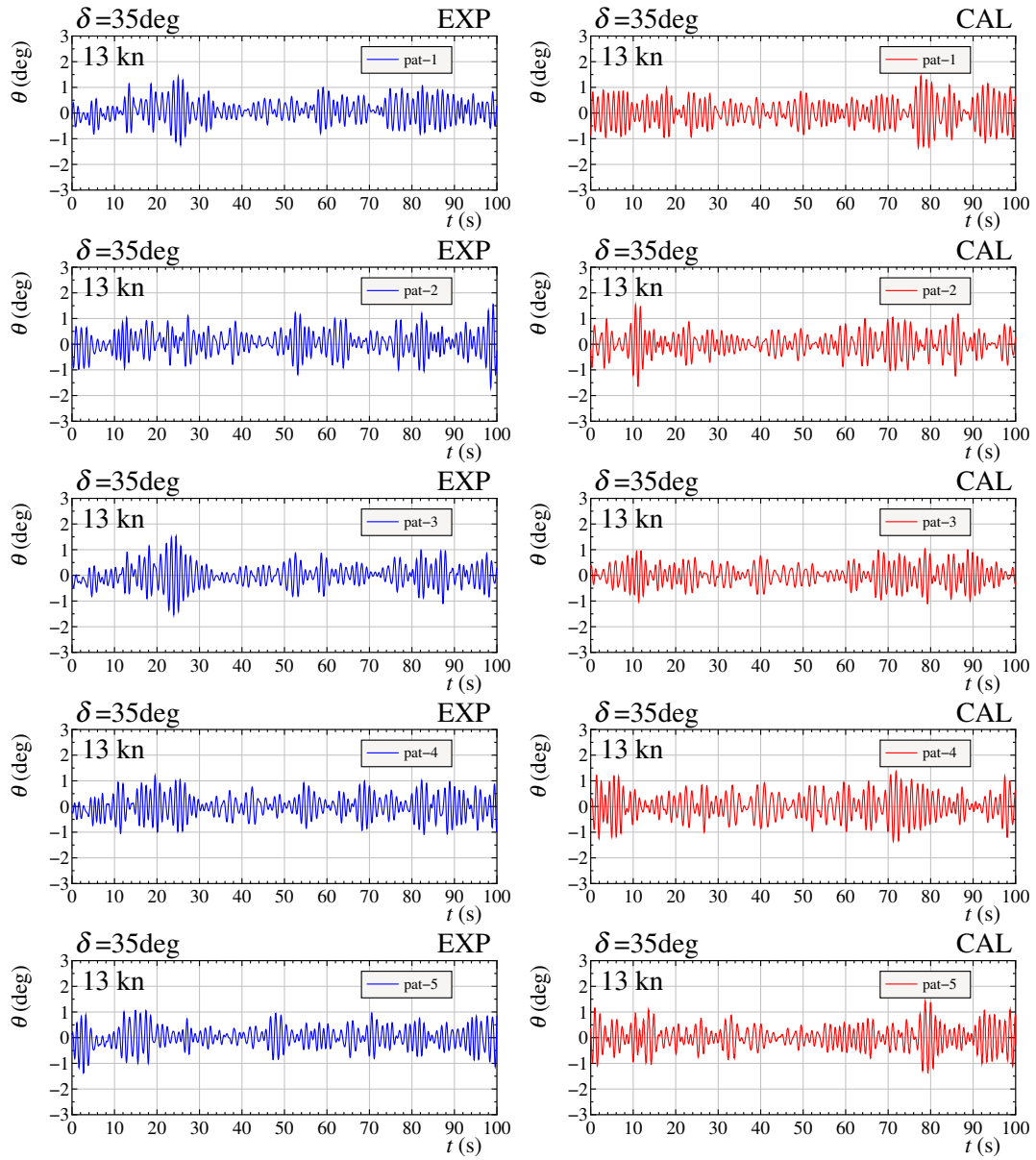
Fig. 5.10: Comparison of time histories of pitch ($\theta$) during $\delta = +35°$ turning in irregular waves at $U_A = 13$ kn
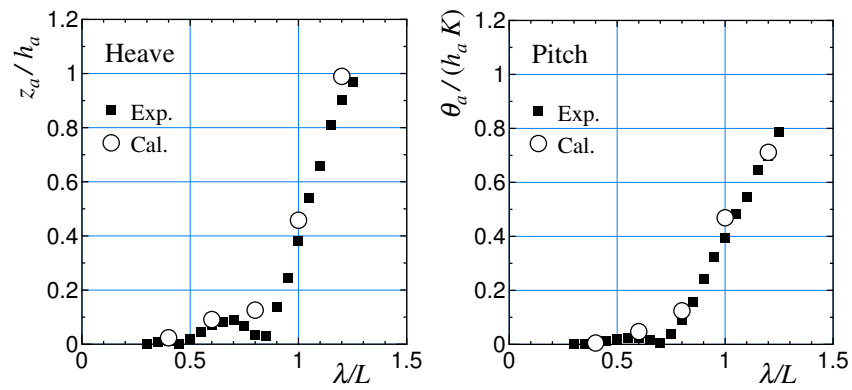
Fig. 5.11: Comparison of non-dimensional amplitudes of heave and pitch during straight moving in regular head waves for KVLCC2 model ($U = 15.5\,\mathrm{kn}$, and incident wave amplitude $h_a = 1.65\,\mathrm{m}$ in full-scale)

## 5.8　Summary for turning simulation in irregular waves

From this chapter, the summary are the followings:

1. Turning simulations for KVLCC2 model with rudder angle $\delta = \pm 35°$ in calm water and short-crested irregular waves were performed by utilizing the proposed method. In order to validate the results from the method, the obtained results were compared with the free-running model test results provided in chapter 3. As a result, it was found that the present method can simulate both the turning motion in the irregular waves and the wave-induced motions during turning with practical accuracy in short computational time, although there is some room for improvement in the low approach speed range (about 5 kn).

2. The validation works in this chapter confirm the reliability of the proposed simulation method. The present method is useful for applying to a ship-handling simulator.

# Chapter 6

# Theoretical Consideration during Turning

## 6.1 Theory of wave-induced drift motion during turning

In this sub-chapter, the wave-induced drift motion of ships during turning is theoretically investigated.

### 6.1.1 Motion equations

In this theoretical analysis, the following assumptions apply:

- Rudder angle $\delta$, lateral velocity $v$, and yaw rate $r$ are small.

- Wave-induced steady lateral force and yaw moment acting on the ship are small.

- Surge-coupling effects on maneuvering are neglected. The ship speed $U$ is given.

Therefore, the motion equations of the ship is simplified to the equations with respect to sway and yaw.

In the framework of the ship-fixed coordinate system, the motion equations in the non-dimensional form are expressed as

$$(m' + m'_y)\dot{v}' + (m' + m'_x)r' = Y', \tag{6.1}$$

$$(I'_{zz} + J'_{zz})\dot{r}' = N', \tag{6.2}$$

where $m$ is the ship's mass, $I_{zz}$ is the moment of inertia for yaw, $m_x$ is the added mass for surge, $m_y$ is the added mass for sway, $J_{zz}$ is the added moment of inertia for yaw, $Y$

is the lateral force acting on the ship, and $N$ is the yaw moment around the center of gravity acting on the ship. These equations are non-dimensionalized by using the water density $\rho$, ship length $L$, ship draft $d$, and ship speed $U$ as

$$m', m'_x, m'_y = \frac{m, m_x, m_y}{(1/2)\rho L^2 d}, \quad I'_{zz}, J'_{zz} = \frac{I_{zz}, J_{zz}}{(1/2)\rho L^4 d},$$

$$Y' = \frac{Y}{(1/2)\rho L d U^2}, \quad N' = \frac{N}{(1/2)\rho L^2 d U^2},$$

$$v' = v/U, \quad r' = rL/U.$$

The dot notation denotes the ordinary differential with respect to non-dimensionalized time $t'(= tU/L)$.

$Y'$ and $N'$ are expressed as

$$\left.\begin{aligned}
Y' &= Y'_v v' + Y'_r r' + Y'_\delta \delta + Y'_W(\chi_r) \\
N' &= N'_v v' + N'_r r' + N'_\delta \delta + N'_W(\chi_r)
\end{aligned}\right\}. \tag{6.3}$$

$Y'_v$, $Y'_r$, $N'_v$, and $N'_r$ are linear hydrodynamic derivatives on maneuvering. $Y'_\delta$ and $N'_\delta$ are rudder force coefficients. $Y'_W(\chi_r)$ and $N'_W(\chi_r)$ are coefficients of the wave-induced steady lateral force and the yaw moment in irregular waves, respectively; are each functions of the relative wave direction $\chi_r(= \chi - \psi)$; and are expressed as follows:

$$\left.\begin{aligned}
Y'_W(\chi_r) &= \frac{2}{F_n^2} \frac{H_{1/3}^2}{Ld} C_Y(\chi_r) \\
N'_W(\chi_r) &= \frac{2}{F_n^2} \frac{H_{1/3}^2}{Ld} C_N(\chi_r)
\end{aligned}\right\}, \tag{6.4}$$

where $F_n$ is the Froude number based on $L$, and $H_{1/3}$ is the significant wave height. $C_Y$ and $C_N$ are defined as

$$\left.\begin{aligned}
C_Y(\chi_r) &= \frac{Y_W(\chi_r)}{\rho g H_{1/3}^2 L} \\
C_N(\chi_r) &= \frac{N_W(\chi_r)}{\rho g H_{1/3}^2 L^2}
\end{aligned}\right\}, \tag{6.5}$$

where $g$ is the acceleration gravity.

$v'$, $r'$, heading angle $\psi$, and $\delta$ are assumed as follows:

$$\left.\begin{aligned}
v' &= v'_0 + \Delta v' \\
r' &= r'_0 + \Delta r' \\
\psi &= \psi_0 + \Delta \psi \\
\delta &= \delta_0
\end{aligned}\right\}. \tag{6.6}$$

The subscript 0 implies the quantity in calm water; substituting $\Delta$ implies the change

in quantity due to the wave effect. $\psi_0$ is assumed to be $O(1)$, and the other terms are assumed to be $O(\varepsilon)$, where $\varepsilon$ is a small quantity.

By substituting eq. (6.6) into eqs. (6.1) and (6.2) and linearizing the equations, obtain two sets of motion equations: one set gives the motion equations in calm water and the other set gives the equations for motion change due to the wave effect. The motion equations in calm water are expressed as

$$(m' + m_y')\dot{v}_0' + (m' + m_x')r_0' = Y_v'v_0' + Y_r'r_0' + Y_\delta'\delta_0, \tag{6.7}$$

$$(I_{zz}' + J_{zz}')\dot{r}_0' = N_v'v_0' + N_r'r_0' + N_\delta'\delta_0. \tag{6.8}$$

By eliminating $v_0'$ in eqs. (6.7) and (6.8), the following equation is obtained:

$$T_1'T_2'\ddot{r}'_0 + (T_1' + T_2')\dot{r}'_0 + r_0' = T_3'\dot{\delta}'_0 + K'\delta_0, \tag{6.9}$$

where

$$T_1'T_2' = (m' + m_y')(I_{zz}' + J_{zz}')/C, \tag{6.10}$$

$$T_1' + T_2' = -\left[(m' + m_y')N_r' + (I_{zz}' + J_{zz}')Y_v'\right]/C, \tag{6.11}$$

$$T_3' = (m' + m_y')N_\delta'/C, \tag{6.12}$$

$$K' = \left(Y_\delta'N_v' - Y_v'N_\delta'\right)/C, \tag{6.13}$$

$$C = Y_v'N_r' - (Y_r' - m' - m_x')N_v'. \tag{6.14}$$

These formulas coincide with the formulas derived by Nomoto et al.[39].

On the other hand, the equations for the motion changes due to the wave effect are expressed as

$$(m' + m_y')\Delta\dot{v}' + (m' + m_x')\Delta r' = Y_v'\Delta v' + Y_r'\Delta r' + Y_W'(\chi_r), \tag{6.15}$$

$$(I_{zz}' + J_{zz}')\Delta\dot{r}' = N_v'\Delta v' + N_r'\Delta r' + N_W'(\chi_r). \tag{6.16}$$

For simplicity, the Taylor expansion is applied to $Y_W'(\chi_r)$ at $\psi = \psi_0$ as follows:

$$Y_W'(\chi_r) \simeq Y_W'(\chi_0) + \Delta\psi\frac{\partial Y_W'}{\partial\psi} + ....$$

$$= Y_W'(\chi_0) + O(\varepsilon^2), \tag{6.17}$$

where $\chi_0$ is defined as $\chi - \psi_0$. Therefore, the following motion equations are obtained as

$$(m' + m_y')\Delta\dot{v}' + (m' + m_x')\Delta r' = Y_v'\Delta v' + Y_r'\Delta r' + Y_W'(\chi_0), \tag{6.18}$$

$$(I_{zz}' + J_{zz}')\Delta\dot{r}' = N_v'\Delta v' + N_r'\Delta r' + N_W'(\chi_0). \tag{6.19}$$

If the heading angle in calm water $\psi_0$ is obtained by solving eq. (6.9), $\chi_0$ is known when $\chi$ is given, and $Y_W'(\chi_0)$ and $N_W'(\chi_0)$ are also known. By eliminating $\Delta v'$ in eqs. (6.18)

and (6.19), the following equation is obtained:

$$T_1' T_2' \Delta \ddot{r}' + (T_1' + T_2') \Delta \dot{r}' + \Delta r' = F_W'(\chi_0), \tag{6.20}$$

where

$$F_W'(\chi_0) = \left[ N_v' Y_W'(\chi_0) - Y_v' N_W'(\chi_0) \right] / C. \tag{6.21}$$

Similarly, eliminating $\Delta r'$ in eqs. (6.18) and (6.19), the following equation is obtained:

$$T_1' T_2' \Delta \ddot{v}' + (T_1' + T_2') \Delta \dot{v}' + \Delta v' = F_V'(\chi_0), \tag{6.22}$$

where

$$F_V'(\chi_0) = \left[ N_r' Y_W'(\chi_0) - (Y_r' - m' - m_x') N_W'(\chi_0) \right] / C. \tag{6.23}$$

Eq. (6.20) for $\Delta r'$ and eq. (6.22) for $\Delta v'$ are base equations for the motion changes due to the wave effect.

## 6.1.2 Ship position

In the space-fixed coordinate system, the equation for the non-dimensionalized ship position $(x', y')$ is expressed as

$$\left. \begin{array}{rcl} \dot{x}' &=& \cos \psi - v' \sin \psi \\ \dot{y}' &=& \sin \psi + v' \cos \psi \end{array} \right\}. \tag{6.24}$$

Substituting eq. (6.6) into eq. (6.24) and linearizing the equation, the followings are obtained:

$$\left. \begin{array}{rcl} \dot{x}' &=& \dot{x}_0' + \Delta \dot{x}' \\ \dot{y}' &=& \dot{y}_0' + \Delta \dot{y}' \end{array} \right\}, \tag{6.25}$$

where

$$\dot{x}_0' = \cos \psi_0 - v_0' \sin \psi_0, \tag{6.26}$$

$$\dot{y}_0' = \sin \psi_0 + v_0' \cos \psi_0, \tag{6.27}$$

$$\Delta \dot{x}' = -(\Delta \psi + \Delta v') \sin \psi_0, \tag{6.28}$$

$$\Delta \dot{y}' = (\Delta \psi + \Delta v') \cos \psi_0. \tag{6.29}$$

$(x_0', y_0')$ represents the ship's position in calm water, and $(\Delta x', \Delta y')$ expresses the change in the ship's position due to the wave effect.

### 6.1.3 Solution of steady turning in calm water

Assuming a step-like steering with rudder angle $\delta_0$ and $T_3' = 0$, the solution of eq. (6.9) is derived under the initial condition of $\dot{r}' = r' = 0$ at $t' = 0$:

$$r' = K'\delta_0 \left[ 1 - \frac{T_1'}{T_1' - T_2'} e^{-t'/T_1'} + \frac{T_2'}{T_1' - T_2'} e^{-t'/T_2'} \right]. \tag{6.30}$$

Considering a steady turning condition after time has elapsed, the exponential terms approach zero, and obtain the following:

$$r_S' = K'\delta_0, \tag{6.31}$$

$$\psi_S = r_S' t' + \psi_{0I}, \tag{6.32}$$

where $r_S'$ is the non-dimensional yaw rate during steady turning, $\psi_S$ is the heading angle during steady turning, and $\psi_{0I}$ is an integration constant. Then, eqs. (6.26) and (6.27) are expressed as

$$\left. \begin{aligned} \dot{x}_0' &= \cos(r_S' t' + \psi_{0I}) - v_S' \sin(r_S' t' + \psi_{0I}) \\ \dot{y}_0' &= \sin(r_S' t' + \psi_{0I}) + v_S' \cos(r_S' t' + \psi_{0I}) \end{aligned} \right\}, \tag{6.33}$$

where $v_S'$ is the non-dimensional lateral velocity during steady turning. Integrating eqs. (6.33) by $t'$, the following is obtained:

$$\left. \begin{aligned} x_0' &= \sin(r_S' t' + \psi_{0I})/r_S' + v_S' \cos(r_S' t' + \psi_{0I})/r_S' + x_{0I}' \\ y_0' &= -\cos(r_S' t' + \psi_{0I})/r_S' + v_S' \sin(r_S' t' + \psi_{0I})/r_S' + y_{0I}' \end{aligned} \right\}, \tag{6.34}$$

where $x_{0I}'$ and $y_{0I}'$ are integration constants. Rewriting eq.(6.34), the following is obtained:

$$\left. \begin{aligned} x_0' &= \sin(r_S' t' + v_S' + \psi_{0I})/r_S' + x_{0I}' \\ y_0' &= -\cos(r_S' t' + v_S' + \psi_{0I})/r_S' + y_{0I}' \end{aligned} \right\}. \tag{6.35}$$

This represents a circular motion with the radius of $1/r_S'$.

### 6.1.4 Solution of turning change due to wave effect

Next considers the solution of eq. (6.20), where the absolute wave direction $\chi$ is assumed to be zero. This means that the head wave is assumed at the time of approaching before steering is initiated. In addition, for analytical treatment of the problem, $F_W'$ and $F_V'$ are assumed to be expressed using the sine function as

$$F_W'(\chi_0) \simeq A_W \sin(\chi_0), \tag{6.36}$$

$$F_V'(\chi_0) \simeq A_V \sin(\chi_0). \tag{6.37}$$

Considering the condition after time has elapsed, we can approximate as $\chi_0 \simeq -r'_S t'$, and the following are obtained:

$$F'_W(\chi_0) = -A_W \sin(r'_S t'), \tag{6.38}$$

$$F'_V(\chi_0) = -A_V \sin(r'_S t'). \tag{6.39}$$

The motion equation (6.20) is then rewritten as

$$T'_1 T'_2 \Delta \ddot{r}' + (T'_1 + T'_2)\Delta \dot{r}' + \Delta r' = -A_W \sin(r'_S t'), \tag{6.40}$$

Here the solution for $\Delta r'$ is assumed to be

$$\Delta r' = A_W \Im[r_C \exp(i r'_S t')], \tag{6.41}$$

where $\Im$ is obtained by taking the imaginary part of the complex number, and $i$ is $\sqrt{-1}$. By substituting eq. (6.41) into eq. (6.40), the following is obtained:

$$
\begin{aligned}
r_C &= \frac{-1}{i(T'_1 + T'_2)r'_S + 1 - T'_1 T'_2 r'^2_S} \\
&= -1 + i(T'_1 + T'_2)r'_S + O(r'^2_S). 
\end{aligned}
\tag{6.42}
$$

Therefore, the solution is expressed as

$$\Delta r' = A_W C_W \sin(r'_S t' + \epsilon_W), \tag{6.43}$$

where

$$C_W = \sqrt{1 + (T'_1 + T'_2)^2 r'^2_S} \simeq 1, \tag{6.44}$$

$$\epsilon_W = \tan^{-1}\left[\frac{(T'_1 + T'_2)r'_S}{T'_1 T'_2 r'^2_S - 1}\right] \simeq -\tan^{-1}\left[(T'_1 + T'_2)K'\delta_0\right]. \tag{6.45}$$

When eq. (6.43) is integrated by $t'$, the heading change due to the wave effect $\Delta\psi$ can be expressed as

$$\Delta\psi = -\frac{A_W}{r'_S}\cos(r'_S t' + \epsilon_W) + \psi_I, \tag{6.46}$$

where $\psi_I$ is an integration constant. Similarly, $\Delta v'$ is obtained as

$$\Delta v' = A_V \sin(r'_S t' + \epsilon_W). \tag{6.47}$$

By substituting the above into eqs. (6.28) and (6.29), the following are obtained:

$$\Delta \dot{x}' = -\left[A_V \sin(r'_S t' + \epsilon_W) - \frac{A_W}{r'_S}\cos(r'_S t' + \epsilon_W) + \psi_I\right]\sin(r'_S t'), \tag{6.48}$$

$$\Delta \dot{y}' = \left[A_V \sin(r'_S t' + \epsilon_W) - \frac{A_W}{r'_S}\cos(r'_S t' + \epsilon_W) + \psi_I\right]\cos(r'_S t'). \tag{6.49}$$

When eqs. (6.48) and (6.49) are integrated by $t'$, the turning trajectory change due to the wave effect $(\Delta x', \Delta y')$ are obtained as

$$
\begin{aligned}
\Delta x' &= -\frac{A_W}{4r_S'^2}\cos(2r_S't' + \epsilon_W) - t'\frac{A_W}{2r_S'}\sin\epsilon_W + \frac{\psi_I}{r_S'}\cos(r_S't') \\
&\quad + \frac{A_V}{4r_S'}\sin(2r_S't' + \epsilon_W) - t'\frac{A_V}{2}\cos\epsilon_W + x_{0I}', \qquad (6.50)
\end{aligned}
$$

$$
\begin{aligned}
\Delta y' &= -\frac{A_W}{4r_S'^2}\sin(2r_S't' + \epsilon_W) - t'\frac{A_W}{2r_S'}\cos\epsilon_W + \frac{\psi_I}{r_S'}\sin(r_S't') \\
&\quad + \frac{A_V}{4r_S'}\cos(2r_S't' + \epsilon_W) + t'\frac{A_V}{2}\sin\epsilon_W + y_{0I}'. \qquad (6.51)
\end{aligned}
$$

Eqs. (6.50) and (6.51) are composed of three terms: a varying term with frequency $2r_S'$, a varying term with frequency $r_S'$, and a term that is proportional to $t'$. Since the first two terms vary periodically with $t'$, it can been seen that the drift motion that occurs during the turning of ships in waves comes from the term that is proportional to $t'$. The term that is proportional to $t'$ emerges from the time integration in terms of $\sin^2(r_S't')$ and $\cos^2(r_S't')$ in eqs. (6.48) and (6.49). Initially, this comes from the interaction between the ship's heading in calm water and the heading change due to the wave effect (see eqs. (6.28) and (6.29)).

Now, consider a condition in which the heading changes by $2\pi$ from a certain time $t' = t_0'$. When $\Delta t'$ is denoted as the time it takes, $\Delta t'$ is expressed as $2\pi/r_S'$. The coordinates of the trajectory change due to waves at $t' = t_0'$ are represented by $(\Delta x_{p0}', \Delta y_{p0}')$, and the coordinates of the trajectory change after the heading changes by $2\pi$ are represented by $(\Delta x_{p2\pi}', \Delta y_{p2\pi}')$. Consequently, the distance between the two coordinates (drifting distance) $l_{01}'$ and the inclination (drifting direction) $\theta_{01}$ are calculated as follows:

$$
\begin{aligned}
l_{01}' &= \sqrt{\left(\Delta x_{p2\pi}' - \Delta x_{p0}'\right)^2 + \left(\Delta y_{p2\pi}' - \Delta y_{p0}'\right)^2} \\
&= \frac{\Delta t'}{2r_S'}\sqrt{A_W^2 + A_V^2 r_S'^2} \\
&\simeq \frac{\pi|A_W|}{r_S'^2}, \qquad (6.52)
\end{aligned}
$$

$$
\begin{aligned}
\theta_{01} &= \tan^{-1}\left[\frac{\Delta x_{p2\pi}' - \Delta x_{p0}'}{\Delta y_{p2\pi}' - \Delta y_{p0}'}\right] \\
&= \tan^{-1}\left[\frac{-A_W\sin\epsilon_W - A_V r_S'\cos\epsilon_W}{-A_W\cos\epsilon_W + A_V r_S'\sin\epsilon_W}\right] \\
&\simeq \epsilon_W. \qquad (6.53)
\end{aligned}
$$

$l_{01}'$ and $\theta_{01}$ are determined independently of time. $l_{01}'$ is proportional to the square of the turning radius in calm water and is proportional to $A_W$. Therefore, as shown in eq. (6.4), $l_{01}'$ is proportional to $H_{1/3}^2$ and is inversely proportional to $F_n^2$. $\theta_{01}$ coincides with $\epsilon_W$ as defined in eq. (6.45). $\epsilon_W$ is calculated using the index of maneuvering response $T_1' + T_2'$, the strength of turning $K'$, and the rudder angle $\delta_0$. $\theta_{01}$ does not depend on ship speed.

## 6.2 Calculation of drifting indices during turning in waves

Using eqs. (6.52) and (6.53), the drifting indices ($H'_D$, $\mu_D$) of KVLCC2 and KCS in waves are calculated. Note that between $H'_D$ and $l'_{01}$, and $\mu_D$ and $\theta_{01}$, there are relationships of $H'_D = l'_{01}$, and $\mu_D = \pi/2 + \theta_{01}$, respectively.

### 6.2.1 Input data used in calculation

Table 6.1 shows linear derivatives and maneuverability indices for KVLCC2 and KCS, which are used for the calculations. These were estimated based on the captive model test data[29][30]. In the table, $Y'_v$, $Y_r - m' - m'_x$, $N'_v$, and $N'_r$ include the propeller and rudder effects. It should be noted that the derivatives of KVLCC2 were slightly tuned so as to be course stable since this ship was originally course unstable with a negative $C$-value.

Table 6.1: Linear derivatives and maneuverability indices for KVLCC2 and KCS

|  | KVLCC2 | KCS |
|---|---|---|
| $Y'_v$ | $-0.3780$ | $-0.2646$ |
| $Y_r - m' - m'_x$ | $-0.2213$ | $-0.1124$ |
| $N'_v$ | $-0.1111$ | $-0.0968$ |
| $N'_r$ | $-0.0757$ | $-0.0608$ |
| $Y'_\delta$ | $-0.0564$ | $-0.0811$ |
| $N'_\delta$ | $0.0277$ | $0.0391$ |
| $C$ | $0.0040$ | $0.0052$ |
| $T'_1 + T'_2$ | $12.49$ | $4.935$ |
| $K'$ | $4.179$ | $3.496$ |

The drifting indices were calculated in the wave conditions shown in Table 3.4 in chapter 3. To calculate drifting indices in waves theoretically, $F'_W$ and $F'_V$ are required. For this purpose, average values of the wave-induced lateral force and the yaw moment in irregular waves must be provided. These averaged values can be obtained by the short-term prediction method based on the wave-induced lateral force and the yaw moment in regular waves calculated using the 3D panel method without a forward speed effect[34]. Fig. 6.1 shows the calculation results of $F'_W$ and $F'_V$ versus the relative wave direction ($\chi_r$) and approximation curves based on the sine function. The accuracy of the approximation curves for $F'_W$ and $F'_V$ is acceptable for practical purposes.
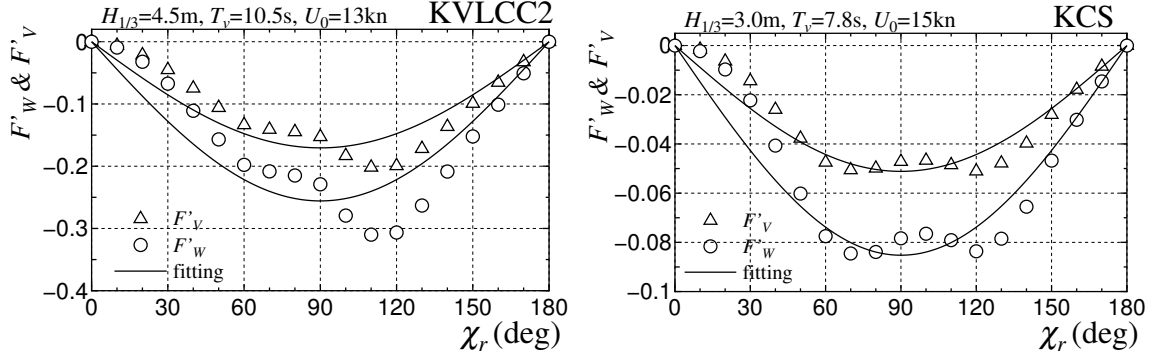
Fig. 6.1: Calculation results of $F'_W$ and $F'_V$ and approximation curves using sine functions for KVLCC2 and KCS

## 6.2.2 Comparison of drifting indices in waves

Figs. 6.2 and 6.3 show the comparisons of $H_D/L$ and $\mu_D$ respectively for both KVLCC2 and KCS. $H_D/L$ and $\mu_D$ were calculated by theoretical formulas with changing ship speed $U_A$ and were compared with the test results. The calculated rudder angle was set at 20° for both models. Based on the comparisons, the overall tendency of $H_D/L$ for both models are captured well. The predicted $H_D/L$ for both models becomes small with the increase of ship speed. $\mu_D$, however, is predicted constant at all ship speeds for both KVLCC2 and KCS and close with the test results only at high ship speeds, and the difference with the test results are gradually becomes larger with the reduction of ship speeds.
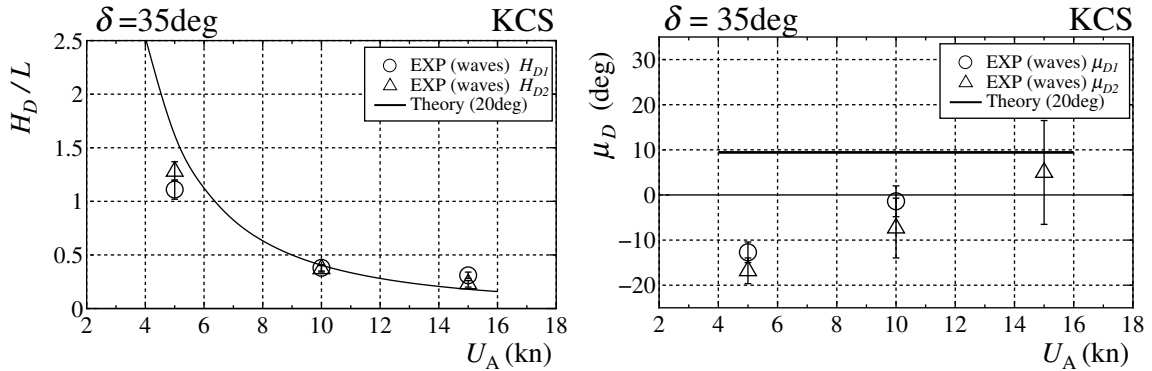


Fig. 6.2: Comparison of $H_D/L$ and $\mu_D$ for KCS in waves

In investigating further, in each graph of $H_D/L$ and $\mu_D$, two calculation results using the formulas are plotted for $\delta = 20°$ and 35° for KVLCC2 as shown in Fig. 6.3. Since the rudder force coefficients ($Y'_\delta$, $N'_\delta$) used in the calculation were obtained based on the measured values at a small rudder angle, the rudder force at $\delta = 35°$ is normally over-estimated. As expected, the result of $H_{D1}/L$ at $\delta = 35°$ is small as a whole, but the result at $\delta = 20°$ captures well a tendency of the test result. On the other hand, the influence of the rudder angle on $\mu_{D1}$ is not significant. In the same graphs, the $H_{D1}/L$ and $\mu_{D1}$ that were calculated using the proposed simulation method for KVLCC2 at 35°

in previous chapter are also included. The calculated value of $H_{D1}/L$ from the simulation method based on two-time scale concept show a close tendency similar to that of the free-running test result, followed by the calculation value from the theoretical formula. The comparison shows the $H_{D1}/L$ is inversely proportional to $F_n^2$ and this is as suggested by the theoretical formula accordingly. Similarly, the calculated value of $\mu_{D1}$ from the simulation predicts with close tendency with test result, followed by the value from the theoretical value where is constant regardless of $U_A$ and the order of magnitude is close to the test result. In the tests, $\mu_{D1}$ increases with an decrease in $U_A$. It is qualitatively different. The reason why formula does not capture this tendency is due to non-linear effects, which are neglected in the derivation of the formula, related to turning motions in waves.
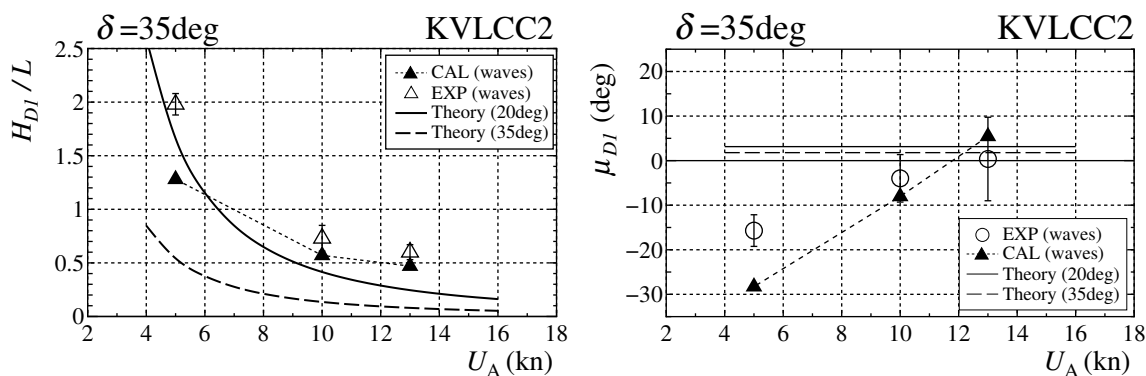


Fig. 6.3: Comparison of $H_D/L$ and $\mu_D$ for KVLCC2 in waves

# 6.3 Summary for analytical study for steady turning in irregular waves

In this analytical study, the effect of speed on ship turning in irregular waves is understood. The calculation results using the present formulas for $H_D/L$ and $\mu_D$ roughly agreed with the turning test results and turning simulation results. The formulas are useful for a better understanding of the wave-induced drift motion of ships during turning. The linear assumption in the theory formulation confirmed the non-linearity effect is exist.

# Chapter 7

# Conclusions and recommendations for future works

## 7.1 Conclusions

This study investigated the turning behavior of ships in short-crested irregular waves using free-running model tests, two-time scale simulation method and theoretically. Two types of ship were selected for the investigation: a KVLCC2 large tanker and a KCS container ship. The tests were performed in head waves at the time of approaching with the significant wave height 4.5 m and 3.0 m for KVLCC2 and KCS respectively. First, a repeat test was conducted for KCS turning in regular waves with rudder angle $\pm 35°$. The repeat test then was performed for KVLCC2, in which the turning test of rudder angle $\pm 35°$ was repeated five times for the same wave pattern. Next, five waves with different patterns were generated with the same wave conditions (significant wave height, mean wave period, and main wave direction). Turning tests were conducted for KVLCC2 and KCS in these waves. From the obtained test results, the average values and standard deviations of turning indices (advance $A_D$ and tactical diameter $D_T$), and drifting indices in waves (drifting distance $H_D$ and drifting direction $\mu_D$) were obtained. The obtained turning indices and drifting indices then were compared with the results from the two-time scale simulation method, together with the time histories motion and wave-induced motion during turning in regular and irregular waves. Finally, theoretical formulas for conventionally calculating $H_D/L$ and $\mu_D$ were derived on the assumptions of small rudder angle, small maneuvering motions and small wave-induced steady forces. As a result, the following conclusions are obtained:

1. With a decrease in the approach speed $U_A$ of the ships running in the same wave condition, $A_D$ decreases and $D_T$ does not change significantly. For the head wave condition in approaching, the wave effect on $A_D$, which is the longitudinal distance during turning, is significant. In contrast, the wave effect on $D_T$ is relatively small as it signifies the lateral distance during turning. When reducing $U_A$ in the same wave condition, the drifting distance $H_D$ increases as the influence of the waves

on the ships becomes relatively larger. The drifting direction $\mu_D$ also increases with decrease in $U_A$, and the tendency of the ship to drift towards the location $(x_s, y_s) = (0, 0)$ of rudder executing point becomes more remarkable. A variation in turning trajectories was observed. This may have resulted from the influence of the slowly varying second-order wave forces acting on the ship models. However, the influence on the trajectories is negligible in view of practical purposes. The experimental data shown in this paper is useful for the validation of the simulation method of ship maneuvering in irregular waves. The two-time scale concept is valid to be used based on the comparisons of time histories and wave-induced motions between ship turning calm water and irregular waves conditions.

2. Based on the results from the conducted free-running test for ship turning in regular and irregular waves, 6-DOF motion simulation method of ships with steering in regular waves and irregular waves based on the two time-scale concept was established. In order to validate the present method, turning simulations for KCS model with rudder angle $\delta = \pm 35°$ in calm water and regular waves were performed and the obtained results were compared with the free-running model test results. Next, KVLCC2 model with rudder angle $\delta = \pm 35°$ in calm water and short-crested irregular waves were performed and the obtained results were compared with the free-running model test results. The wave condition for the irregular waves was the significant wave height $H_{1/3} = 4.5$ m, the average wave period $T_0 = 10.5$ s at full-scale, and main wave direction $\chi = 0°$ when approaching. As a result, it was found that the present method can simulate both the turning motion in the irregular waves and the wave-induced motions during turning with practical accuracy in short computational time, although there is some room for improvement in the low approach speed range (about 5 kn). The present method is useful for applying to a ship-handling simulator.

3. The calculation results using the present theoretical formulas for $H_D/L$ and $\mu_D$ roughly agreed with the turning test results. The formulas are useful for a better understanding of the wave-induced drift motion of ships during turning. It was confirmed that the $H_D$ is proportional to the $H_{1/3}$ and inversely proportional to $U_A$. However, for $\mu_D$ is constant regardless of $U_A$ in the theory calculation due to non-linear effect is neglected in the theoretical derivation formula.

## 7.2  Recommendations for future works

The recommendations for the future works include:

1. The experiment in this research has limitation such as the wave conditions of the irregular waves. The turning test should consider more significant wave heights and average wave periods for comprehensive analysis. Besides that, it also useful to conduct turning tests with smaller rudder angle which are smaller than 35°. Then, the data are used for the validations with the simulation methods.

2. The proposed simulation method that is based on two-time scale concept in this research has limitation on both maneuvering and wave-induced motion models. As for maneuvering model, rudder normal force and propeller thrust do not include the effect of the high-frequency components. Furthermore, the speed effect on the calculation of wave-induced steady lateral force and steady yaw moment are assumed to be negligible. Meantime, the wave-induced motion model has limitation in predicting the ship motion especially the heave and pitch motions during turning in following waves.

3. The analytical study in this research is based on the assumption of steady turning condition. The calculated value of drifting direction $\mu_D$ is constant regardless of $U_A$ in the theory calculation due to non-linear effect is neglected in the theoretical derivation formula. Thus, the analytical study should extend by considering the non-linear effect.

# Bibliography

[1] Hirano, M., Takashina, J., Takeshi, K. and Saruta, T. (1980): Ship Turning Trajectory in Regular Waves, Trans. West-Japan Society of Naval Architects, No.60, pp.17-31.

[2] Ueno, M., Nimura, T. and Miyazaki, H. (2003): Experimental Study on Manoeuvring Motion of a Ship in Waves, Proc. International Conference on Marine Simulation and Ship Maneuverability (MARSIM'03), Kanazawa, Japan.

[3] Nishimura, K. and Hirayama, T. (2003): Maneuvering and Motion Simulation of a Small Vessel in Waves, Proc. International Conference on Marine Simulation and Ship Maneuverability (MARSIM'03), Kanazawa, Japan.

[4] Yasukawa, H. (2006): Simulations of Ship Maneuvering in Waves (1st report: turning motion), J. Japan Society of Naval Architects and Ocean Engineers, Vol.4, pp.127-136. (in Japanese)

[5] Yasukawa, H. (2006): Simulation of Wave-Induced Motions of a Turning Ship, J. Japan Society of Naval Architects and Ocean Engineers, Vol.4, pp.117-126. (in Japanese)

[6] Yasukawa, H. (2008): Simulation of Ship Maneuvering in Waves (2nd report: zig-zag and stopping maneuvers). J. Japan Society of Naval Architects and Ocean Engineers, Vol.7, pp.163-170. (in Japanese)

[7] Yasukawa, H., and Nakayama, Y. (2009): 6-DOF Motion Simulations of a Turning Ship in Regular Waves, Proc. International Conference on Marine Simulation and Ship Maneuverability (MARSIM'09), Panama City.

[8] Lee, S., Hwang, S., Yun, S., Rhee, K. and Seong, W. (2009): An Experimental Study of a Ship Manoeuvrability in in Regular Waves, Proc. International Conference on Marine Simulation and Ship Maneuverability (MARSIM'09), Panama City.

[9] Sanada, Y., Tanimoto, K., Takagi, K., Gui, L., Toda, Y., and Stern, F. (2013): Trajectories for ONR Tumblehome Maneuvering in Calm Water and Waves, Ocean Engineering, Vol.72, pp.45-65.

[10] Sanada, Y., Elshiekh, H., Toda, Y., and Stern, F. (2018): ONR Tumblehome Course Keeping and Maneuvering in Calm Water and Waves J. Marine Science and Technology, DOI 10.1007/s00773-018-0598-3 (published on line; Oct. 2018)

[11] Sprenger, F., Maron, A., Delefortrie, G., van Zwijnsvoorde, T., Cura-Hochbaum, A., Lengwinat, A. and Papanikolaou, A. (2017): Experimental Studies on Seakeeping and Maneuverability of Ships in Adverse Weather Conditions, J. Ship Research, Vol.61, No.3, pp.131-152.

[12] Nonaka, K. (1990): Manoeuvring Motion of a Ship in Waves, Proc. International Conference on Marine Simulation (MARSIM1990), Tokyo, pp.422-430.

[13] McCreight, W. R. (1986): Ship Maneuvering in Waves, Proc. 16th Symp. on Naval Hydrodynamics, Berkeley, pp.456-469.

[14] Hamamoto, T. and Saito, K. (1992): Time Domain Analysis of Ship Motions in Following Waves, 11th Australian Fluid Mechanics Conference, University of Tasmania, Hobart, Australia.

[15] Hamamoto, T. and Kim, J.-S. (1993): A New Coordinate System Describing the Steering Motion in the Waves and its Equation of Motion, J. Society of Naval Architects of Japan, Vol.173, pp.209-220. (in Japanese)

[16] Nishimura, K., Hirayama, T., Takayama, T., Hirakawa, H. and Ma, N. (2004): One Proposal for Numerical Simulation Method in Time Domain for Motion of Maneuvering Small Ship in Steep Waves, J. Society of Naval Architects of Japan, Vol.195, pp.203-210. (in Japanese)

[17] Fang, M.-C., Luo, J.-H. and Lee, M.-L.: A Nonlinear Mathematical Model for Ship Turning Circle Simulation in Waves, J. Ship Research, Vol.49, No.2 (2005), pp.69-79.

[18] Skejic, R. and Faltinsen, O. M. (2008): A Unified Seakeeping and Maneuvering Analysis of Ships in Regular Waves, J. Marine Science and Technology, Vol.13, pp.371-394.

[19] Yen, T. G., Zhang, S., Weems, K. and Lin, W. M. (2010): Development and Validation of Numerical Simulations for Ship Maneuvering in Calm Water and in Waves, Proc. 28th Symp. on Naval Hydrodynamics, Pasadena, pp.12-17.

[20] Seo, M.-G. and Kim, Y. (2011): Numerical Analysis on Ship Maneuvering Coupled with Ship Motion in Waves, Ocean Engineering, Vol.38, pp.1934-1945.

[21] Cura-Hochbaum, A. and Uharek, S. (2016): Prediction of Ship Manoeuvrability in Waves based on RANS Simulations, Proc. the 31st ONR symp. on Naval Hydrodynamics, Monterey, CA.

[22] Zhang W., Zou, Z.-J and Deng, D.-H. (2017): A Study on Prediction of Ship Maneuvering in Regular Waves, Ocean Engineering, Vol.137, pp.367-381.

[23] Skejic, R. and Faltinsen, O. M. (2013): Maneuvering Behavior of Ships in Irregular Waves, Proc. ASME 32nd International Conference on Ocean, Offshore and Arctic Engineering (OMAE2013), Nantes, France.

[24] SIMMAN 2008: Workshop on Verification and Validation of Ship Manoeuvering Simulation Methods, Copenhagen, http://www.simman2008.dk/

[25] Yasukawa, H., Hirata, N. and Yamazaki, Y. (2018): Effect of Bilge Keels on Maneuverability of a Fine Ship, J. Marine Science and Technology, Vol.23, No.2, pp.302-318.

[26] Hamamoto, T. and Kim, J.-S. (1993): A New Coordinate System Describing the Steering Motion in the Waves and its Equation of Motion, J. Society of Naval Architecture, Japan, No.173, pp.209-220. (in Japanese)

[27] Iseki, T. and Ohtsu, K. (1994): Bayesian Estimation of Directional Wave Spectra Based on Ship Motions (2nd Report), J. Society of Naval Architects of Japan, Vol.176, pp.99-105. (in Japanese)

[28] Matsuda, A., Hashimoto, H., Terada, D., Taniguchi, Y. (2016): Validation of Free Running Model Experiments in Heavy Seas, Proc. 3rd International Conference on Violent Flows, Japan.

[29] Yasukawa, H. and Yoshimura, Y., (2015): Introduction of MMG Standard Method for Ship Maneuvering Predictions, J. Marine Science and Technology Vol.20, pp.37-52.

[30] Yasukawa, H. and Sano, M. (2008): Maneuvering Simulation of MOERI Container Ship, Workshop on Verification and Validation of Ship Manoeuvring Simulation Methods (SIMMAN 2008), Copenhagen.

[31] Watanabe, I., Toki, N., and Ito, A. (1994): Theory of Seakeeping performance and its Application to Ship Design, Chapter 2 Strip Method, 11th Marine Dynamic Symposium, Society of Naval Architects of Japan, pp.167-187. (in Japanese)

[32] Kim, D. J., Yun, K., Park, J. Y., Yeo, D. J., and Kim, Y. G. (2019): Experimental Investigation on Turning Characteristics of KVLCC2 Tanker in Regular Waves, Ocean Engineering, Vol.175, pp.197-206.

[33] Kashiwagi, M. et al. (2003): Hydrodynamics of Floating Bodies, Seizan-Do Shoten, ISBN4-425-71321-4. (in Japanese)

[34] Yasukawa, H., Hirata, N., Matsumoto, A., Kuroiwa, R. and Mizokami, S. (2019a): Evaluations of Wave-Induced Steady Forces and Turning Motion of a Full Hull Ship in Waves, J. Marine Science and Technology, Vol.24, No.1, pp.1-15.

[35] Yasukawa, H., Sakuno, R. and Yoshimura, Y. (2019b): Practical Maneuvering Simulation Method of Ships Considering the Roll-Coupling Effect, J. Marine Science and Technology, Vol.24, No.4, pp.1280-1296.

[36] Maruo, H. (1960): Wave Resistance of a Ship in Regular Head Sea, Bulletin of the Faculty of Eng., Yokohama National University, Vol.9, pp.73-91.

[37] Takahashi, T. (1988): A Practical Prediction Method of Added Resistance of a Ship in Waves and the Direction of its Application to Hull Form Design, Trans. West-Japan Society of Naval Architects, No.75, pp.75-95. (in Japanese)

[38] Hasnan, M. A. A., Yasukawa, H., Hirata, N., Terada, D. and Matsuda, A. (2020): Study of Ship Turning in Irregular Waves, J. Marine Science and Technology, doi:10.1007/s00773-019-00698-1. (in press)

[39] Nomoto, K., Taguchi, T., Honda, K. and Hirano, S. (1957): On the Steering Qualities of Ships, Technical report, International Shipbuilding Progress, Vol.4, pp.354-370.